

Organization of Sterols in Model Membranes

by

Bibhu Ranjan Sarangi

**Thesis submitted to the
Jawaharlal Nehru University
for the award of the degree of
Doctor of Philosophy**

2010



Raman Research Institute

Bangalore 560 080

India

CERTIFICATE

This is to certify that the thesis entitled “**Organization of Sterols in Model Membranes**” submitted by Bibhu Ranjan Sarangi for the award of the degree of DOCTOR OF PHILOSOPHY of Jawaharlal Nehru University is his original work. This has not been published or submitted to any other University for the award of any other Degree or Diploma.



Prof. R Subrahmanyam

Director

Raman Research Institute

Bangalore 560 080 INDIA



Dr. V. A. Raghunathan

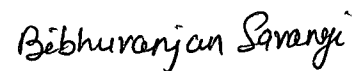
(Thesis Supervisor)

DECLARATION

I hereby declare that the work reported in this thesis is entirely original. This thesis is composed independently by me at Raman Research Institute under the supervision of Dr. V. A. Raghunathan. I further declare that the subject matter presented in this thesis has not previously formed the basis for the award of any degree, diploma, membership, associateship, fellowship or any other similar title of any university or institution.



(Dr. V. A. Raghunathan)



(Bibhu Ranjan Sarangi)

SCM Group

Raman Research Institute

Bangalore 560 080 - INDIA

ACKNOWLEDGEMENTS

I am deeply indebted to my supervisor Dr. V. A. Raghunathan for his invaluable guidance, support, encouragement and help. I thank him for everything that I learnt from him. He has been a wonderful teacher. Every discussions with him has made me learn something new. It has been a pleasure working with him.

I am extremely thankful to Dr Georg Pabst for his active support and interest in my work. It was a great learning experience working with him at ELLETRA beamline, Trieste. The experiments on cell blebs were done at National Center for Biological Sciences, Bangalore with active support from Dr. Satyajit Mayor. I thank him for his support. I am extremely thankful to Dr. Madan Rao for his keen interest in my research and a lot of fruitful discussions. I thank Dr. Pramod Pullarkat for making me learn various aspects of biological experiments. It has been a pleasure working with him. I thank Dr. Yashodhan Hatwalne for many helpful discussions. I thank Dr. Arun Roy for his support. I express my gratitude to Prof Ravi Subrahmanyam and Prof. N. Kumar for their encouragement and support. My sincere thanks are due to Prof. N. V. Madhusudana, Prof. B. K. Sadashiva and all other faculty members of the SCM group for their encouragement and help.

I thank Mr. Mani, Mr. Dhason and Mr. Ram for their extremely valuable help at various stages of the experimental work. I thank Mr. Md. Ishaq for his help. I am thankful to the staff of the chemistry laboratory for supplying needed chemicals, distilled water etc.

I sincerely thank all the library staff for their prompt help in getting several references and related materials. My special thanks to Dr. Y. M. Patil, Mr. Kiran, Mr. Nagaraj, Mr. Manjunath, Ms. Girija, Ms. Geetha, Ms. Vrinda, Mr. Hanumappa and Mr. Chowdappa. I would like to thank everyone at the computer section for their help. I thank everyone in the administrative department. Special thanks to Mr. Krishnamarju, Mr. Radhakrishna, Ms. Marisa and Ms. Radha for their administrative help.

I specially thank Sanat for making me understand minute details of sample preparation

and related experiments. It was a great pleasure working with him. I also thank Subhshri Ghosh from NCBS for helping me learn the cell culture.

I am fortunate to have a friend like Susanta who has been a constant source of encouragement and support. I express my heartfelt thank for him. I thank Tripta for her support and encouragement. I have learnt a great deal during many discussions with her. I thank Lipsa, Sunita and Jagadish for their support. It has been a an enjoyable life at RRI because of my friends like Bharat, Suresh, Hari and Radhakrishnan. I also thank Dibyendu, Marjan and Amiri, Rahul, Nagaraju, Rakesh, Satyam, Jayakumar, Sandeep, Radhika, Nandan. Special thanks to Bharat, Suresh and Madhukar for reading my thesis chapters and their suggestions. I am thankful to all my former and present labmates Sanat, Sajal, Rema, Sowmya, Radhakrishnan, Arif, Antara, Madhukar, Santosh, Shabib, and Vasudha. I also thank the biophysics labmates Santanu, Giri, Renu, Anagha for their help.

I take this oppotunity to express my gratitude to my school teachers Mr. Dharendra Kumar Behera and Mr. Uttam Kumar Sahu for helping me shape my academic carrear.

I thank all my Brothers and Sisters and family members for their constant support. I express my heartfelt thanks to my loving parents who have sacrificed a lot for helping me realize my dreams.

Finally my sincere thanks to all the taxpayers of India and Government of India for the financial support.

PREFACE

This thesis deals with the structure and phase behaviour of lipid-sterol model membranes. Sterols such as cholesterol, are essential components of plasma membranes. They play important roles in several biological processes. Cholesterol rich functional domains called “rafts”, have been proposed to exist in the plasma membranes. It is also interesting to note that sterols have evolved in a biochemical pathway. There are several sterols which share similar chemical structures with cholesterol. However specific sterols have been found to be present in particular organisms. For example higher order eukaryotic membranes contain cholesterol, whereas yeast and fungi have ergosterol in their membranes. Our motivation was to study the influence of the sterol structure on the structure and thermodynamic phase behaviour of lipid membranes.

In **chapter 1**, we give a brief introduction to model membranes constituted from various lipid-sterol mixtures. Then we describe the experimental techniques employed in this thesis to study these systems.

The biological membranes are based on a frame work of lipid bilayers. Lipids are amphiphilic molecules, consisting of two parts; a polar hydrophilic head and non-polar hydrophobic chain(s). Due to the presence of innumerable molecular species biological membranes are generally far too complex for quantitative experiments. Therefore model membranes containing fewer lipid species are widely used to understand the membrane structure and interaction between its various components.

The phase behaviour of such lipid bilayers depend on the hydration level and and temperature of the medium. At high hydration lipids exhibit a fluid (L_α) phase above the chain melting transition temperature (T_m). In this phase the hydrocarbon chains are molten and disordered. At lower temperatures this fluid phase transforms into a gel phase. In this phase the hydrocarbon chains are predominantly in the fully stretched all *trans* conformational state. Lipids which have a larger head group, such as phosphatidylcholine (PC), show the $L_{\beta'}$ gel

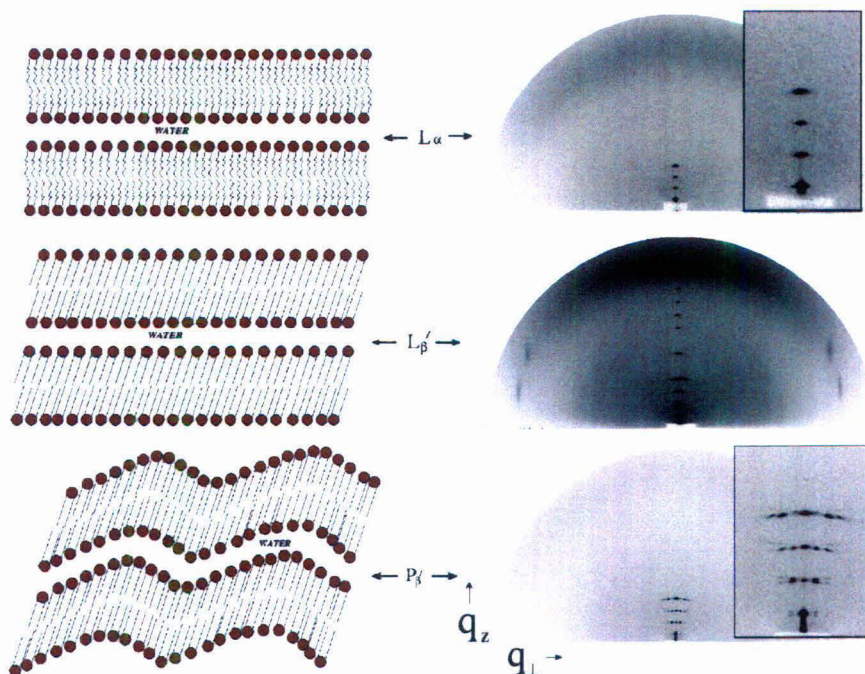


Figure 1: Schematic of various phases of lipid bilayer and their characteristic diffraction patterns. The real space z direction is along the bilayer normal

phase, where the hydrocarbon chains are tilted with respect to the bilayer normal. In the gel phase the lipid chains exhibit a quasihexagonal inplane ordering. Some PCs exhibit a ripple ($P_{\beta'}$) phase in between L_{α} and $L_{\beta'}$ phases. The $P_{\beta'}$ phase is characterized by a two dimensional oblique lattice formed by height modulated bilayers. The different phases of the lipid bilayers can be identified by their characteristic diffraction patterns. The schematics of various phases of the lipid bilayers along with the characteristic diffraction patterns are shown in fig. 1.

Presence of sterols influences the phase behaviour of lipid bilayers significantly. There have been numerous studies on lipid-sterol model membranes to understand such influence. Cholesterol has been used in majority of such studies because of its biological importance. On addition of cholesterol to lipid membranes, both $L_{\alpha} - P_{\beta'}$ (main-transition) and $P_{\beta'} - L_{\beta'}$ (pre-transition) temperatures decrease with increasing cholesterol concentration (X_c). At sufficiently high X_c (> 20 mol%), both the main- and pre-transition are completely abolished resulting in a single fluid phase. In lipid-cholesterol binary mixtures below T_m , the gel

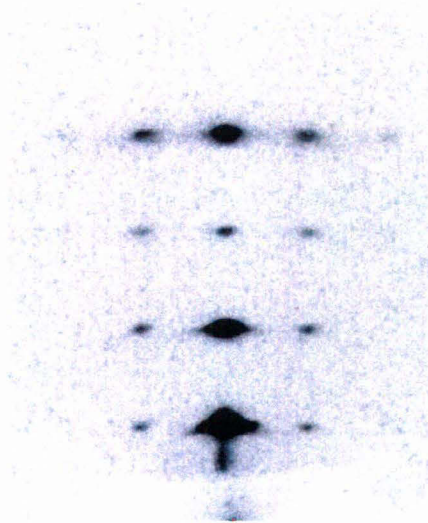


Figure 2: Small angle diffraction pattern of the P_β phase.

phase was found to coexist with a cholesterol-rich phase for $\sim 5 < X_c < \sim 20$. Although spectroscopic techniques such as NMR have found a fluid-fluid coexistence above T_m in similar range of X_c , there has been no evidence for such a coexistence in diffraction studies. A novel modulated phase denoted as P_β was found to exist in PC-cholesterol mixtures at intermediate cholesterol concentrations. Unlike the normal ripple phase diffraction data from this phase can be indexed on a two dimensional rectangular lattice suggesting that the two arms of the ripple are symmetric (fig. 2).

Ternary mixtures of a saturated lipid, an unsaturated lipid and cholesterol exhibit fluid-fluid phase separation. The two fluid phases are called as liquid-ordered (l_o) and liquid disordered (l_d) phases. This kind of phase separation has been often linked to the “rafts” in the plasma membranes. It has been shown that the l_o phase basically contains the saturated lipid and the l_d phase contains the unsaturated lipid. Though l_o phase is believed to be richer in cholesterol, partitioning of cholesterol between these two fluid phases is not yet fully established.

Apart from cholesterol there have been several studies on other sterols in model membranes. The main aim of such studies were to find the effect of sterol structure on various aspects of lipid bilayers.

We have systematically investigated the structure and phase behaviour of lipid-sterol model membranes as a function of sterol concentration and temperature. We have used various sterols such as cholesterol, ergosterol, lanosterol, 15-hydrocholesterol (25HC), cholestenone etc. We have prepared binary and ternary mixtures of lipid and sterols in the form of unoriented multilamellar vesicle (MLVs) dispersions, oriented stacks of bilayers and giant unilamellar vesicles (GUVs). The MLVs and oriented samples were studied using small angle x-ray scattering. The calculation of electron density maps from the observed diffraction data requires both the magnitude and phases of the reflections. Magnitude of the structure factors were obtained from the experiments. For retrieving the phase information we have used either a brute force method or a model function approach. GUVs were prepared by electroformation method. The GUVs obtained by electroformation were of size 10-100 μm hence can be easily observed using light microscopy. Confocal fluorescence microscopy was used to image these GUVs.

In **chapter 2** we present our experimental results of x-ray diffraction studies on the structure and phase behaviour of dipalmitoyl phosphatidylcholine (DPPC) and dimiristoyl phosphatidylcholine (DMPC) membranes at various cholesterol concentrations (X_c) as well as at different relative humidities (RH). The hydration level of a lipid strongly influences both its main and pre-transition temperatures. Also the chain tilt of the PC lipids decreases with decreasing degree of hydration. At very low hydration the tilt of the PC molecules vanishes.

DMPC-cholesterol bilayers were probed at 30% and 65% RH. Significant increase in T_m was observed with decrease in hydration level. Earlier reports on pure DMPC bilayers suggest a similar behaviour. The increase in the main transition temperature suggests that the gel phase ($L_\beta/L_{\beta'}$) is stabilized at lower humidities. This may be due to the fact that the effective area per lipid molecule decreases as the hydration level decreases. This helps in the lipid packing facilitating the gel phase stabilization. In agreement with earlier results we did not see the $P_{\beta'}$ phase at both 65% and 30% RH. Which suggests that the pre-transition completely disappears at lower hydration. From our studies we also found out that amount

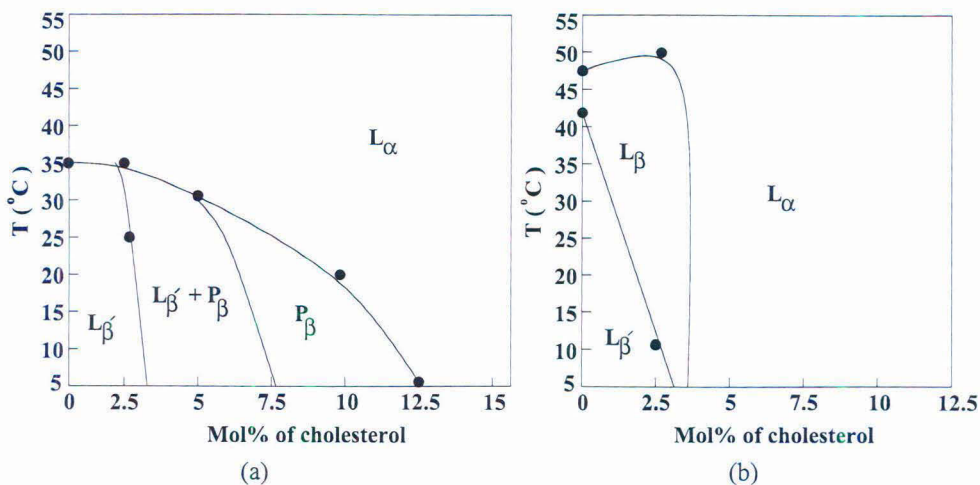


Figure 3: Phase diagrams of DMPC-cholesterol mixtures at (a) 65 % RH, (b) 30% RH.

of cholesterol required to abolish the main transition completely, decreases significantly as the RH decreases. At very low hydration (30% RH) 2.5 mol% of cholesterol is sufficient to abolish the main transition. Our results on DPPC-cholesterol in excess water suggest that the modulated phase ceases to exist in excess water. Instead we observe a fluid phase (L'_{α}) with higher lamellar periodicity.

In **chapter 3**, we present a comparative study of the effects of ergosterol and Lanosterol on the phase behaviour of DPPC membranes using x-ray diffraction on aligned samples. We also compare the chain orientational order parameter obtained from the wide angle x-ray scattering studies of these systems. The phase behaviour of DPPC-lanosterol mixtures is very similar to that of DPPC-cholesterol mixtures reported in earlier x-ray scattering studies. Above T_m a single fluid phase (L_{α}) was observed at all sterol concentrations. At intermediate sterol concentrations we observed the modulated phase (P_{β}) as reported earlier in DPPC-cholesterol mixtures. The P_{β} phase was preceded by a coexistence region of $L_{\beta'}$ and P_{β} phase. Though major aspects of the phase diagram of DPPC-ergosterol system remain the same as cholesterol system but we have observed a three phase coexistence region at intermediate ergosterol concentrations.

The electron density profiles constructed for both ergosterol and lanosterol do not show any significant differences. The bilayer thickness is similar for both sterols. By following

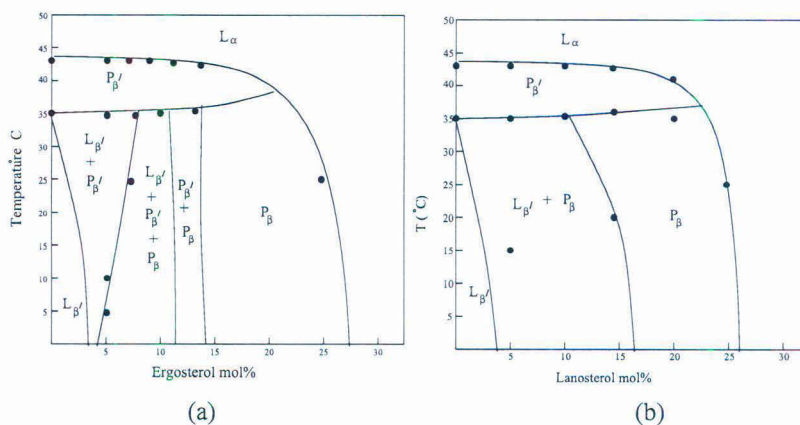


Figure 4: Phase diagrams of (a) DPPC-ergosterol and (b) DPPC-lanosterol mixtures at 98% RH.

an existing method we analyzed the wide angle chain scattering to calculate an average order parameter of the acyl chains in DPPC bilayers containing cholesterol, ergosterol and lanosterol. Our results suggest that ergosterol is most efficient of the three in ordering the acyl chains of DPPC bilayers. The order parameter values follows the trend ergosterol \geq cholesterol > lanosterol.

In **chapter 4**, we describe our studies on DPPC bilayers with several other sterols such as cholestenone, 25HC, cholestane and 7DHC. We have studied the phase behaviour of these binary mixtures using x-ray scattering. Our results show that the DPPC-cholestenone system has a similar phase behaviour as DPPC-cholesterol mixtures. However 25-hydrocholesterol shows a very different phase behaviour. The modulated phase was not observed in DPPC-25HC mixtures. Instead a two phase coexistence was observed in a very broad region of this phase diagram. The two phases were identified as the gel phase and a fluid phase (fig. 5). DPPC-cholestane system also shows a very similar phase behaviour as that of DPPC-25HC. We observed a three phase co-existence in DPPC-7DHC bilayers at ~ 10 mol % sterol concentration. This is very similar to our studies on DPPC-ergosterol bilayers described earlier. This indicates that structural changes in the steroid skeleton play a key role in influencing the bilayer properties.

In **chapter 5**, we describe the phase behaviour of ternary raft mixtures composed of equimolar mixture of dipalmitoyl phosphatidylcholine (DPPC) and dioleoyl phosphatidyl-

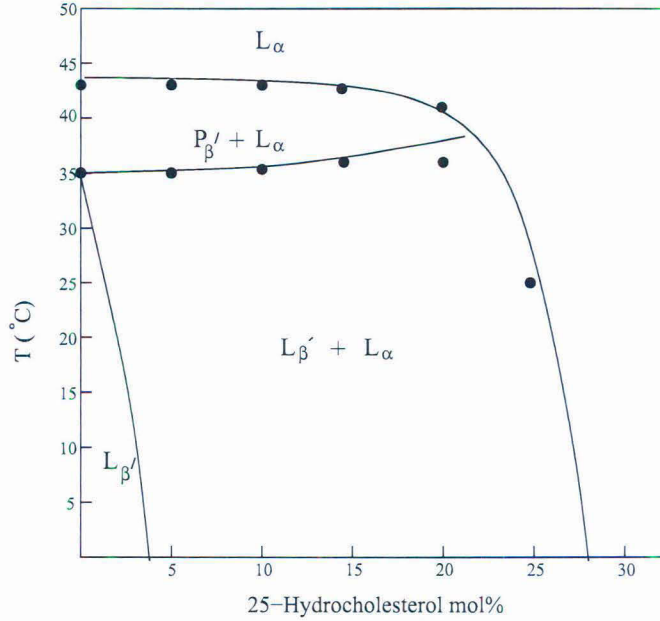


Figure 5: Phase diagram of DPPC-25HC mixture at 98% RH.

choline (DOPC) at various concentrations of ergosterol and cholesterol. The important result of our studies on these two systems is the observation of fluid-fluid co-existence at intermediate sterol concentrations for both ergosterol and cholesterol. However at ergosterol concentration ~ 33 mol% we observed demixing of the sterols evident from sharp scattering coming from ergosterol crystallites. For cholesterol similar demixing was observed at a lower concentration (~ 25 mol%).

We have also studied GUVs of these ternary mixtures at a few sterol concentrations using fluorescence microscopy. For ergosterol concentration ~ 30 mol% we observed domains which were circular in shape reminiscent of a fluid domain (fig. 6). Though the domains observed have a circular shape resembling the fluid domains, but the fact that they do not coalesce with each other suggests that they are more ordered than the normal fluid phase domains. This is in agreement with our scattering studies.

We also describe our approach to find the partitioning of cholesterol from x-ray diffraction studies of DSPC-DOPC-cholesterol mixtures. We propose a method to find such a partitioning from scattering data provided the electron density profile (edp) in absolute scale is given. However we found that a method that has been used in the literature to put the edp in

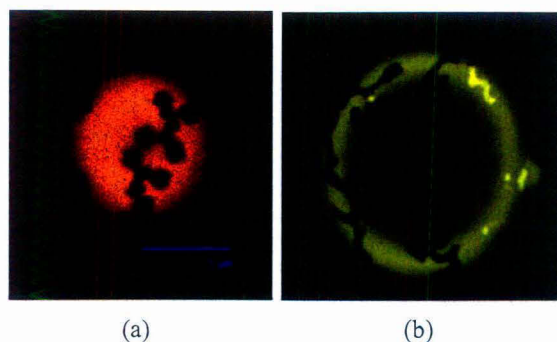


Figure 6: Fluorescence micrographs of GUVs of (a) DPPC-DOPC-ergosterol and (b) DPPC-DOPC-cholestenone mixtures showing the coexistence of two phases.

absolute scale gives inconsistent values for lateral area per lipid when calculated separately from the head and chain region of the edp. We propose a way to construct edp on absolute scale while maintaining the consistency. Subsequently we describe some critical aspects of the determination of the absolute electron density profile from scattering data.

In **chapter 6**, we present our experimental result on cell blebs. Blebs are spherical cellular protrusions that occur in many physiological situations such as cytokinesis, cell spreading, virus uptake, and apoptosis. Freshly plated fibroblast cells with a dynamically unstable cortical actin mesh exhibit spontaneous blebbing. These cell blebs can be detached from the parent cells. Being a part of the plasma membrane such detached blebs provide a very simple yet biological system for studying several aspects of plasma membranes. For example the active coupling of the cytoskeleton to the membrane organization can be studied in such a system of detached blebs. Motivated by this idea we tried to prepare cell detached blebs following several existing protocols. In this chapter we describe our studies on these cell blebs. We found out that such cell detached blebs contain actin (fig. 7), and hence can be ideal for studying the coupling of the cytoskeleton to membrane organization. Although formaldehyde+DTT treatment produce cell detached blebs, we believe the blebs produced by this method will not have any biological activity because formaldehyde is known to fix the cells by cross linking the proteins. On the other hand, detached blebs produced using osmotic shock may retain their biological activity and could be very useful for a variety of experiments aimed at understanding the plasma membranes.

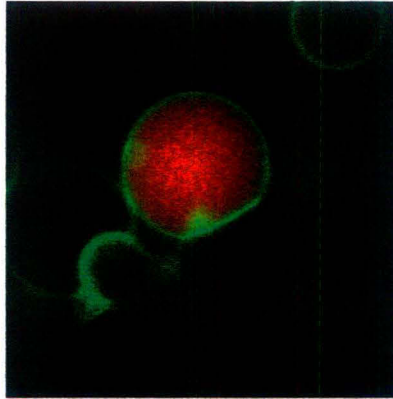


Figure 7: Detached blebs labelled with green fluorescent protein (shown green) and cherry actin (shown red).

The last chapter discusses the conclusions that can be drawn from the studies in this thesis and some future directions.

Publications:

1. Phase behaviour of lipid–cholesterol membranes
S. Karmakar S, B. R. Sarangi, and V. A. Raghunathan. *Solid State Communications*, 2006, **139**, 630.
2. Phase behaviour of phosphatidylcholine (PC)–cholesterol membranes
S. Karmakar S, B. R. Sarangi, and V. A. Raghunathan. *DAE Solid State Physics Symposium*, 2006, **51**.
3. X-ray and neutron scattering studies on lipid-sterol model membranes,
B. R. Sarangi, S. Karmakar, V. A. Raghunathan
Advances in planner lipid bilayers and liposomes, Vol. **12**, Edited by Ales Iglic, Elsevier, 2010.
4. Influence of sterols on model lipid membranes : A comparative study
B. R. Sarangi and V. A. Raghunathan
(To be submitted)

Contents

1	Introduction	1
1.1	Introduction to membranes	2
1.1.1	Cell membranes and model membranes	2
1.1.2	Lipid bilayers as model membranes	4
1.1.3	Structure and phase behaviour of lipid bilayers	7
1.1.4	Sterols in membranes	10
1.1.5	Influence of sterols on the structure and phase behaviour lipid bilayers	13
1.1.6	Cell membrane Vs model membrane	17
1.2	Experimental techniques	18
1.2.1	X-ray diffraction	18
1.2.1.1	X-ray diffraction of lipid bilayers	18
1.2.1.2	Preparation of samples for diffraction studies	21
1.2.1.3	Experimental setup	22
1.2.1.4	Data analysis	24
1.2.1.5	Calculation of transbilayer electron density profile by Fourier reconstruction method	27
1.2.2	Optical microscopy	29
1.2.2.1	Preparation of giant unilamellar vesicles (GUVs) for mi- croscopic studies	29
1.2.2.2	Fluorescence microscopy	31
1.2.2.3	Laser scanning confocal fluorescence microscopy	32

2	Influence of hydration on the phase behaviour of PC-cholesterol membranes	38
2.1	Introduction	38
2.2	Experimental results	40
2.2.1	Phase behaviour of DMPC-cholesterol mixtures at low humidity	40
2.2.1.1	RH=65%	41
2.2.1.2	RH=30%	41
2.2.2	Phase behaviour of DPPC-cholesterol in excess water condition	43
2.3	Discussion	49
2.4	Conclusion	52
3	Phase behaviour of DPPC bilayer containing ergosterol and lanosterol	55
3.1	Introduction	55
3.2	Experimental results	57
3.2.1	Small angle x-ray scattering (SAXS) studies	58
3.2.1.1	Phase behaviour of DPPC-ergosterol mixtures	58
3.2.1.2	Phase behaviour of DPPC-lanosterol mixtures	62
3.2.1.3	Trans-bilayer electron density profiles: Influence of sterol on bilayer thickness	62
3.2.2	Wide angle x-ray scattering (WAXS) studies	64
3.2.2.1	Theoretical background	66
3.2.2.2	Results	68
3.3	Discussion	71
3.4	Conclusion	75
4	Universal behaviour of sterols in PC membranes	78
4.1	Introduction	78
4.2	Experimental results	80
4.2.1	Phase behaviour of DPPC-cholestenone bilayers	81
4.2.2	Phase behaviour of DPPC-25HC and DPPC-cholestane bilayers	81

4.2.3	Phase behaviour of DPPC-7DHC bilayers	85
4.3	Discussion	86
4.4	Conclusion	89
5	Phase behaviour of ternary mixtures with ergosterol and cholestenone and the problem of cholesterol partitioning between l_o and l_d phases	91
5.1	Introduction	91
5.2	Experimental studies on ternary mixtures with ergosterol and cholestenone .	93
5.2.1	SAXS studies on DPPC-DOPC-ergosterol mixtures	93
5.2.2	SAXS studies on DPPC-DOPC-cholestenone mixtures	95
5.2.3	Microscopy of GUVs	95
5.3	Cholesterol partitioning between l_o and l_d phases	99
5.3.1	Calculation from scattering data	100
5.3.1.1	Principle	100
5.3.1.2	l_o - l_d phase separation in DSPC-DOPC-cholesterol mixtures	103
5.3.2	Constructing electron density profile on absolute scale	105
5.3.2.1	Using head group contrast	107
5.3.2.2	Using a model	108
5.3.2.3	Another way for obtaining electron density profile with minimum constraints	110
5.3.2.4	Effect of the limiting number of Bragg peaks	111
5.3.3	Scheme of calculation of partitioning in two component system . .	113
5.3.3.1	Binary mixture with cholesterol	115
5.3.3.2	Binary mixture with a cholesterol like molecule with higher electron density	116
5.3.3.3	Binary mixture of two lipid molecules with contrast in electron density	117
5.4	Discussion	118

5.5	Conclusion	122
6	Preparation of a simple cellular environment: Cell blebs	126
6.1	Introduction	126
6.2	Experimental results	127
6.2.1	Cell culture and imaging	127
6.2.2	Cell blebbing	128
6.2.2.1	Ethanol treatment	129
6.2.2.2	Osmotic shock	130
6.2.2.3	Formaldehyde treatment	131
6.2.2.4	Actin detection in detached cell blebs	131
6.3	Discussion	133
6.4	Conclusion	135

Chapter 1

Introduction

Cell membrane acts as an interface for biological cells providing support to the cells and also allowing transport through it at the same time. Like many other biological structures cell membranes are complex multifunctional soft materials. These membranes are made up of a framework of lipid bilayers in which embedded molecules such as proteins are free to diffuse. Model membranes containing a few lipid components provide a much simpler platform to understand the structure and interaction of such soft materials at a fundamental level.

The present thesis deals with x-ray diffraction and fluorescence microscopy studies on binary and ternary lipid-sterol membranes. In this chapter we give a brief introduction and motivation for the work described in the thesis. This chapter is broadly divided into two main sections. Section. 1.1 gives a brief introduction to the structure and properties of membranes. Section. 1.2 gives the experimental methodology employed in this thesis to study these systems.

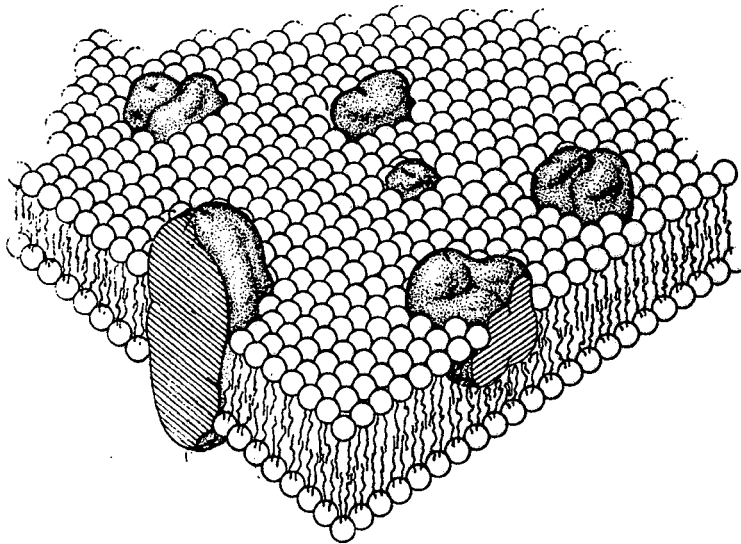


Figure 1.1: A cartoon of the Fluid Mosaic model of Cell membranes proposed by Singer and Nicolson [2].

1.1 Introduction to membranes

1.1.1 Cell membranes and model membranes

All eukaryotic cells are compartmentalized by membranes of various morphologies and compositions. Most common to all cells is the plasma membrane which is basically the cell surface. The central structural element of a plasma membrane is the lipid bilayer. In addition, it contains various macromolecules like proteins, sterols, sugars etc. The membrane with such structural complexity takes part in many biological processes. While providing support for the intracellular materials, it also facilitates selective transportation of materials and signals which are essential for various cellular activities. In a way the plasma membranes play a key role in many cellular processes like metabolism, transport, growth, mobility, signalling etc. [1]. Due to such importance, there has been on-going research interest in understanding cell membranes from both biologist's and physicist's points of view. Majority of such studies are aimed at understanding the structure of the membranes and the functionality of the various molecules present in it. From the structural point of view the most widely accepted model

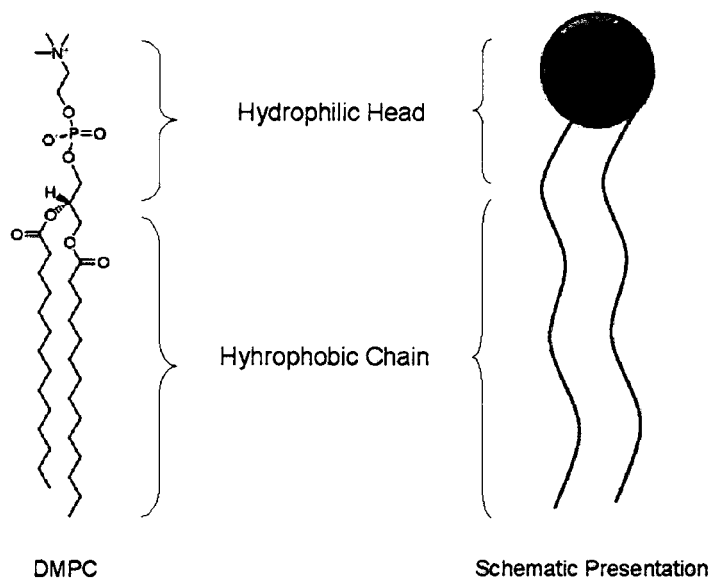


Figure 1.2: Typical structure of a lipid molecule with hydrophilic and hydrophobic parts. Left: Dimyristoyl phosphatidylcholine (DMPC) lipid, Right: A schematic representation

that best explains the properties of cell membranes is the fluid mosaic model proposed by Singer and Nicolson [2]. This model views the cell membrane as a continuous bilayer of phospholipid molecules in which various other molecules like proteins are embedded. A cartoon of the fluid mosaic model taken from [2] is shown in fig. 1.1.

Because of the presence of innumerable molecular species, quantitative studies on cell membranes invite several experimental difficulties. However model membranes containing a few lipids and sterols offer a much simpler platform for detailed study of various physical properties of membranes and their structure and phase behaviour. Because of the self assembling properties of the lipid molecule, described in the following section, it is rather easy to prepare model membranes using a few lipid components. In particular there have been many studies on model membranes containing cholesterol because of its immense biological importance. However studies on model membrane systems have their own limitations as discussed in section 1.1.6.

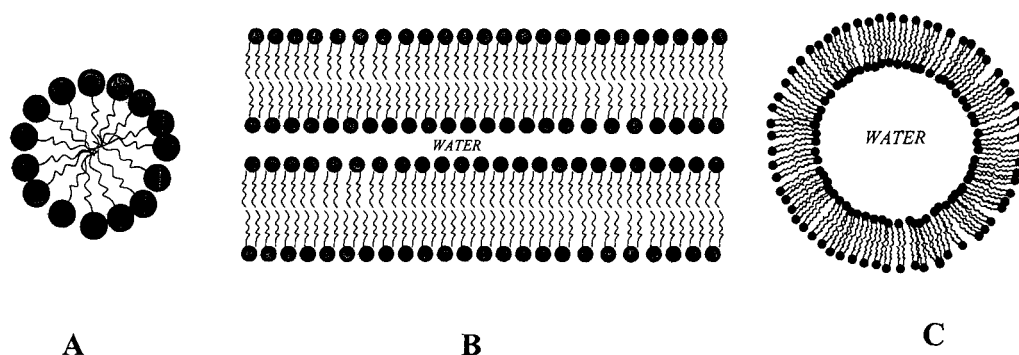


Figure 1.3: Different self-assembled structures. A: Micelle, B: Bilayer, C: Vesicle

1.1.2 Lipid bilayers as model membranes

Lipids are mostly amphiphilic molecules, i.e they have both water soluble (hydrophilic) and water insoluble (hydrophobic) parts in the same molecule. In general a lipid molecule has a polar head which is hydrophilic and a nonpolar part consisting of one or more hydrocarbon chains which is hydrophobic. A schematic representation of a two chain lipid molecule along with the structure of a typical phospholipid molecule with the phosphatidylcholine (PC) head-group is shown in fig. 1.2. When such molecules are dispersed in an aqueous medium they tend to self assemble to minimize the free energy. For example in case of lipids dispersed in water, because the chains do not like to be in contact with water and heads want to be in water the molecules will rearrange themselves in compact structures shielding their chains from water and exposing the heads to water. This phenomenon is a result of the hydrophobic interaction which is basically of entropic origin [3]. The concentration above which self-assembly of amphiphiles occurs is called the critical micellar concentration (CMC). The CMC of a molecule depends strongly on its chemical structure. Typical CMC of a two-chain lipid molecule is of the order of $\sim 10^{-9}$ moles/liter. Depending on the chemical structure and shape of the lipid molecule involved, various self assembled structures can be formed [3, 4, 5]. The most common structure formed by lipid molecules which are present in biological membranes is a bilayer. Other structures which can be formed by such amphiphilic molecules are micelles which are formed mostly by single chain lipids. A schematic representation of three of such structures is given in fig. 1.3. The focus of the present thesis is on

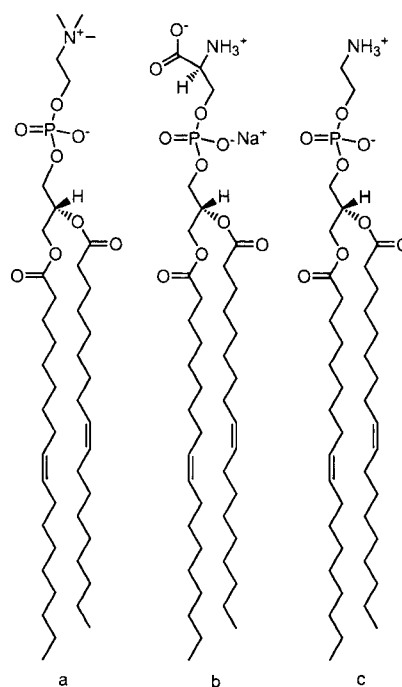


Figure 1.4: Structure of some of the common head groups of phospholipids a: PC, b: PS, c: PE

lipid bilayers.

Cell membranes contain numerous lipid species. But phospholipids and sphingolipids are the most abundant species in the plasma membranes. Depending on the chemical structure of the head group, phospholipids are classified into several groups such as phosphatidylcholines (PCs), phosphatidylethanolamines (PEs), phosphatidylserines (PSs) and phosphatidylinositols (PIs). Typical structures of phospholipids with various head groups are shown in fig. 1.4. PCs and PEs are known as zwitterionic lipids as they possess a dipole moment when dissolved in water, but no net charge, whereas PSs and PIs are electrically charged. Lipid molecules having the same headgroup can have different chain lengths and degree of unsaturation. These differences can lead to different physical and biochemical properties of the lipid. The chemical structures of some PC lipids with different chain lengths and degrees of unsaturation are shown in fig. 1.5.

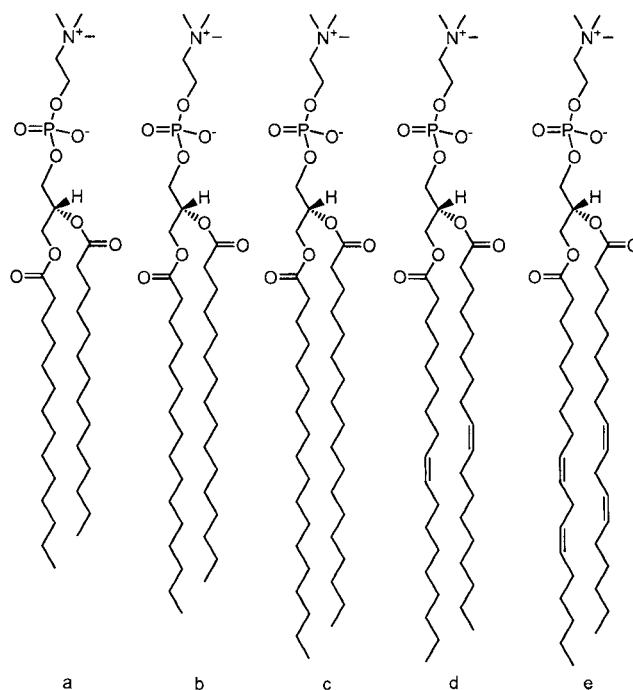


Figure 1.5: Chemical structures of phosphatidylcholine lipids with different chain lengths and degree of unsaturation. The abbreviations are used for the names of the lipids (see table. 1.1). The first and the second number in the parenthesis are chain length and the number of double bonds present in the chains of the corresponding lipid. a: DMPC (14:0), b: DPPC (16:0), c: DSPC (18:0), d: DOPC (18:1), e: DLPC (18:2)

1.1.3 Structure and phase behaviour of lipid bilayers

Lipid molecules mostly form lamellar phases in an aqueous medium, made up of a periodic stack of bilayers separated by water. Such a lamellar structure can exhibit various liquid crystalline phases depending upon the structure of the lipid molecule involved and the temperature of the medium. Lipid bilayers exhibit a fluid phase known as L_α above a certain temperature known as the chain melting transition temperature or the main-transition temperature (T_m). T_m depends on various factors like the structure of the headgroup, chain length of the lipid, degree of unsaturation of the hydrocarbon chains etc. Also for a particular lipid T_m varies with the hydration level of the lipid bilayer. The known T_m s of a few representative lipids with various chain lengths and degree of unsaturation are given in table. 1.1. It is evident from the table that the presence of unsaturation in the hydrocarbon chain reduces T_m drastically as compared to the saturated lipid of same chain length and head group structure.

Table 1.1: Known values of the T_m of a few Lipids. The acronyms of the lipids are given besides their names. The number of carbon atoms in the chains and the number of double bonds are also given.

Saturation	Lipids	Chain lengths	T_m (°C)
Saturated	Dilauryl phosphatidylethanolamine (DLPC)	12:0/12:0	-1
	Dimyristoyl phosphatidylcholine (DMPC)	14:0/14:0	23
	Dipalmitoyl phosphatidylcholine (DPPC)	16:0/16:0	41
	Dilauryl phosphatidylethanolamine (DLPE)	12:0/12:0	29
	Dipalmitoyl phosphatidylethanolamine (DPPE)	16:0/16:0	63
	Dipalmitoyl phosphatidylserine (DPPS)	16:0/16:0	54
	Sphingomyelin (from bovine brain)	Distribution of chains	40
Unsaturated	Di-oleoyl phosphatidylcholine (DOPC)	18:1/18:1	-18
	Dilinoleoyl phosphocholine (DLPC)	18:2/18:2	-53
	Di-oleoyl phosphatidylserine (DOPS)	18:1/18:1	-11

In the fluid L_α phase the hydrocarbon chains of the lipid molecules are completely molten and disordered. The bending rigidity of the bilayer is $\sim 10^{-19}$ J ($\sim 10 - 20 k_B T$) in this phase whereas the self-diffusion constant of the lipid molecule is $\sim 10^{-11} m^2 s^{-1}$. Typical diffraction pattern of a stack of oriented bilayers in the L_α phase consists of a set of peaks in the small

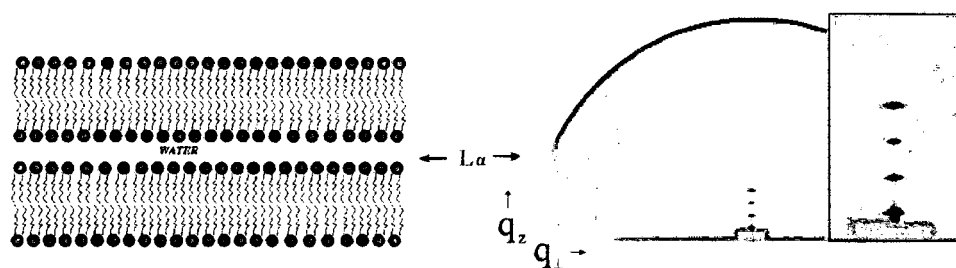


Figure 1.6: Schematic of the L_α phase and its diffraction pattern. The z axis is along the bilayer normal.

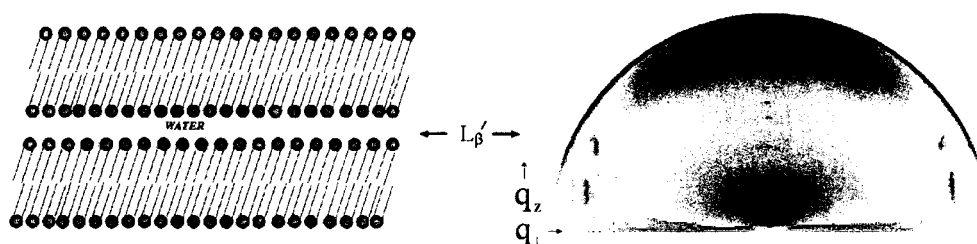


Figure 1.7: Schematic of the $L_{\beta'}$ phase with a typical diffraction pattern. The condensed wide angle peaks correspond to the chain lattice. The z axis is along the bilayer normal.

angle region corresponding to the lamellar periodicity of the bilayer stack. The scattering from the chains gives rise to a very weak diffuse peak in the wide angle region. A schematic representation of the L_α phase along with its typical diffraction pattern is shown in fig. 1.6.

Below T_m , the bilayers exhibit a more ordered phase, known as the gel phase (L_β or $L_{\beta'}$). In this gel phase hydrocarbon chains are predominantly in the fully stretched all *trans* conformation. Chains form a quasi-hexagonal lattice in the plane of the bilayer. In the case of lipids with large head groups such as PCs, to accommodate the large headgroup area, the hydrocarbon chains are tilted with respect to bilayer normal in the gel phase. Such a gel phase with tilt is denoted as $L_{\beta'}$ where prime indicates the tilt of the chains. Typical tilt angle for PCs is of the order of 30° . A schematic of the $L_{\beta'}$ phase along with its diffraction pattern is shown in fig. 1.7. Here in addition to the lamellar peaks along the q_z direction, a set of wide angle peaks are also obtained which correspond to the chain lattice. The position of these peaks at $q_z \neq 0$ signifies the tilt of the chains. Three different types of gel phases have been found to form at different levels of hydration [6, 7]. These different gel phases are characterized by different tilt directions of the chains.

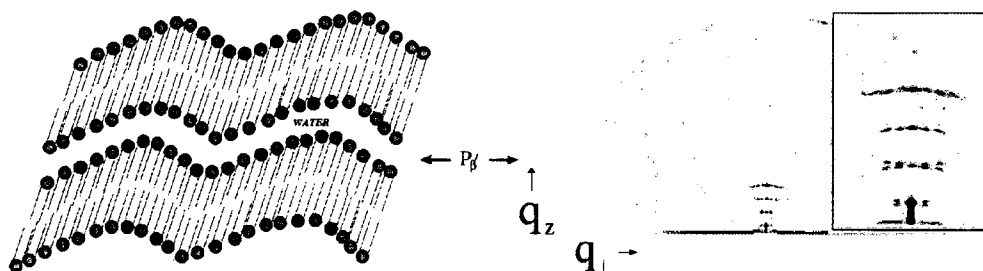


Figure 1.8: Schematic of the $P_{\beta'}$ phase with a typical diffraction pattern. The satellite peaks present in the small angle region corresponds to an oblique lattice formed by the height modulations of the bilayers. The z axis is along the bilayer normal.

Many lipids which exhibit the $L_{\beta'}$ phase show an intermediate phase in between L_{α} and $L_{\beta'}$. This is called as the ripple ($P_{\beta'}$) phase. $P_{\beta'} \rightarrow L_{\beta'}$ transition is known as pre-transition. For lipids such as phosphatidylethanolamine (PE) which do not show the tilted gel phase, $P_{\beta'}$ phase is absent. $P_{\beta'}$ phase is characterized by a two dimensional oblique lattice formed by height modulated bilayers. Typical diffraction pattern in the $P_{\beta'}$ phase is shown in fig. 1.8. The wavelength of the modulation is about 150 Å. In $P_{\beta'}$ hydrocarbon chains show quasi-hexagonal inplane ordering, similar to that in the gel phase. The pre-transition temperature also depends on hydration level of the lipid bilayers. At low hydration levels pre-transition disappears and gel phase is stabilized over a large temperature range [8]. Presence of sterols in the lipid bilayer also affects the main and pre-transitions thereby influencing the phase behaviour of lipid bilayers. Such kind of phase behaviour will be discussed in subsequent sections.

Apart from these three phases, lipids exhibit another phase, known as the L_c phase at temperatures below the gel phase [9]. In general, L_c phase occurs after a long incubation at lower temperatures typically at 4°C. The L_c phase is a highly ordered phase where hydrocarbon chains as well as head groups are strongly correlated [10].

As stated above lipids with unsaturated hydrocarbon chains have very low T_m . For example for DOPC the T_m (-18.3°C) is way below the room temperature. Hence such lipids show only fluid phase over the temperature range of interest. Similarly when two or more lipid species with different individual T_m s are mixed the overall transition temperature of

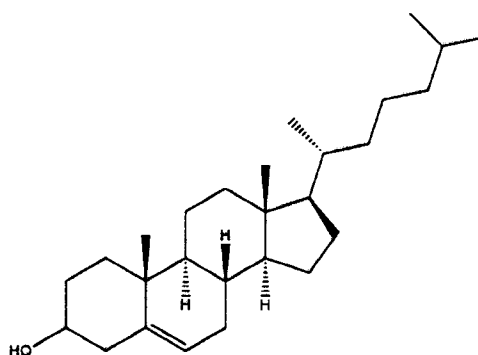


Figure 1.9: Chemical structure of cholesterol.

the system takes an intermediate value. Example of such systems are egg-PC and brain-SM where the head group is same but the hydrocarbon chains differ in length and degree of unsaturation. The plasma membrane is a classic example of such a mixed lipid bilayer.

1.1.4 Sterols in membranes

Sterols are a class of lipids with a very different structure than that of the phospholipids described earlier. They belong to the category of polycyclic organic compounds. The most common structural feature of all sterol molecules is the bulky hydrophobic part consisting of steroid rings. This steroid skeleton is often attached to a small hydrocarbon chain. The most well known example of a sterol molecule is cholesterol whose structure is shown in fig. 1.9. It has a very small polar head in the form of a hydroxyl (-OH) group. Four steroid rings form the bulky hydrophobic skeleton to which a small hydrocarbon chain is attached. There are many other biologically relevant sterol molecules with similar structural features. Ergosterol, lanosterol and sitosterol are examples of such sterol molecules. The structures of a few of these sterol molecules are shown in fig. 1.10.

These sterols play a very important role in various biological processes involving the membranes. For example cholesterol in membrane has been associated with many cellular functions like protein sorting, signalling etc. Sterols also influence membrane organization. It is believed that cholesterol rich domains called “rafts” exist in plasma membranes, which are proposed to play very important role in various cellular activities. However the existence

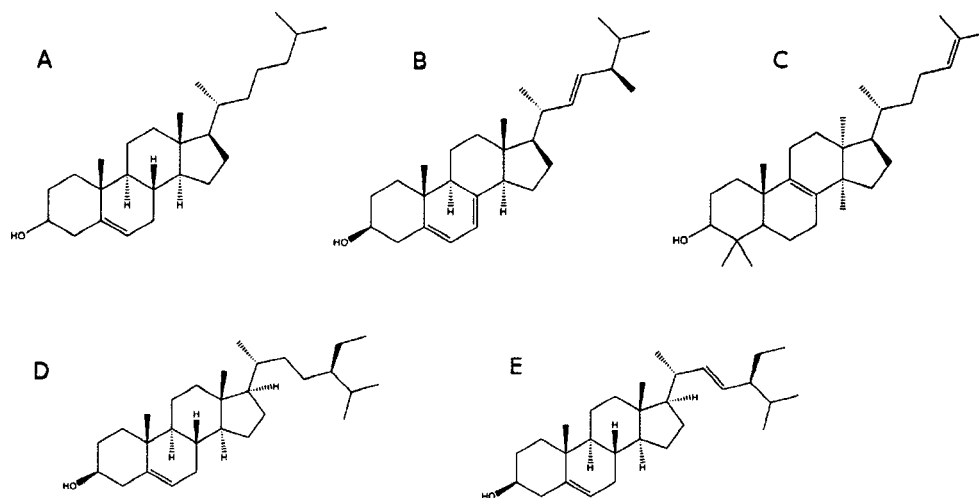


Figure 1.10: Structures of different sterols A: Cholesterol, B: Ergosterol, C: Lanosterol, D: Sitosterol, E: Stigmasterol. Ergosterol is present in the membranes of yeast and fungi. Lanosterol is the common precursor of both cholesterol and ergosterol in the biochemical synthesis. Sitosterol and stigmasterol are found in plant cells. The structural differences between the sterols can be very small, such as the position of the double bond as in the case of ergosterol and cholesterol or it can be the presence of additional methyl group as in the case of lanosterol.

of such domains, their organization and functionality is still far from fully established.

Such a raft hypothesis traces its origin to the experimental evidence that epithelial cells polarize their cell surfaces into apical and basolateral domains with different protein and lipid compositions in each of these domains. In this regard the most prominent experimental result *in vivo* is based on detergent resistant membranes (DRM) techniques [11]. DRM is the insoluble fraction of the membranes when Triton X-100 is added at $\sim 1\text{mol}\%$ to the membranes at 4°C . It is found to consist of sphingolipids, cholesterol and GPI anchored proteins which are believed to be the components of rafts. Motivated by this proposal a large number of experimental studies have been carried out to probe the details of raft formation [12, 13, 14].

Nanoscale heterogeneity in lateral membrane organization has been observed using homo-FRET [15] and more recently by stimulated emission depletion (STED) far-field fluorescence nanoscopy [16]. In model membrane systems microscopic phase separation has

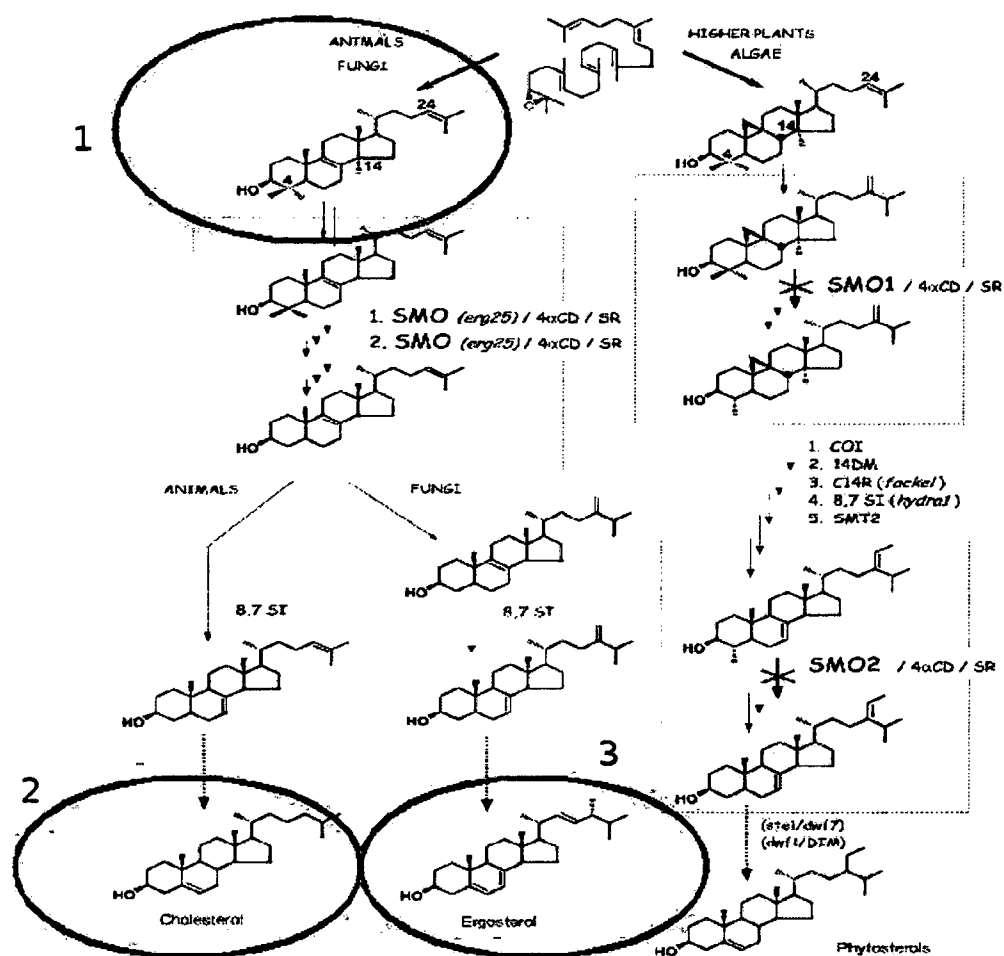


Figure 1.11: Simplified sterol biosynthesis pathway[19] . The positions of lanosterol(1), cholesterol(2), and ergosterol(3) are marked.

been observed in ternary mixtures of a saturated lipid, with an unsaturated lipid and cholesterol [8, 17]. Such kind of phase separation has been proposed to mimic the raft like domains of the biological membranes.

Apart from cholesterol, there are many other sterol molecules which are biologically relevant. In this context it is interesting to note that sterols have evolved in a biochemical pathway. As argued by Bloch, cholesterol in our cells is a result of long biochemical synthesis [18]. Depending on the cell types, plasma membranes contain sterols of different structure and concentration. Cholesterol is found in almost all higher order eukaryotic cell membranes in various concentrations whereas lower order eukaryotes like yeast and fungi do not contain cholesterol in their membranes, instead they have ergosterol. Similarly two other sterols,

sitosterol and stigmasterol are only found in plant cell membranes. Even though some sterol molecules have minute structural differences, it is very puzzling to find the selectiveness of nature in choosing a particular sterol for a particular type of membrane. It seems nature has optimized the sterol structure through biochemical evolution in accordance with the cell type to perform various functions.

A simplified sterol biosynthesis pathway is shown in fig. 1.11 [19]. In the sterol evolution one important sterol is lanosterol, which is the common precursor to both ergosterol and cholesterol. The difference in the chemical structure of these sterols can be seen from fig. 1.10. Lanosterol has additional $-CH_3$ groups protruding out of its hydrophobic skeleton. Cholesterol and ergosterol are very similar in structure apart from the additional double bond. These minute structural differences significantly influence the physical properties of model membranes. Differential effects of ergosterol and lanosterol on PC membranes will be discussed in Chapter 3.

1.1.5 Influence of sterols on the structure and phase behaviour lipid bilayers

As described in the earlier section, sterol structure seems to have important consequences on its functionality in the membrane. Hence there have been many studies on lipid-sterol model membranes. Most of the studies involve cholesterol as the sterol molecule because of its immense biological relevance. So our present day understanding of sterol functionality is mostly based on these studies on lipid-cholesterol systems [20]. However there have also been several studies on model membranes containing other sterols. In this section we describe some of the important results of these studies.

Various experimental techniques such as differential scanning calorimetry (DSC), spectroscopic techniques (NMR, ESR, fluorescence etc.), diffraction techniques (x-ray, neutron), microscopy (freeze-fracture electron microscopy, fluorescence microscopy and atomic force microscopy) have been widely used to probe membrane characteristics in the presence of cholesterol. Addition of cholesterol to the lipid bilayer brings about various structural

changes thereby influencing bilayer properties. The main-transition (T_m) and pre-transition temperatures decrease with increasing cholesterol concentration indicating that cholesterol transforms the gel phase into a fluid phase [21].

Partial phase diagrams of lipid-cholesterol mixtures have been determined using several experimental techniques [22, 23, 24, 26, 27] and theoretical modelling [28]. A comparison of these phase diagrams is shown in fig. 1.12. There are several common features of these results. Below T_m coexistence of the gel phase with a cholesterol-rich phase, known as liquid ordered (l_o) phase is observed. But one major difference between these phase diagrams is the observation of a two phase coexistence called as liquid ordered (l_o) and liquid disordered (l_d) phases above T_m as evident from the spectroscopic studies. However such a coexistence is not observed in scattering studies.

Another important result is the observation of a cholesterol induced modulated phase in oriented PC bilayers [27]. This phase denoted by P_β was found to be different from the normal ripple phase ($P_{\beta'}$) in several structural aspects. The phase diagram with the modulated phase as observed by Karmakar *et al.* is shown in fig. 1.13. A typical diffraction pattern along with the proposed bilayer model of the P_β phase is shown in fig. 1.14.

Another important structural parameter influenced by cholesterol is the bilayer thickness. But the change depends on the structure of the lipid and the phase state of the bilayer. Bilayer thickness increases with cholesterol concentration in the gel phase of phosphatidylcholine bilayers for chain length from 12 to 16, as cholesterol is known to remove the chain tilt. However, for longer chain length like DSPC, bilayer thickness is decreased in the gel phase [29]. In L_α phase bilayer thickness increases due to the increase in conformational order by straightening the hydrocarbon chain of lipids in the presence of neighboring cholesterol molecules. However at low cholesterol concentrations, this effect is not significant [30]. The influence of cholesterol on bilayers of monounsaturated PCs has also been studied using SANS on unilamellar vesicles. The membrane thickness, lateral area of the lipid and the headgroup hydration are found to monotonically increase with increasing cholesterol concentration up to 45 mol% [31]. The bending modulus (K_c) of the bilayer increases with

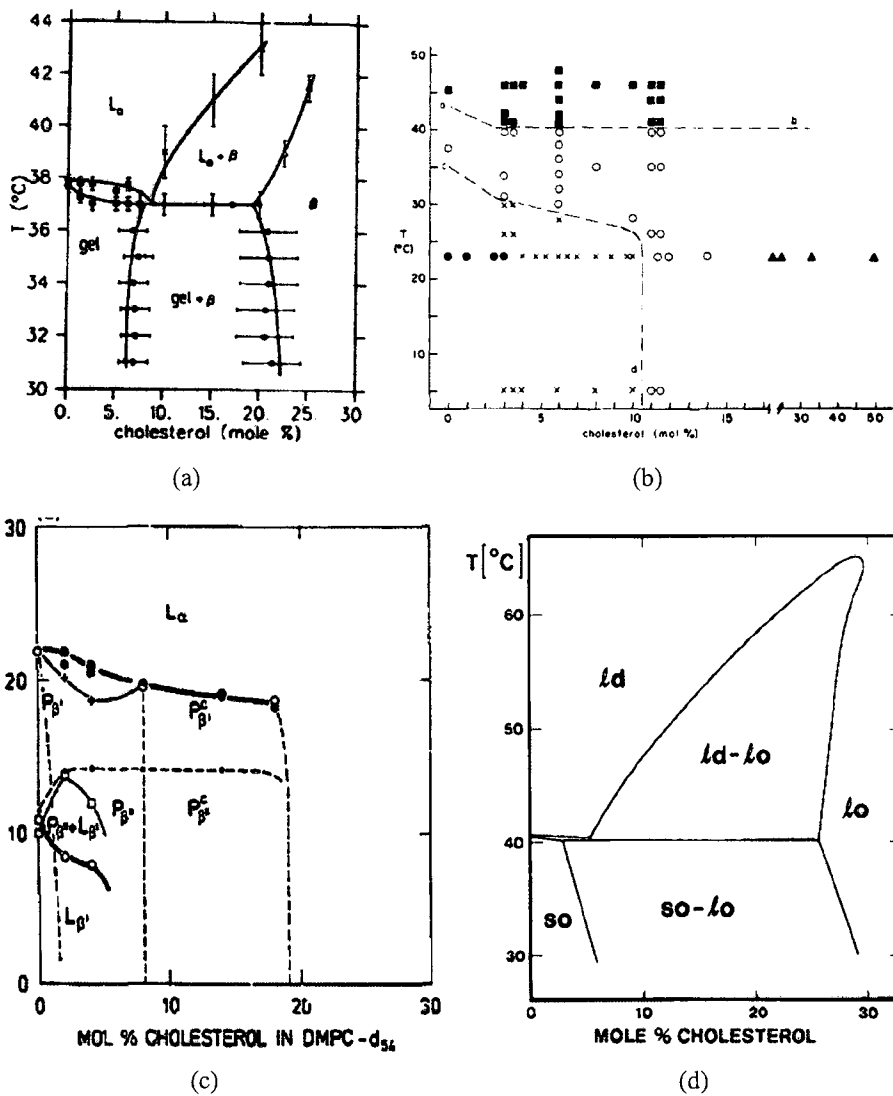


Figure 1.12: Phase diagrams of PC–cholesterol mixtures obtained from (a) NMR studies [22],(b) x-ray Scattering [23],(c) neutron scattering [24] and (d) theoretical model [28]. L_{α}/l_d is fluid phase, β is a cholesterol-rich phase, $L_{\beta'}/s_o$ represent the gel phase, $P_{\beta'}$ represent the ripple phase.

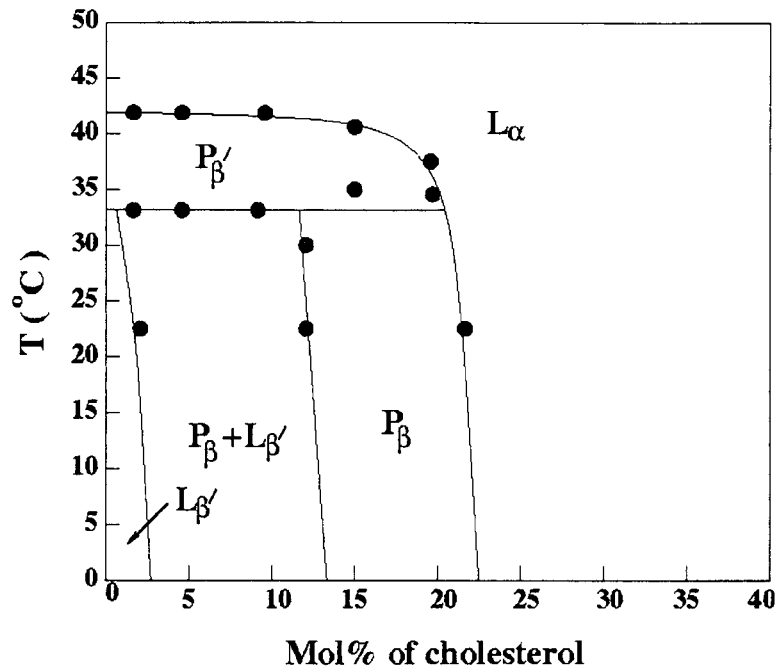


Figure 1.13: Partial phase diagram of DPPC-cholesterol mixtures obtained from x-ray scattering studies on oriented bilayers [27].

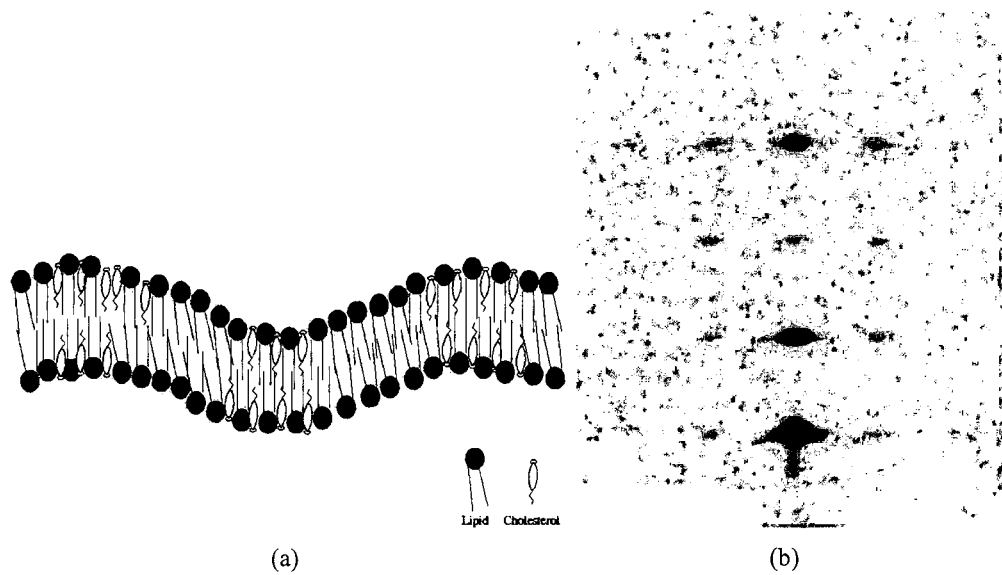


Figure 1.14: Proposed model of the P_{β} phase (a) along with its characteristic small angle diffraction pattern (b). It is proposed that cholesterol distribution in the bilayer is inhomogeneous. Coupling of this inhomogeneity to the local bilayer curvature can induce the height modulated P_{β} phase.

cholesterol concentration [32]. This effect is more enhanced in the case of saturated lipids like DMPC.

Though a lot of studies have focused on cholesterol in model membranes, still there have been a few studies on the influence of other sterols on bilayer properties. Most of these studies aim to compare the differential effect of various sterols on the membrane properties with that of cholesterol. Using SANS on ULVs it has been shown that ergosterol and lanosterol, which are structurally closely related to cholesterol, produce similar changes in the bilayer thickness, although large differences in their influence on the membrane thermal expansion coefficient is observed [33]. The influence of the plant sterols, stigmasterol and sitosterol on membrane properties has been studied using SAXS. For all the lipids studied, these sterols are found to be not as efficient as cholesterol in increasing the bilayer thickness and rigidity, which is attributed to the additional methyl group in their alkyl chains [34]. To our knowledge there have been no systematic studies on the influence of various sterols on the phase behaviour of model membranes. We have carried out a systematic study on the influence of many such sterols on various properties of the PC bilayers which will be described in the subsequent chapters.

1.1.6 Cell membrane Vs model membrane

Though model membranes are much simpler systems to study, some caution is required in applying the results of such studies to processes in cell membranes. As described earlier, model membranes often consist of very few lipids and sterol, whereas cell membranes are very complex in composition with innumerable molecular species. Another major difference is the dynamical functionality of cell membrane. In biological cells, plasma membranes are not isolated entities, rather their functions are coupled to the intracellular organelles in various ways. This kind of co-ordination makes the cell membrane an active system. Also various processes in the plasma membrane use energy from the ATP hydrolysis process. Hence plasma membrane system are not necessarily in thermodynamic equilibrium. On the other hand in the case of model membranes one is most often interested in the passive

behaviour. And it is difficult to bring in the activity at the scale of cellular level in a model membrane system. However, when one needs to understand the basic interactions involving different molecular species such as lipid-sterol interactions, model membranes provide an ideal platform. In view of all these, a careful approach is needed to draw biologically relevant conclusions from studies of model membrane systems.

1.2 Experimental techniques

In this section we briefly describe the experimental techniques used in this thesis. We have mainly used x-ray diffraction and light microscopy in all our experiments. In section 1.2.1 we describe x-ray diffraction from lipid bilayers, related experimental setup and data analysis. In section 1.2.2 various microscopic techniques are described in brief.

1.2.1 X-ray diffraction

X-ray scattering is a very powerful tool to probe different condensed matter systems at very small length scales. It has been widely used to find out the structures of very diverse class of materials from pure metal to proteins and macromolecular assemblies. Scattering techniques have contributed immensely in the development of biological sciences. For example, using x-ray diffraction the structures of DNA and tobacco mosaic virus (TMV) were solved which led to ground breaking developments in the field of biology. It has also become a very important tool in model membrane research for finding the membrane structure and interaction.

1.2.1.1 X-ray diffraction of lipid bilayers

X-ray scattering has been widely used to study the structure and phase behaviour of lipid-sterol bilayers. Both small angle x-ray scattering (SAXS) and wide angle x-ray scattering (WAXS) techniques have been used to study multilamellar stacks of lipid bilayers. SAXS provides information about the structure of the bilayers, whereas the organization of the molecules within each bilayer can be deduced from WAXS. Several structural parameters,

such as membrane thickness, lateral area per lipid and number of water molecules per lipid, can be extracted from the x-ray diffraction data [35, 36].

In a typical diffraction experiment the corrected scattered intensity from the system is described by

$$I(q) \propto \langle |f(q)|^2 s(q) \rangle \quad (1.1)$$

where q is the absolute value of scattering vector whose magnitude is given by $|q| = \frac{4\pi \sin\theta}{\lambda}$ (θ and λ are scattering angle and wavelength of incident x-ray respectively), $f(q)$ is the form factor which can be represented in terms of electron density profile $\rho(r)$ of the bilayer as

$$f(q) = \int \rho(r) e^{-iqr} dr$$

$s(q)$ is the structure factor corresponding to the lattice which in the present case is the lamellar stack.

$f(q)$ and $s(q)$ contain information about the lattice and ordering of the bilayers and also the electron density distribution in a single bilayer. However there are several limitations in getting accurate structural data from such kind of bilayer-water system. Lipid bilayers are smectic liquid crystals where long-range crystalline order is destroyed by long wavelength thermal fluctuations. So what they possess is quasi-long range order, characterized by power-law decay of positional correlations. Because of this only a few Bragg reflections are obtained for a fully hydrated bilayer in the fluid phase. Even in the low temperature gel phase where in-plane crystalline order of the chains exists, local thermal fluctuations broadens the Bragg peak which in turn broadens the electron density profile corresponding to individual component thereby limiting the ability to extract finer details from diffraction data. So it is very important to analyze the diffraction data in a proper way. Two different frameworks have been used to analyze the scattering data from these systems, namely the Paracrystalline theory and the Caillé theory. The paracrystalline theory addresses the issue of thermal and lattice disorder within a stochastic approach. Such kind of disorder is known as stacking disorder [37, 38]. In addition to the above mentioned stacking disorder, Caillé theory also

takes into account the local molecular fluctuations which results in the undulation of the bilayers. Unlike the stochastic approach employed in paracrystalline theory, Caillé theory is based on a Hamiltonian model [39]. Caillé theory was later modified to take in to account the finite size of the bilayer stack [40]. There have been several attempts to get more accurate structural data from diffraction experiments [35, 36, 41].

One can construct an electron density profile from the form factor data by Fourier reconstruction method. The electron density profile $\rho(z)$ for a lipid-bilayer is given by the expression

$$\rho(z) = \rho_w + \frac{F(0)}{d} + \frac{2}{d} \sum_{h=1}^{h_{max}} \alpha_h |F_h| \cos\left(\frac{2\pi hz}{d}\right) \quad (1.2)$$

where ρ_w is the electron density of water. d is the lamellar periodicity, F_h s are the discrete values of form factor ($f(q)$) corresponding to $q_h = \frac{2\pi h}{d}$. $F(0)$ is the zero order form factor, α_h are the phases of different Fourier components $|F_h|$. The phases α_h can only take the values ± 1 as discussed later in this section. From the scattering experiments $|F_h|$ can be calculated as

$$F_h = C_h \times \sqrt{I_h} \quad (1.3)$$

where I_h is the intensity corresponding to the h^{th} order diffraction and C_h is the correction factor which depends on the sample morphology and the experimental geometry as will be discussed later. But from the scattering experiments only the absolute ratios $r_h = \frac{|F_h|}{|F_1|}$ of the discrete bilayer form factor can be correctly determined because F_h involves an unknown scaling factor. For this reason the electron density profile can only be obtained on a relative scale as

$$\rho(z)_{relative} \propto \sum_{h=1}^{h_{max}} \alpha_h r_h \cos\left(\frac{2\pi hz}{d}\right) \quad (1.4)$$

The electron density profile can be obtained on an absolute scale if the scaling factor is determined correctly. Such a methodology will be described in detail in Chapter-5.

But all this can only be done if the phases of the various Fourier components can be retrieved accurately. In a scattering experiment only intensities $I_h = |F_h|^2$ can be measured.

TH-18174

Hence the magnitude of F_h can be obtained. But F_h is a complex quantity, hence requires the phase information to be deduced correctly. This problem of finding the phases of diffraction peaks is known as the “phase problem in crystallography”. In general the phases can take any arbitrary values. But for a centro-symmetric object like the lipid bilayers, since the electron density function is an even function with respect to the center of the bilayer, the phases can only take values of 0 or π . With this restriction, for a bilayer-water system having n diffraction peaks the phase problem effectively boils down to finding the right combination of phases amongst the 2^n possibilities.

In practice several methods are followed to retrieve the phase information in such systems. One such method employs swelling experiments where the bilayer form factor is sampled at different hydration levels [42]. Assuming that the change in the hydration level only changes the thickness of the intermediate water layer without changing the bilayer structure in any way, this kind of sampling enables to retrieve the phases of different Fourier components.

For the samples where only a few reflections (3-4) are observed, one can also use a brute force method by testing all possible combinations (2^n). Ideally only one set of phases will give a physically realizable electron density profile and hence is taken to be the correct one. But for systems with large number of diffraction peaks a more suitable method employed in retrieving the phase information is modelling the electron density of the bilayer by a suitable function involving some adjustable parameters and then fitting the calculated intensities with the experimental data. The best fit will give the correct phase information. This kind of approach is described in detail in section 1.2.1.5.



1.2.1.2 Preparation of samples for diffraction studies

In all the x-ray scattering experiments described in this thesis, two sample morphologies have been used. Unoriented lipid bilayers in the form of multilamellar vesicles and oriented samples in the form of bilayer stacks. All lipids and sterols used in the experiments were purchased from *Sigma-Aldrich-Fluka, USA* and were used without further purification. Some

of the samples were tested by thin layer chromatography (TLC) which gave a single spot confirming the purity.

For preparation of unoriented samples an appropriate amount of the lipid-sterol mixture in desired molar ratios was dissolved in chloroform (*HPLC grade, Merk*). Typical total lipid concentration was ~ 10 mg/ml. Then the solvent was evaporated in glass capillaries (*Hampton Research*) of diameter 1 mm under ambient conditions. Typical evaporation time was 2-3 days. After all traces of solvent evaporated the sample was hydrated with excess water and sonicated to ensure proper mixing. To enhance sample concentration in the scattering volume the sample capillaries were centrifuged at ~ 3000 RPM for ~ 20 minutes. After that the sample capillary was sealed in candle flame and glue to ensure thorough sealing. The sample capillaries were placed in locally designed temperature controlled heater for x-ray diffraction.

For preparation of oriented samples an appropriate amount of lipid-sterol mixture in desired molar ratio was dissolved in chloroform in a typical concentration of 5mg /ml. The sample was deposited on the clean outer surface of a glass beaker (radius ≈ 17 mm). The beaker was kept overnight inside an evacuated dessicator to remove all traces of the solvent. Typical area density of dried lipid film was $\sim 5 \mu\text{g}/\text{mm}^2$. It was then kept inside a sealed airtight container along with some amount of Millipore water for a couple of days to ensure proper hydration of the bilayer in a water saturated atmosphere. In this condition the temperature of the sample was cycled across the main transition a few times while hydrating to get a well oriented sample, where the bilayers are oriented parallel to the substrate. The sample was then transferred to the sealed chamber for x-ray studies.

1.2.1.3 Experimental setup

For diffraction studies, unoriented samples as described above were taken in glass capillaries (*Hampton Research*) having a diameter of 1 mm. They were placed inside a locally built heater, whose temperature could be controlled using a standard PID controller program to an accuracy of $\pm 0.1^\circ\text{C}$. A schematic of the experimental setup for unoriented samples is shown

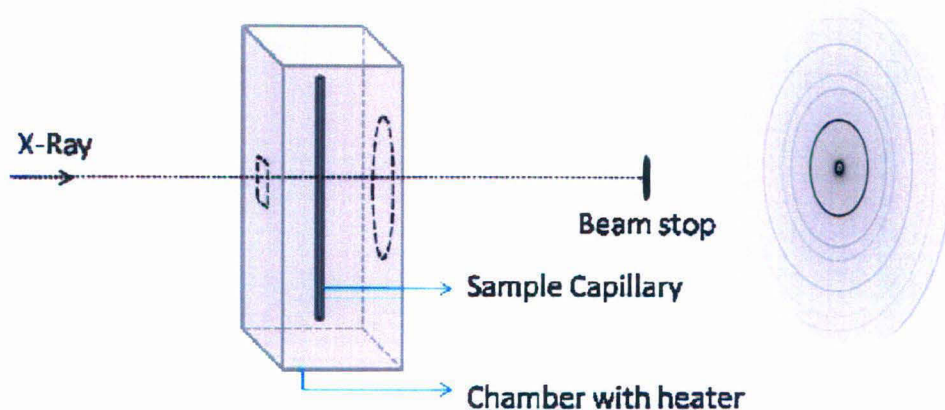


Figure 1.15: Schematic of the experimental set up for unoriented samples.

in fig. 1.15.

For aligned samples, a locally built heater was used which is made up of a double walled nickel-plated brass chamber through which water can be circulated [43]. Temperature of the heater can be changed by circulating water at the desired temperature from a water bath (*Julabo*). The inlet and outlet windows of the chamber were covered with mylar sheets. The chamber was made airtight to achieve a constant relative humidity (RH) inside. A schematic of the experimental set up for aligned sample is shown in fig. 1.16.

High RH close to 100% was achieved by keeping a reservoir of water inside the chamber. Lower values of RH were obtained using saturated salt solutions. A small electric fan was used to make the temperature and RH uniform inside the chamber. Water condensation on the inlet and outlet windows due to the temperature differences between the inside and the outside was prevented by gently blowing hot air on the windows. A thermo-hygrometer probe (*Testo 610*) was inserted into the chamber to monitor both the temperature and RH close to the sample.

A rotating anode generator (*Rigaku UltraX 18*) operating at 50 kV and 80 mA was used as our laboratory x-ray source. A multilayered mirror optics (*Xenocs*) was used to select the CuK_{α} radiation ($\lambda = 1.54 \text{ \AA}$). Monochromatic x-rays then pass through a collimator which consists of two sets of slits. Adjusting the slits we can obtain required beam size at the

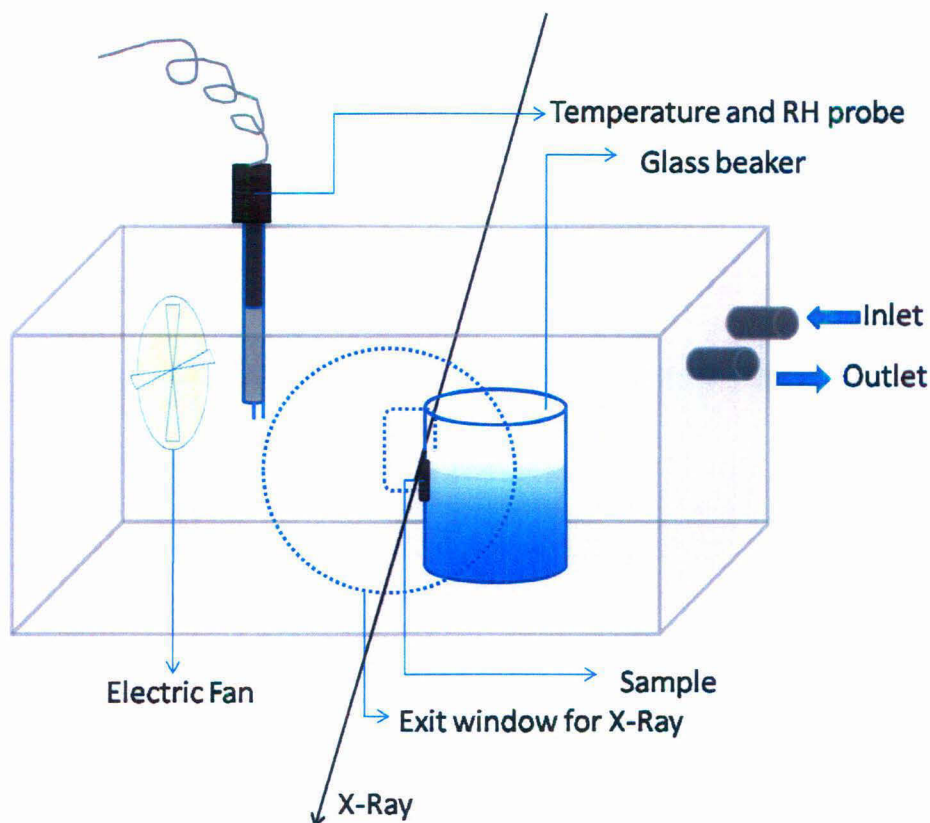


Figure 1.16: Schematic of the experimental set up for aligned samples.

sample and avoid parasitic scattering. Typical beam diameter after collimation was ~ 1 mm. A 2D image plate detector (*Marresearch*) was used for recording the diffraction intensities. Diffraction patterns recorded on the image plate detector (diameter 180 or 240 mm) were scanned and transferred to a computer in the form of 16 bit binary data using a software provided by Marresearch for data collection. The pixel size was $100 \mu\text{m}$. The exposure time was selected depending on the sample. Typical exposure time for unoriented samples was ~ 1 hour where as ~ 20 minutes of exposure time was sufficient to get optimum intensities for most of the aligned samples. An optimal sample to detector distance D ($\sim 200 - 260$ mm) was selected for getting all the data in the q range of interest.

1.2.1.4 Data analysis

The sample to detector distance D was calculated using a standard sample. Diffraction patterns collected on the image plate were viewed and analyzed using the software provided by

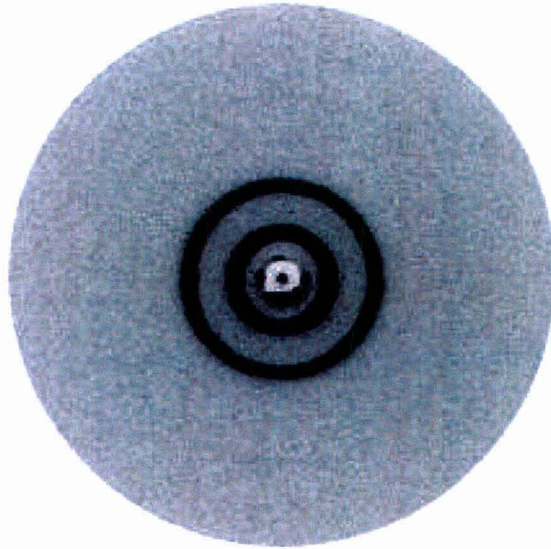


Figure 1.17: Typical diffraction pattern from powder sample. Only the small angle part is shown.

Marresearch.

Diffraction pattern from an unoriented sample consists of concentric rings as shown in fig. 1.17. The corresponding values of d ($= \frac{n\lambda}{2\sin\theta}$) and q ($= \frac{4\pi\sin\theta}{\lambda}$) were calculated from the radius R of the diffracted ring by evaluating θ ($= \frac{1}{2}\tan^{-1}\frac{R}{D}$), where D is the sample to detector distance. The integrated intensity $I(q)$ Vs q was obtained by integrating over the azimuthal angle.

In the oriented sample geometry the x-ray beam was incident tangential to the sample

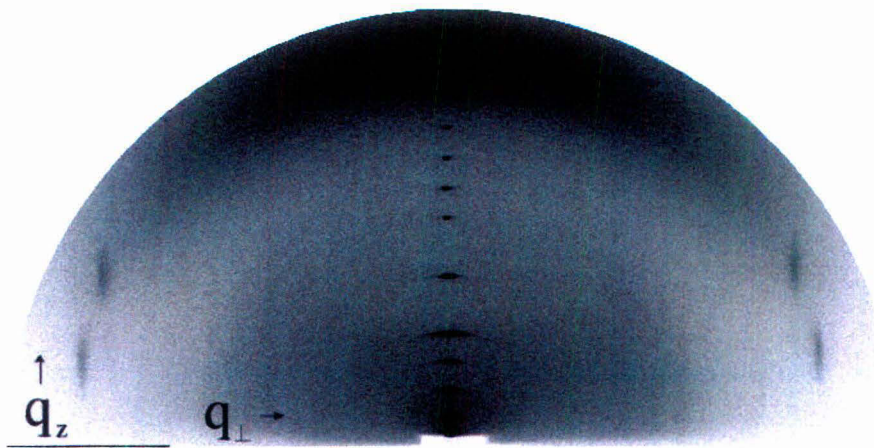


Figure 1.18: Typical diffraction pattern from an aligned sample.

coated beaker as shown in fig. 1.16. The diffraction pattern from such a geometry consists of isolated spots in the $q_z - q_\perp$ plane (fig. 1.18). The peaks along q_z corresponds to the lamellar periodicity of the bilayer stack. For the case where the bilayers exhibit inplane modulation, additional peaks are observed at $q_\perp \neq 0$. These are known as satellite reflections. Lattice parameters can be directly determined from the diffraction pattern in the case of a two dimensional lattice. To obtain integrated intensity, a rectangular box which covers the entire spot was drawn with its edges parallel to q_\perp and q_z . $I(q)$ Vs q were obtained by integrating along one of the edges of the box after subtracting the background. The background was assumed to vary linearly across each diffraction peak. Intensity profile was obtained from a fit to a Gaussian after background subtraction. Gaussian fit was especially required to resolve two partially overlapping peaks.

Intensity Corrections

Because of sample mosaicity and experimental geometry, necessary corrections are needed for getting the accurate values of the intensity. These corrections are different for peaks along q_z and those with non-zero q_\perp . In general two types of corrections are employed : geometric correction and absorption correction.

For the main reflections (q_z peaks) after applying geometric correction the corrected intensity (I_c) can be written as [44]

$$I_c = I_o q \Delta \cos \theta = I_o \frac{2\pi \Delta}{\lambda} \sin 2\theta \quad (1.5)$$

where I_o is the observed intensity, Δ is the sample mosaicity. Estimated value of Δ (mosaicity) is about 10° [45]. And for satellite peaks the geometric correction becomes

$$I_c = I_o 2\pi R' = I_o \frac{4\pi^2}{\lambda_r} |k| \quad (1.6)$$

where k is the Miller index of the corresponding peak, λ_r is the periodicity of in-plane modulation.

The need of absorption correction arises because of the nonuniform path travelled by both the incident and scattered x-ray through the curved aligned sample. Because of the non uniformity the reduction of intensities are different at different q values. But we have not applied any absorption correction in our analysis as it is difficult to measure the thickness of the sample accurately. Also previous study on the $P_{\beta'}$ phase has shown that the electron density map is not affected much by neglecting absorption corrections [45].

1.2.1.5 Calculation of transbilayer electron density profile by Fourier reconstruction method

As described earlier the electron density profile (edp) for a bilayer system on a relative scale can be calculated from the absolute ratios of the form factor as

$$\rho(z)_{relative} = \sum_{h=1}^{h_{max}} \alpha_h r_h \cos\left(\frac{2\pi hz}{d}\right) \quad (1.7)$$

But for this the phases (α_h) of the various Fourier components need to be determined. We have used both brute force and electron density model methods to retrieve the phase information. When the number of peaks are few (3-4) which is the case for most of our bilayer samples in fluid phase, we employ a brute force method. We fix the phase of the first peak and then plot the electron density profile by considering all the combinations (2^{n-1} for n peaks) for the rest. With this approach only one set of phases gives rise to the physically acceptable electron density profile. The phase combination which gives correct edp for most of our sample in fluid phase with four order of diffraction was found to be (-1,-1,+1,-1).

When the number of peaks are more which is the case of many of our gel phase samples we employ a modelling approach as described in [44]. One very common form applied to such a procedure is to write the bilayer electron density profile as sum of three Gaussian functions corresponding to the two electron rich headgroups and one electron deficient terminal methyl group (fig. 1.19). The transbilayer electron density profile using such a Gaussian

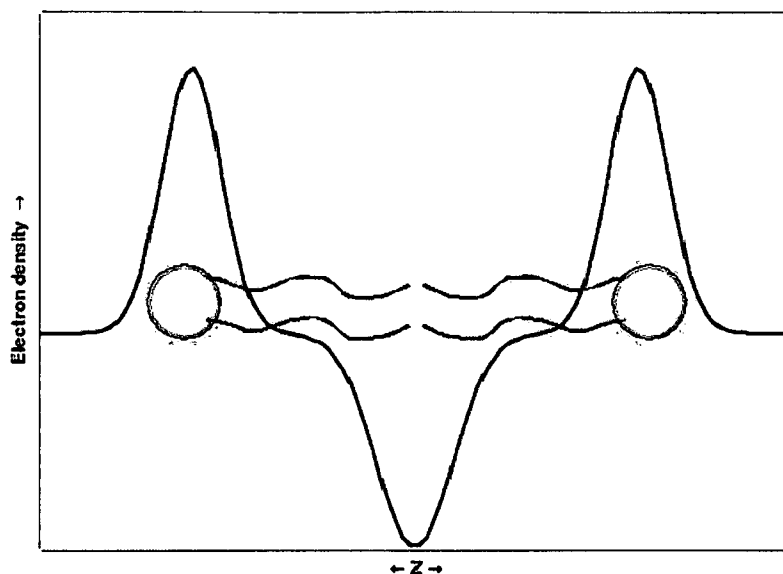


Figure 1.19: Electron density profile of the bilayer can be modelled as a sum of three Gaussian functions corresponding to the two head groups and the terminal methyl region

model can be described as

$$\rho(z) = \rho_H \left\{ e^{-\frac{(z+x_h)^2}{2\sigma_h^2}} + e^{-\frac{(z-x_h)^2}{2\sigma_h^2}} \right\} - \rho_M e^{-\frac{z^2}{2\sigma_m^2}} \quad (1.8)$$

where ρ_H and σ_h are the height and width of headgroup Gaussian function where as ρ_M and σ_m are the corresponding parameters for the terminal methyl groups. Then the bilayer form factor is calculated by taking Fourier transform of model edp function as

$$F_T(q) = \sigma_m \rho_M \left[\frac{2\rho_H \sigma_h}{\rho_M \rho_M} \left\{ e^{-\frac{q^2 \sigma_h^2}{2}} \cos(q_z x_h) \right\} - e^{-\frac{q^2 \sigma_m^2}{2}} \right] \quad (1.9)$$

$F_T(q)$ is sampled at $q_h = \frac{2\pi h}{d}$ and squared to get the intensities of the peaks. The adjustable parameters in the model namely x_h , σ_m , σ_h and $\frac{\rho_h}{\rho_m}$ are varied over a physically realizable range to get the best fit between the calculated and the observed data. From this fit the phases of different Fourier components are obtained. After getting the correct set of phases (α_h) from the model and the magnitude from the experimental data the transbilayer electron

density profile can be obtained using equation (1.7).

1.2.2 Optical microscopy

In all our scattering studies we have mainly used two kind of sample morphologies that is, aligned bilayer stacks and multilamellar vesicles. Apart from these, model membranes can also be prepared in the form of giant unilamellar vesicles (GUVs) as shown in the fig. 1.3(c) which are closed structures made up of a single bilayer. Since the typical diameter of the GUVs are of the order of ~ 10 to $100 \mu m$ well above the optical resolution, the most convenient way to study the system is that of light microscopy. Using different kinds of microscopy techniques such as phase contrast, fluorescence and confocal microscopy it is easy to visualize the shape, phase separation in the bilayer etc.

We have studied these GUVs prepared from lipid-sterol mixtures using mainly fluorescence and confocal microscopy. In this section we describe the preparation of GUVs and various microscopy techniques used to study them.

1.2.2.1 Preparation of giant unilamellar vesicles (GUVs) for microscopic studies

GUVs are self assembled structures. However formation of such a structure requires specific conditions. Since these are closed structures, bilayer has to overcome the associated bending energy to form such a structure. Therefore it is energetically more favorable in the fluid (L_α) phase which has a lower rigidity than in the gel phase. Although several methods have been proposed for the preparation of GUVs [46, 47, 48, 49], the most widely used is the “electroformation method” proposed by Angelova *et al.* [49, 50, 51], since this method gives very high yield of unilamellar vesicles with diameters in the range of 10 - $100 \mu m$ [52]. In the electroformation method a small alternating voltage (1-3 volts) at a low frequency (~ 10 Hz) is applied for 2-3 hours to a lipid film in excess water. During this, the temperature of the sample is maintained above T_m so as to keep the lipid bilayer in the fluid phase.

We have used the electroformation method for preparation of GUVs of lipid-sterol mixtures. For the same purpose we have designed a chamber consisting of a hollow Cu block

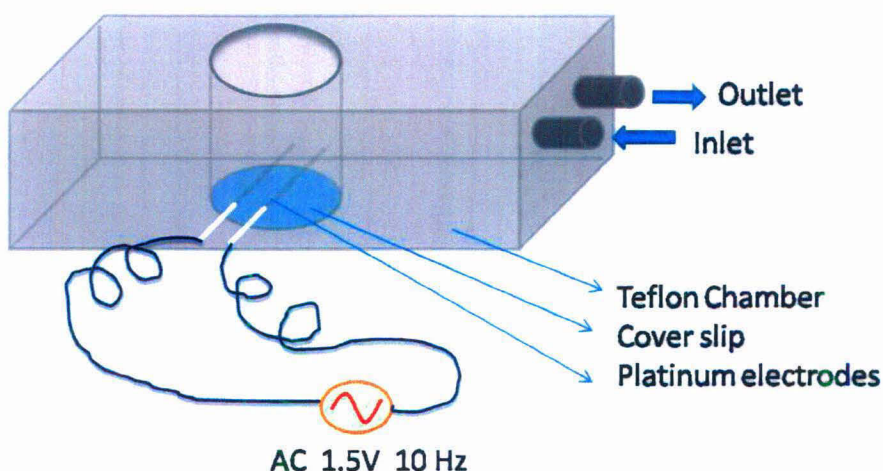


Figure 1.20: Schematic of electroformation chamber for preparation of GUVs.

with a provision for water circulation. Two platinum wires were inserted through two-bore nonconducting ceramic tubes to avoid contact between the two electrodes. The whole chamber is covered with a thin Teflon sheet to increase its thermal stability. A schematic of the chamber used in our experiments is shown in fig. 1.20.

All lipids and sterols used in the preparation of the GUVs were purchased either from *Sigma-Aldrich-Fluka* or *Avanti*. All fluorescent dyes were purchased from *Molecular Probes(USA)*. All chemicals were used without further purification. To confirm the purity some of the samples were tested by TLC and they produced a single spot. The stock solutions of lipid-sterol mixture were prepared by dissolving lipids and sterol in chloroform (*HPLC grade, Merck*) in desired molar ratios. Typical concentration of the stock solution was 0.5 mg/ml. For fluorescence and confocal microscopy a desired dye molecule was added to the stock solution at a molar fraction ~ 0.1 to 0.4 depending upon the excitation sources used and the intended extent of visualization. For preparation of GUVs a small amount (1-2 microliter) of this stock solution was taken in a Hamilton syringe and deposited on the two platinum wire surface of the electroformation chamber described above. It was left for drying for approximately one hour. After all traces of the solvent evaporated the dried lipid film was hydrated by adding $500\mu\text{l}$ of Millipore water. An ac field of 1 to 2 volts amplitude and ~ 10 Hz frequency was applied by connecting the platinum wires to a frequency generator

(*Aplab, India*). The temperature of the chamber was maintained $\sim 5^{\circ}\text{C}$ above the T_m of the lipid used, by water circulation using a Julabo water bath. After ~ 2 hours GUVs were observed on the platinum wires. For microscopy observation the GUVs were transferred to either a coverslip or to another temperature controlled chamber depending on the experimental purpose. Fluorescence microscopy and laser scanning confocal fluorescence microscopy were used for observing these GUVs. These two microscopy techniques are described in the following sections.

1.2.2.2 Fluorescence microscopy

Fluorescence microscopy makes use of a very well known phenomena of fluorescence emission of selective class of molecules known as fluorophores. These fluorophores when excited by a characteristic wavelength of light, emit light of a longer wavelength. The excitation and emission wavelengths are specific to a fluorophore. In fluorescence microscopy the specimen to be studied is labelled with fluorophores. Then the sample is excited by light of appropriate wavelength. The emitted photons are detected using various photo detector devices such as charge couple device (CCD), photodiodes or photomultiplier tube (PMT). Depending on the application, several excitation sources are used for fluorescence microscopy [53, 54]. In all our fluorescence microscopy experiments we have used either a Hg lamp or a metal halide lamps as excitation sources and CCD as detecting device.

In a typical fluorescence microscope the sample is illuminated through the objective lens and the emitted photons are also collected through the same objective lens. Such an arrangement is known as epi-fluorescence. To facilitate such selective propagation of light, various optical filters are used.

The choice of fluorophores depends on various factors such as sample to be labelled, available excitation source and filters. We have used mostly rhodamine DHPE fluorescence dye for our experiments. The molecular structure of the same along with its fluorescence spectra is shown in fig. 1.21.

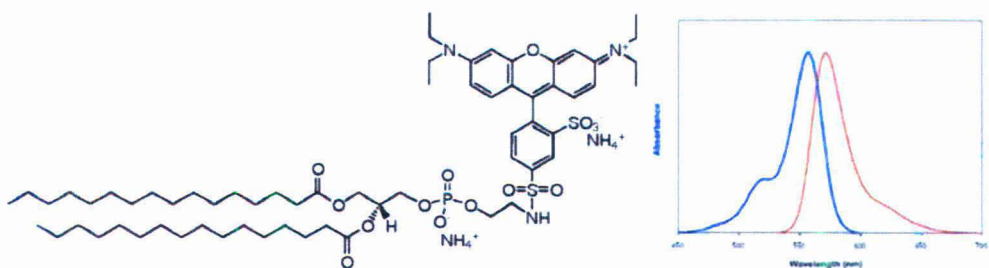


Figure 1.21: Structure of rhodamine DHPE and its absorption and emission spectra.

1.2.2.3 Laser scanning confocal fluorescence microscopy

Confocal fluorescence microscopy has significant advantage over other conventional optical microscopy such as bright field and fluorescence microscopy. Especially for biological samples it has been widely used for various imaging purposes. In conventional microscopy the image of the sample is constructed by collecting all emerging photons from the sample. This signal also includes the light coming from outside the region of interest or the focal plane. For this reason the image constructed will be blurred, thereby limiting the resolution. On the other hand in confocal microscopy this kind of problem is avoided with the help of a confocal pinhole placed in front of the detector at the conjugate plane of focal plane of the objective. The pinhole when set with correct aperture, blocks the light coming from outside the focal plane of the objective. This enables to view thin optical sections of the sample with high resolution [53, 54].

In laser scanning confocal fluorescence microscopy (LSCFM) lasers of different wavelengths are used as excitation source. The specimen is excited with a very tightly focused laser beam of required wavelength. The emitted wavelength from that point is collected by PMT through the pinhole. Then the excitation point is moved both in XY direction in the focal plane with the help of a set of scanning mirrors. After all points of the focal plane are scanned, a different section of the specimen is selected for scanning either by moving the stage or the objective. Thus the image of the whole sample is constructed by stacking all such optical sections.

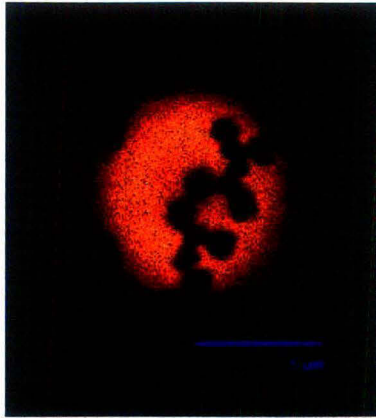


Figure 1.22: Fluorescence image of a GUV showing phase separation. Rhodamine DHPE was used as the fluorescence marker.

A typical fluorescence micrograph of the surface of the GUV showing phase separation is shown in fig. 1.22

Bibliography

- [1] B. Alberts, D. Bray, J. Lewis, M. Raff, K. Roberts, and J. D. Watson, *Molecular Biology of the Cell* Garland publishing, Taylor and Francis Group, (1994).
- [2] S. J. Singer and G. L. Nicolson, *Science*, **175**, 720 (1972).
- [3] J. N. Israelachvili, *Intermolecular and Surface Forces*, Academic Press, London (1991).
- [4] W. M. Gelbart, A. Ben-Shaul, and D. Roux, ed. *Micelles, Membranes, Microemulsions, and Monolayers*, Springer Verlag, New York (1994).
- [5] R. Lipowsky and E. Sackmann, ed. *Handbook of Biological Physics*, Volume 1, Elsevier Science B. V, (1995).
- [6] G. S. Smith, E. B. Sirota, C. R. Safinya, R. J. Plano and N. A. Clark, *J. Chem. Phys.*, **92**, 4519 (1990).
- [7] S. Tristram-Nagle, Y. Liu, J. Legleiter and J. F. Nagle, *Biophys. J.*, **83**, 3324 (2002).
- [8] S. Karmakar, B. R. Sarangi and V. A. Raghunathan, *Solid State Communication*, **139**, 630 (2006).
- [9] S. C. Chen, J. M. Sturtevant and B. J. Gaffney, *Proc. Natl. Acad. Sci. USA*, **77**, 5060 (1980)
- [10] V. A. Raghunathan and J. Katsaras, *Phy. Rev. Lett.*, **74**, 4457 (1995).
- [11] K. Simons and E. Ikonen, *Nature*, **387**, 569 (1997).

- [12] K. Simons and W. L. C. Vaz, *Annu. Rev. Biophys. Biomol. Struct.*, **33**, 269 (2004).
- [13] M. Edidin, *Annu. Rev. Biophys. Biomol. Struct.*, **32**, 257 (2003).
- [14] C. A. Daya and A. K. Kenworthy, *Biochimica et Biophysica Acta*, **1788**, 245 (2009).
- [15] P. Sharma, R. Varma, R. C. Sarasij, K. G. Ira, G. Krishnamurthy, M. Rao and S. Mayor, *Cell*, **116**, 577 (2004).
- [16] C. Eggeling, C. Ringemann, R. Medda, G. Schwarzmann, K. Sandhoff, S. Polyakova, V. N. Belov, B. Hein, C. Middendorff, A. Schnle and S. W. Hell, *Nature*, **457**, 1159 (2009).
- [17] T. Baumgart, S. T. Hess, and W. W. Webb, *Nature*, **425**, 821 (2003).
- [18] K. Bloch, *Science*, **150**, 19 (1965).
- [19] S. Darnet and A. Rahieri, *Biochem. J.*, **378**, 889 (2004).
- [20] L. Finegold, ed. *Cholesterol in Membrane Models*, CRC press, Boca Raton, FL (1993).
- [21] T. P. W. McMullen and R. N. McElhaney, *Biochemistry*, **36**, 4979 (1997).
- [22] M. R. Vist and J. H. Davis, *Biochemistry*, **29**, 451 (1990).
- [23] R. P. Rand, V. A. Parsegian, J. A. C. Henry, L. J. Lis, M. McAlister, *Can. J. Biochem.*, **58**, 959 (1980).
- [24] W. Knoll, G. Schmidt, K. Ibel and E. Sackmann, *Biochemistry*, **24**, 5240 (1985).
- [25] K. Mortensen, W. Pfeiffer, E. Sackmann and W. Knoll, *Biochim. Biophys. Acta*, **945**, 221 (1988).
- [26] M. B. Sankaram and T. E. Thompson, *Proc. Natl. Acad. Sci. USA*, **88**, 8686 (1991).
- [27] S. Karmakar and V. A. Raghunathan, *Phys. Rev. Lett.*, **91**, 098102 (2003).
- [28] J. H. Ipsen, G. Karlström, O. G. Mouritsen, H. Wennerström and M. J. Zuckermann, *Biochim. Biophys. Acta*, **905**, 162 (1987).

- [29] T. P. W. McMullen, R. N. A. H. Lewis and R. N. McElhaney, *Biochemistry*, **32**, 516 (1993).
- [30] S. W. Hui and N. B. He, *Biochemistry*, **22**, 1159 (1983).
- [31] N. Kučerka, J. Pencer, M. P. Nieh and J. Katsaras, *Eur. Phys. J. E*, **23**, 247 (2007).
- [32] J. Pan, T. T. Mills, S. T. Nagle and John F. Nagle, *Phy Rev Lett.*, **100**, 198103 (2008).
- [33] J. Pencer, M. P. Nieh, T. A. Harroun, S. Krueger, C. Adams and J. Katsaras, *Biochim. Biophys. Acta*, **1720**, 84 (2005).
- [34] A. Hodzic, M. Rappolt, H. Amenitsch, P. Laggner and G. Pabst, *Biophys. J.*, **94** 3935 (2008).
- [35] J. F. Nagle and S. Tristram-Nagle, *Biochim. Biophys. Acta*, **1469**, 159 (2000).
- [36] J. F. Nagle and M. C. Wiener, *Biophysical J*, **55**, 309 (1989).
- [37] A. Guinier, in: *X-Ray Diraction, Freeman, San Francisco*, (1963).
- [38] R. Hosemann and S. N. Bagchi, *Direct Analysis of Diraction by Matter, North-Holland, Amsterdam*, (1962).
- [39] A. Caillé, *C. R. Acad. Sci. Paris, Series. B*, **274**, 891 (1972).
- [40] R. Zhang, R. M. Suter and J. F. Nagle, *Phys. Rev. E*, **50**, 5047 (1994).
- [41] G. Pabst, M. Rappolt, H. Amenitsch and Peter Laggner, *Phys. Rev. E*, **62**, 4000 (2000).
- [42] Y. Lyatskaya, Y. Liu, S. T. Nagle, J. Katsaras and J. F. Nagle, *Phy Rev E*, **63**, 011907 (2000).
- [43] J. Katsaras and M. J. Watson, *Rev. Sci. Instrum.*, **71**, 1737 (2000).
- [44] S. Karmakar, *Phase Behaviour of lipid-cholesterol membranes*, Thesis submitted to JNU, Delhi, 2001.

- [45] K. Sengupta, V. A. Raghunathan and J. Katsaras, *Phys. Rev. E*, **68**, 031710 (2003).
- [46] F. M. Menger and K. D. Gabrielson, *Angew. Chem. Int. Ed. Engl.*, **34**, 2091 (1995).
- [47] A. Moscho, O. Orwar, D.T. Chiu, B. P. Modi, and R. N. Zare, *Proc. Natl. Acad. Sci. U.S.A.*, **93**, 11443 (1996).
- [48] K. Akashi, H. Miyata, H. Itoh, and K. Kinoshita. Jr, *Biophys. J.*, **71**, 3242 (1996).
- [49] M. I. Angelova, S. Soléau, Ph. Méleard, J. E. Faucon, and P. Bothorel, *Progr. Colloid. Polym. Sci.*, **89**, 127 (1992).
- [50] M. I. Angelova and D. S. Dimitrov, *Mol. Cryst. Liq. Cryst.*, **152**, 89 (1987).
- [51] M. I. Angelova and D. S. Dimitrov, *Faraday Discuss. Chem. Soc.*, **81**, 303 (1986).
- [52] L. A. Bagatolli, T. Parasassi, and E. Gratton, *Chem. Phys. Lipids*, **105**, 135 (2000).
- [53] Douglas B. Murphy, *Fundamentals of Light Microscopy and Electronic Imaging*, Wiley-Liss; 1st edition (2001).
- [54] J. R. Lakowicz, *Principles of Fluorescence Spectroscopy*, Plenum Press, New York (1983).

Chapter 2

Influence of hydration on the phase behaviour of PC-cholesterol membranes

2.1 Introduction

Cholesterol is the most important sterol molecule from a biological perspective because of its strikingly singular presence in almost all higher order eukaryotic cell membranes. Phosphatidylcholine (PC) lipids are major components of cell membranes. Therefore, there have been many studies on PC-cholesterol model membranes to understand the influence of cholesterol on various membrane properties. In particular, the phase behaviour of lipid cholesterol membranes has been given central importance in these studies. Various experimental techniques like DSC, NMR, x-ray and neutron scattering, microscopy etc. have been used to study the phase behaviour of lipid-cholesterol mixtures [1, 2, 3, 4, 5, 6, 7]. Phase diagrams constructed using various experimental techniques are given in chapter-1. The main results of these studies can be summarized as follows

1. A cholesterol rich β phase was found to coexist with both L_α and $L_{\beta'}$ phases over a wide cholesterol concentration range at temperatures above and below the main transition, respectively. Degree of ordering of the hydrocarbon chains and the in-plane diffusion rates in this phase were found to be intermediate between those in the fluid (L_α) and gel ($L_{\beta'}$) phases.

2. At higher cholesterol concentrations (> 20 mol%) the β phase exists throughout the temperature range. The β and L_α phases are often referred to as the liquid ordered (l_o) phase and liquid disordered (l_d) phase respectively in the literature [4, 8, 9].
3. The two phase region above the main transition observed in NMR studies has not been seen in diffraction experiments [10, 11, 12, 13]. However, these studies have found two phase coexistence below the main transition at cholesterol concentration < 10 mol%. One of these two phases, which is presumably richer in cholesterol can swell more [10]. This phase persists even at higher cholesterol concentrations, whereas the cholesterol-poor phase disappears above 10 mol%.
4. The l_o phase is believed to be rich in cholesterol, whereas the l_d phase is poor in cholesterol. Hydrocarbon chain segmental order parameters in the l_o phase is found to be almost twice compared to that in the pure lipid at temperatures above the chain melting transition [3].

X-ray diffraction studies on oriented bilayers of DPPC-cholesterol and DMPC-cholesterol mixtures at close to full hydration (98% relative humidity) was carried out by Karmakar *et al.* A novel modulated phase denoted as P_β was observed at intermediate cholesterol concentrations [13].

Most of the above studies were carried out at full or close to full hydration, the reason being that the full hydration condition truly mimics the environment of the biological membranes. However the hydration levels strongly influences both the main and pre-transition temperatures of the pure lipid bilayers [14]. Also the chain tilt of the lipid decreases with decreasing degree of hydration. At very low hydration the tilt of the PC molecules vanishes [15, 12]. So it is an interesting problem to look at the effect of hydration on the phase behaviour of lipid-cholesterol membranes.

In this chapter we present our experimental results of x-ray diffraction studies on the structure and phase behaviour of dipalmitoyl phosphatidylcholine (DPPC) and dimiristyl phosphatidylcholine (DMPC) membranes at various cholesterol concentrations (X_c) as well

as at different relative humidity (RH) conditions.

2.2 Experimental results

We have carried out x-ray diffraction studies on DPPC-cholesterol and DMPC-cholesterol mixtures in the form of both oriented and unoriented bilayers at various cholesterol concentrations. In this section we describe briefly the experimental methodology and results of our studies.

Both oriented and unoriented multilayers of DPPC-cholesterol and DMPC-cholesterol were prepared at required molar ratios as described in the previous chapter. Small angle x-ray scattering was used to probe these mixtures. The oriented samples were probed at various relative humidity conditions in a specially designed chamber. Various RH s were obtained by keeping a reservoir of saturated salt solutions in the chamber. Different salts give rise to different values of RH depending on their saturated vapor pressure. For example a saturated *NaCl* solution gives $\sim 75\%$ RH where as *CaCl₂* gives $\sim 30\%$ RH. A general empirical relation describing the relation of RH with the salt is given by $RH = ae^{-b/T}$. Where a, b are characteristic constants for the particular salt.

2.2.1 Phase behaviour of DMPC-cholesterol mixtures at low humidity

Oriented bilayer stacks of DMPC-cholesterol mixtures were probed at various cholesterol concentrations and hydration levels. The partial phase diagrams were obtained by small-angle x-ray scattering studies. At low hydration levels a large number of Bragg peaks are observed even in the disordered fluid (L_α) phase. This is due to the fact that at low water content the bilayers come closer and hence the correlation length increases due to decreased thermal undulations of the bilayers. At full hydration or close to full hydration (98% RH) only ~ 4 Bragg peaks are obtained from the L_α phase. Whereas in more rigid gel phase number of Bragg peaks is typically ~ 10 . The phase behaviour of DMPC-cholesterol mixture at 65% RH and 30% RH are described below.

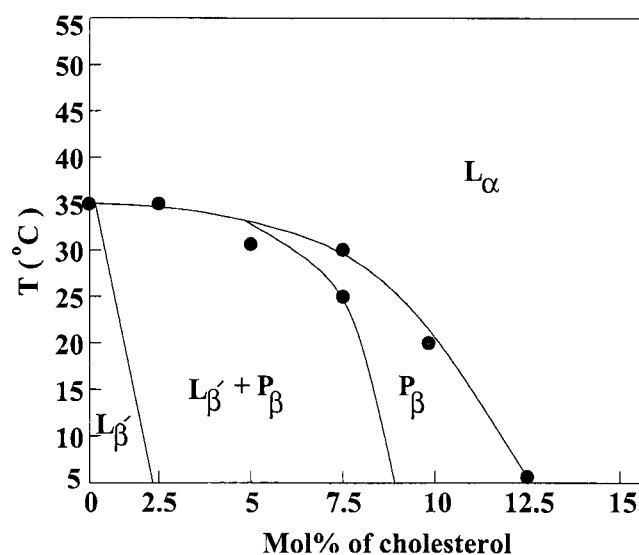


Figure 2.1: Phase diagram of DMPC–cholesterol mixtures at 65% RH.

2.2.1.1 RH=65%

Partial phase diagram obtained from the diffraction study of DMPC-Cholesterol mixtures at 65% RH is shown in fig. 2.1. At 65 % RH an increase of $\sim 10^\circ\text{C}$ was observed in the main transition temperature (T_m). For low cholesterol concentrations T_m was observed to be 35°C and the value was found to decrease with cholesterol content up to 12.5 mol% where the transition was completely abolished. Interestingly the pre-transition was completely abolished at all cholesterol concentration as the $P_{\beta'}$ phase was not observed. As seen in the phase diagram a relatively broad region of two phase coexistence of $L_{\beta'}$ and P_{β} was observed between 2.5 to 7.5 mol% of cholesterol. At cholesterol concentration ~ 10 mol% a narrow region of modulated phase was observed. The modulated phase was identified by the satellite peaks in the small angle region (see fig. 2.2).

2.2.1.2 RH=30%

Lowering the RH to 30% influences the phase behaviour of DMPC-cholesterol mixture significantly. Both main and pre-transitions were abolished at a very low cholesterol concentration. Even for the pure lipid the pre-transition was not observed which is in agreement with earlier studies by Smith *et al.* [14]. The small angle diffraction patterns showing the

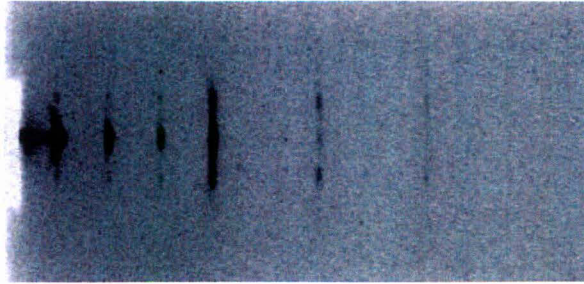


Figure 2.2: Small angle diffraction pattern of the P_β phase of DMPC–cholesterol mixtures at 65% RH. Cholesterol concentration = 10mol%, $T = 10^\circ\text{C}$.

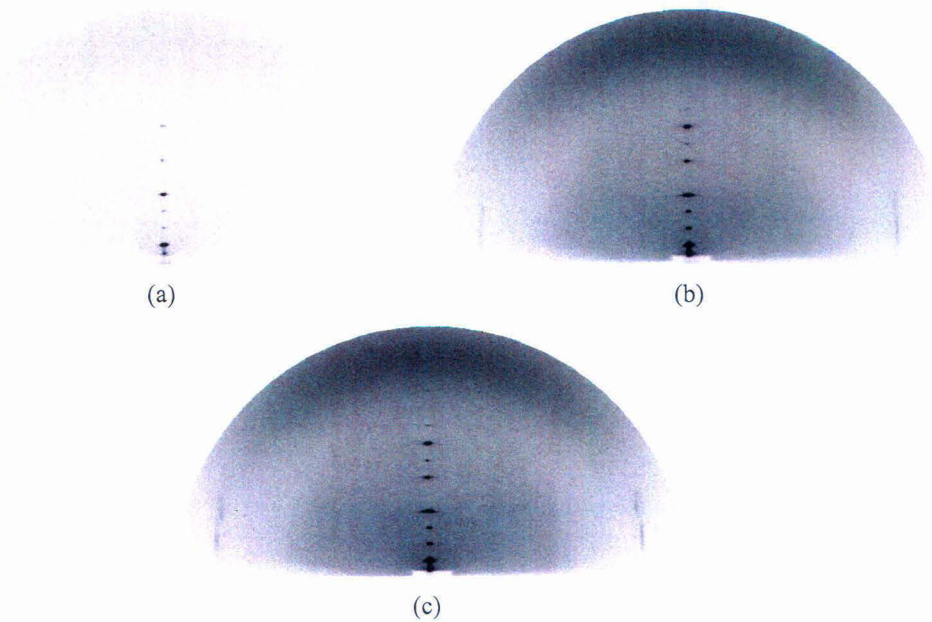


Figure 2.3: Diffraction pattern of DMPC bilayers at 30% RH (a) fluid phase (L_α) at $T=47^\circ\text{C}$, (b) gel phase (L_β) at $T=43^\circ\text{C}$, and (c) gel phase (L_{β_r}) at $T=20^\circ\text{C}$.

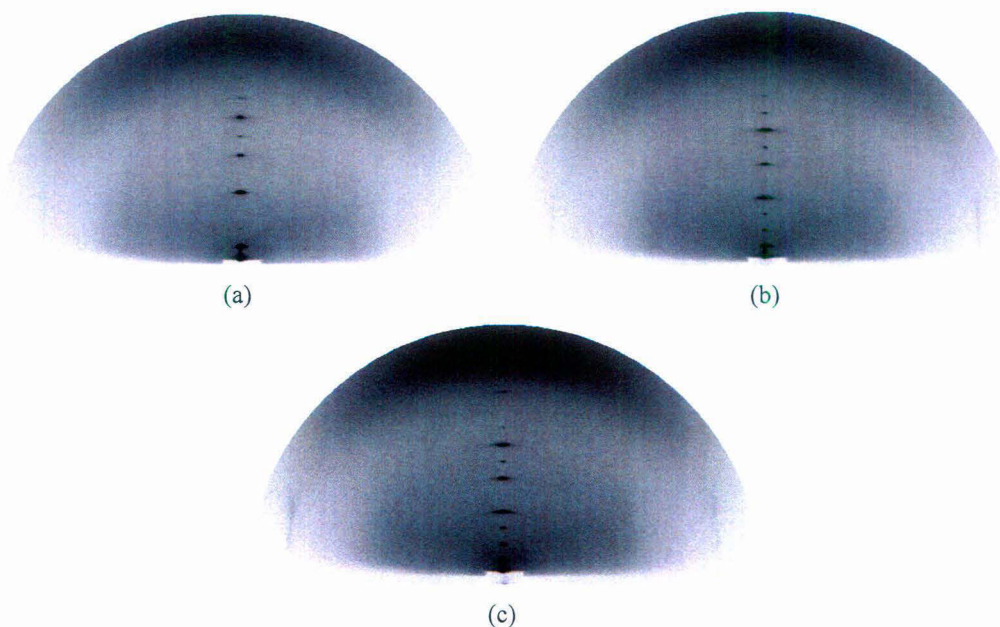


Figure 2.4: Diffraction pattern of DMPC-cholesterol mixture at 2.5 mol% of cholesterol at RH=30%. (a) fluid phase (L_α) at T=55 °C, (b) gel phase (L_β) at T=20 °C, and (c) gel phase ($L_{\beta'}$) at T=5 °C.

phase transition of pure DMPC bilayers at 30% RH are shown in fig. 2.3. At 5 mol% of cholesterol we observe the fluid phase at all temperatures. Only at 2.5 mol% of cholesterol a fluid-gel transition was observed. The T_m at that concentration was $\sim 50^\circ\text{C}$. At 2.5 mol% of cholesterol the phase sequence $L_\alpha \rightarrow L_\beta \rightarrow L_{\beta'}$ was observed. The L_β and $L_{\beta'}$ phases were identified from the characteristic chain reflections in the wide angle region (see fig. 2.4).

Based on our diffraction study we have constructed a partial phase diagram (shown in fig. 2.5) for DMPC-cholesterol mixture at 30 % RH.

2.2.2 Phase behaviour of DPPC-cholesterol in excess water condition

Unoriented samples of DPPC-cholesterol mixtures at different cholesterol concentrations were probed in excess water. A partial phase diagram was constructed by analyzing the diffraction peaks and is shown in fig: 2.6.

The main transition temperature was found to decrease slightly with cholesterol content up to about 20 mol%, beyond which it drops sharply. At temperatures above $\sim 40^\circ\text{C}$ the

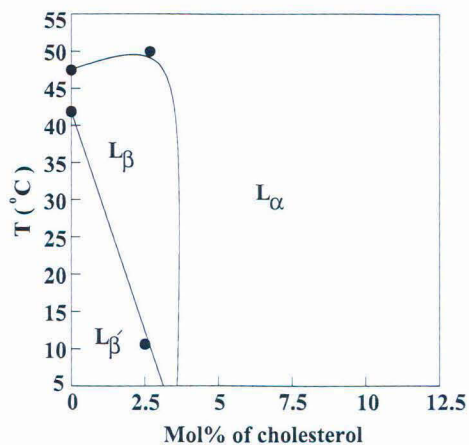


Figure 2.5: Phase diagram of DMPC–cholesterol mixtures at 30% RH.

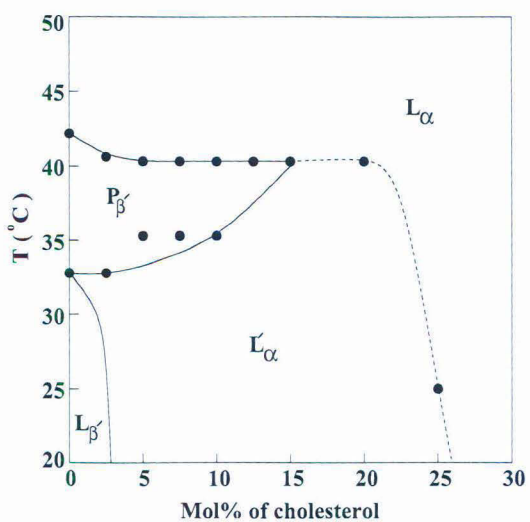
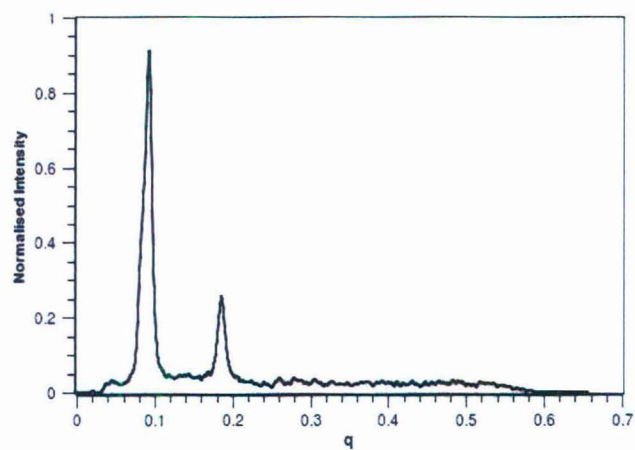
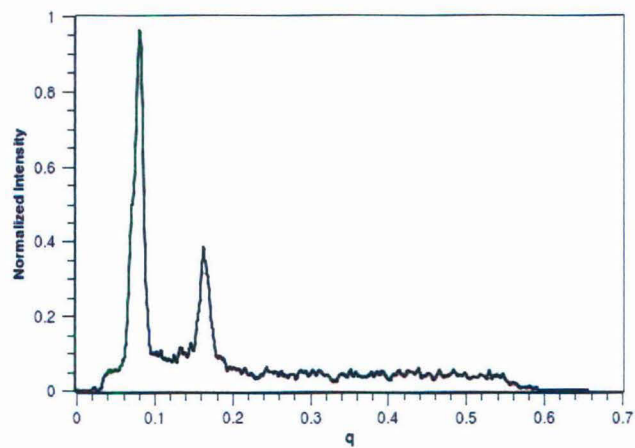


Figure 2.6: Phase diagram of DPPC-cholesterol mixtures in excess water.



(a)



(b)

Figure 2.7: I-q plots for DPPC-cholesterol mixtures at 20 mol% of cholesterol. (a) $T=50^{\circ}\text{C}$, (b) $T=30^{\circ}\text{C}$. Intensity scales are normalized.

Table 2.1: Lamellar spacings d (Å) of DPPC-cholesterol mixtures as a function of temperature in excess water (100% RH). The error in d is ± 0.3 Å.

T (°C)	X_c (mol%)								
	2.5	5	7.5	10	12.5	15	20	25	40
60	63.2	64.5	63.8	63.8	64.5	64.5	64.5	63.8	63.2
50	63.7	65.1	64.5	64.5	65.1	65.8	65.8	65.1	64.5
45	64.5	65.1	65.1	65.8	66.5	67.2	67.2	65.1	64.5
40	65.1	69.5	67.2	69.5	72.7	72.7	70.2	65.8	65.2
35	65.8	75.3	72.7	75.3	74.4	74.4	71.0	66.5	65.8
30	69.5	75.3	75.3	76.2	75.3	75.3	71.0	68.7	66.5
25	72.7	75.3	78.1	78.1	76.7	76.2	71.0	69.5	67.3

fluid phase (L_α) was observed at all cholesterol concentrations. For X_c between 0 to 15 mol%, below T_m the ripple phase ($P_{\beta'}$) was observed. We were not able to see the gel ($L_{\beta'}$) phase even at 2.5 mol% cholesterol. Also gel-fluid coexistence region was not observed. The reason for this may be the coarse steps taken along the composition axis (~ 2.5 mol%). Interestingly the modulated phase (P_β) was not seen in this phase diagram, rather that region of the phase diagram was occupied by a fluid phase which is denoted by L'_α . Such a notation was introduced to differentiate this region of phase diagram from that of the normal fluid phase L_α region. Though L'_α was characterised as a fluid phase but the lamellar periodicity is ~ 5 Å larger than that of the L_α phase. The $I-q$ plot at 20 mol% of cholesterol is shown in fig. 2.7 and the $I-q$ plot at 20 mol% of cholesterol as a function of temperature is shown in fig. 2.8. The jump in lamellar periodicity can be clearly seen from the plot of lamellar periodicity Vs temperature as shown in fig. 2.9. The abrupt increase in the lamellar periodicity by about 0.5 nm across the $L_\alpha - L'_\alpha$ transition, suggests that the latter might be a distinct phase [16]. The lamellar periodicity data at various cholesterol concentrations and temperatures are given in table. 2.1.

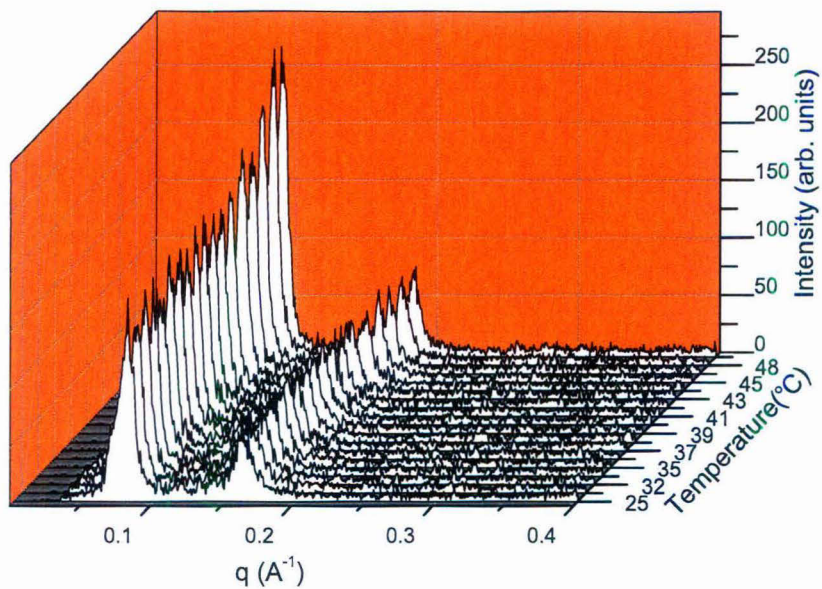


Figure 2.8: $I - q$ plots as a function of temperature at 20 mo% of cholesterol.

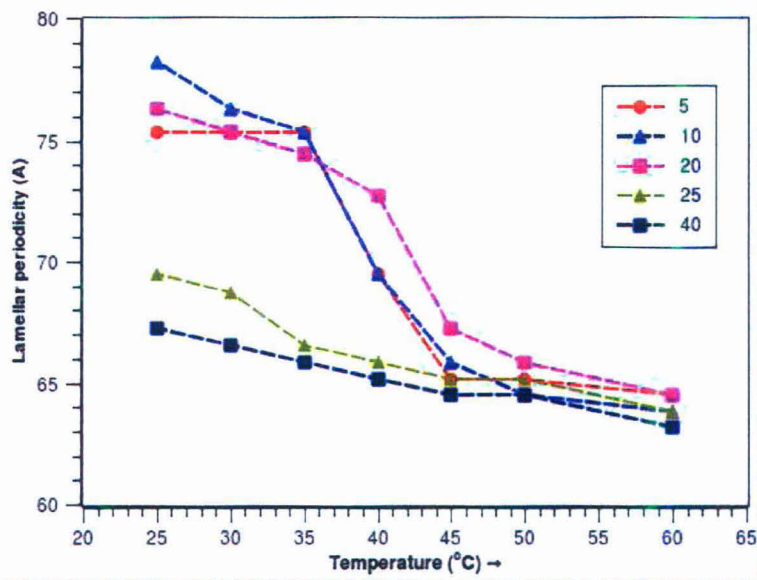


Figure 2.9: Lamellar periodicity (d in Å) as a function of temperature at various cholesterol concentration.

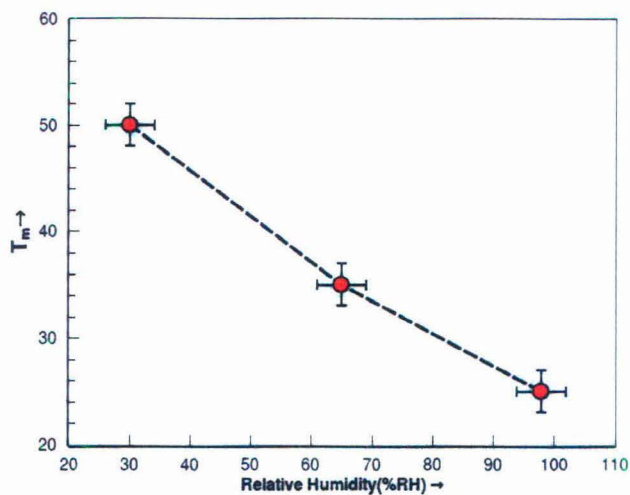


Figure 2.10: T_m (°C) of DMPC at different RH s. Error bars in temperature axis signifies the coarse steps taken and error bar in RH axis arises from the accuracy of the RH meter.

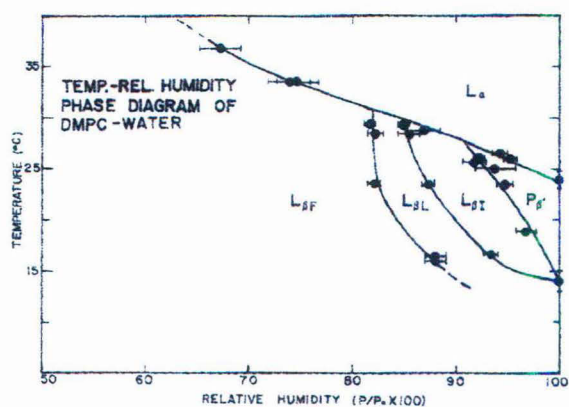


Figure 2.11: Temperature-RH phase diagram of DMPC-water taken from reference [14]. Note the increase in T_m as RH decreases and the absence of ripple phase at low RH.

2.3 Discussion

Phase behaviour of DMPC-cholesterol mixture at 98% RH was studied by Karmakar *et al.* [17] where the ripple phase was observed below T_m for cholesterol concentration up to 20 mol%. Beyond that the main and pre-transitions are abolished. At intermediate cholesterol concentrations the P_β phase was observed at low temperatures. Our studies on DMPC-cholesterol mixtures show that T_m increases as RH decreases. A plot of T_m as a function of RH is shown in fig. 2.10. The increase in the main transition temperature suggests that the gel phase ($L_\beta/L_{\beta'}$) is stabilized at lower humidities. This may be due to the fact that the effective lateral area per lipid molecule decreases as the hydration level decreases. This helps in the lipid packing facilitating the gel phase stabilization. We did not see the $P_{\beta'}$ phase at both 65% and 30% RH. Which suggests that the pre-transition completely disappears at lower hydration. Our results are consistent with earlier studies on DMPC-water system [14]. The DMPC-RH phase diagram obtained by Smith *et al.* is given in fig. 2.11.

At 65% RH the phase behaviour of DMPC-cholesterol is very similar to DPPC-cholesterol mixture at 75% RH [17]. The modulated phase was observed at 65% RH. However at 30% RH we did not see the modulated phase. Earlier studies show that the tilt of the hydrocarbon chains of the PC molecule decreases as the hydration level decreases and at very low hydration the tilt completely vanishes [12]. Hence at low hydrations a PC molecule will behave similar to a lipid molecule having no tilt like the phosphatidylethanolamines (PEs). The phase behaviour of PC-cholesterol membrane should therefore be very similar to that of PE-cholesterol membranes. The phase behaviour PE-cholesterol membrane was reported by Karmakar *et al.* [17] where it was observed that cholesterol does not induce the P_β phase in DLPE bilayers. We also obtain a very similar result from our studies on DMPC-cholesterol mixture at 30% RH where we observe a relatively broad region of the L_β phase. This again ascertains the fact chain tilt plays an important role in inducing the modulated phase in lipid bilayers.

Consistent with earlier scattering studies on PC-cholesterol membranes we also do not

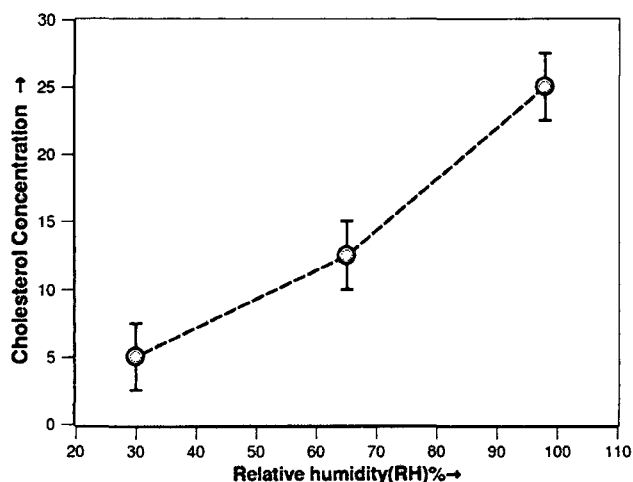


Figure 2.12: Cholesterol concentration required to abolish the main transition as a function of RH.

observe any l_o - l_d co-existence above T_m in DMPC-cholesterol bilayers. The observation of l_o - l_d co-existence above T_m from spectroscopic measurement may be attributed to the timescale of observation employed in such probes. We think that there are transient concentration fluctuations of cholesterol in the lipid bilayer above T_m . The lipid molecule in the vicinity of cholesterol will have higher chain ordering. This can be picked up by the spectroscopic probes. Whereas scattering techniques like x-ray which probe the system at a much longer timescale will average out all such transient behaviour [16]. The phase behaviour below T_m depends on the cholesterol concentration and degree of hydration. Cholesterol concentration required to completely abolish the main transition decreases with decrease in degree of hydration (see fig. 2.12).

Another interesting aspect of our result is that phase behaviour of DPPC-cholesterol at excess water condition has certain differences from the phase behaviour at a slightly lower RH (98%) reported earlier [13]. In excess water we do not see the modulated phase P_β . That region of phase diagram is occupied by a fluid phase which we have denoted as L'_α . The reason for differentiating this phase from the normal fluid phase L_α is that we see a jump of $\sim 5\text{\AA}$ in lamellar periodicity across $L_\alpha \rightarrow L'_\alpha$ transition. The increase in lamellar periodicity may be attributed to the decrease in membrane rigidity. This can be understood from the

following discussion -

If we assume that the cholesterol concentration fluctuation can couple with the local bilayer curvature, as indicated by the formation of P_β phase, then we can write the the expression for the free energy density (f) of the bilayer in terms of concentration fluctuation (δX) of cholesterol as-

$$f = \frac{1}{2}\kappa C^2 + \alpha C\delta X + \beta(\delta X)^2$$

where κ is the bending rigidity of a single bilayer, C is the mean curvature of the bilayer. α and β are two parameters. Here α can be either +ve or -ve depending on the particular systems, but β can only take +ve values since the system wants to maintain a homogeneous concentration.

Minimizing f w.r.t δX we get $\delta X = -\frac{\alpha}{2\beta}$. Hence

$$f = \frac{1}{2}\left(\kappa - \frac{\alpha^2}{2\beta}\right)C^2 = \frac{1}{2}\kappa' C^2$$

where $\kappa' = \kappa - \frac{\alpha^2}{2\beta}$ is the effective bending rigidity. Since the quantity $\frac{\alpha^2}{2\beta}$ always assumes a +ve value for reasons mentioned above, $\kappa' < \kappa$. Hence the bending rigidity of the bilayer decreases in presence of such concentration fluctuations, provided these fluctuations can be coupled to the local membrane curvature. Such a decrease in the bending rigidity can lead to increase in the steric repulsion between bilayers as the the undulation/steric repulsion interaction (f_U) per unit area is related to κ as-

$$f_U \propto \frac{(K_B T)^2}{K_c a^2}$$

where $K_c = \kappa \times d$ represents the bending rigidity of the lamellar stack and a is the interbilayer separation, K_B is Boltzman constant, T is the temperature.

Therefore the decrease in κ can effectively increase the steric repulsion between the bilayers and hence can increase the inter bilayer separation. This can account for the observed jump in the lamellar periodicity across $L_\alpha \rightarrow L'_\alpha$ transition.

2.4 Conclusion

We have studied the phase behaviour of DMPC-cholesterol mixtures at two different RHs (65 and 30%). We compared the results with earlier results obtained at 98% RH. Significant increase in T_m was observed at low hydration. The gel phase is stabilized at low RH and we do not see the ripple phase at these low RHs. However the P_β phase exists at low RH as long as the tilt angle of the chains in the gel phase is non zero. This result highlights the importance of the chain tilt in the formation of this phase. Our results on DPPC-cholesterol in excess water seems to suggest that the modulated phase ceases to exist in excess water. Instead we observe a fluid phase (L'_α) with higher lamellar periodicity, which can arise from a lowering of the membrane rigidity due to the coupling between cholesterol concentration and the tilt of the chain.

Bibliography

- [1] W. Knoll, G. Schmidt, K. Ibel, and E. Sackmann, *Biochemistry*, **24**, 5240 (1985).
- [2] M. R. Vist and J. H. Davis, *Biochemistry*, **29** 451 (1990).
- [3] M. B. Sankaram, T. E. Thompson, *Proc. Natl. Acad. Sci. USA*, **88**, 8686 (1991).
- [4] M. B. Sankaram and T. E. Thompson, *Biochemistry*, **29**, 10670 (1990).
- [5] T. P. W. McMullen, R. N. A. H. Lewis, and R. N. McElhaney, *Biochim. Biophys. Acta*, **1416**, 119 (1999).
- [6] T. P. W. McMullen, R. N. A. H. Lewis, and R. N. McElhaney, *Biochemistry*, **32**, 516 (1993).
- [7] S. W. Hui and N. B. He, *Biochemistry*, **22**, 1159 (1983).
- [8] J. H. Ipsen, G. Karlström, O. G. Mouritsen, H. Wennerström , and M. J. Zuckermann, *Biochim. Biophys. Acta*, **905**, 162 (1987).
- [9] A. Filippov, G. Orädd, and G. Lindblom, *Biophys. J.*, **84**, 3079 (2003).
- [10] R. P. Rand, V. A. Parsegian, and J. A. C. Henry, L. J. Lis, M. McAlister, *Can. J. Biochem.*, **58**, 959 (1980).
- [11] K. Mortensen, W. Pfeiffer, E. Sackmann, and W. Knoll, *Biochim. Biophys. Acta*, **945**, 221 (1988).
- [12] T. J. McIntosh, *Biochim. Biophys. Acta*, **513**, 43 (1978).

- [13] S. Karmakar and V. A. Raghunathan, *Phys. Rev. Lett*, **71**, 061924 (2003).
- [14] G. S. Smith, E. B. Sirota, C. R. Safinya, R. J. Plano, and N. A. Clark, *J. Chem. Phys.*, **92**, 4519 (1990).
- [15] S. Tristram-Nagle, R. Zhang, R. M. Suter, C. R. Worthington, W J Sun, and J F Nagle, *Biophys J.*, **64**, 1097 (1993).
- [16] S. Karmakar, B. R. Sarangi and V. A. Raghunathan, *Solid State Communication*, **139**, 630 (2006).
- [17] S. Karmakar and V. A. Raghunathan, *Phys. Rev. E*, **71**, 061924 (2005).

Chapter 3

Phase behaviour of DPPC bilayer containing ergosterol and lanosterol

3.1 Introduction

Sterols are essential for many biological processes involving the plasma membrane. The sterol type present in a given membrane is the result of a long evolutionary pathway [1, 2]. Many studies have been carried out in order to understand the molecular basis of the biological functions of these sterols. Higher order eukaryotes like humans contain cholesterol in their plasma membranes. Plasma membranes of lower eukaryotes such as yeast and fungi do not contain cholesterol, instead they contain ergosterol. Cholesterol and ergosterol have very similar structures. As argued by Mouritsen and others, in the biochemical evolution, cholesterol in the membranes has been selected for its ability to optimize certain physical properties [3]. In the plasma membranes, cholesterol influences both the structural properties like organization, ordering, rigidity and functional properties like signaling, trafficking etc. [4]. Lanosterol, which is a constituent of prokaryotic cell membranes, is a common precursor of both cholesterol and ergosterol in the sterol biosynthesis pathway [5, 6, 7]. Lanosterol is not present in any eukaryotic cell membranes. It is very appropriate to ask why cholesterol has been preferred over other sterols having structural similarity.

The structures of cholesterol, ergosterol and lanosterol are shown in fig. 3.1 for compar-

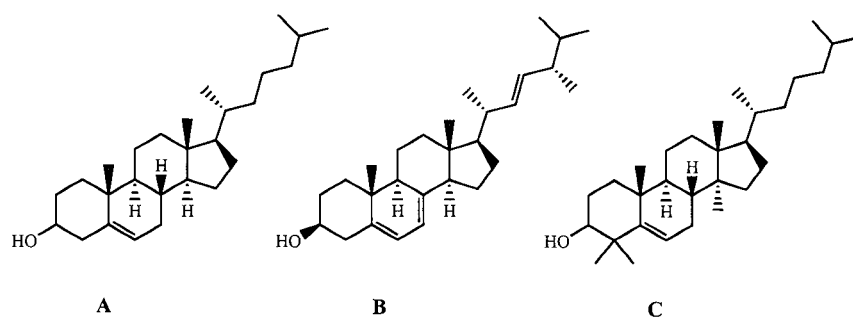


Figure 3.1: Structure of A. cholesterol, B. ergosterol and C. lanosterol.

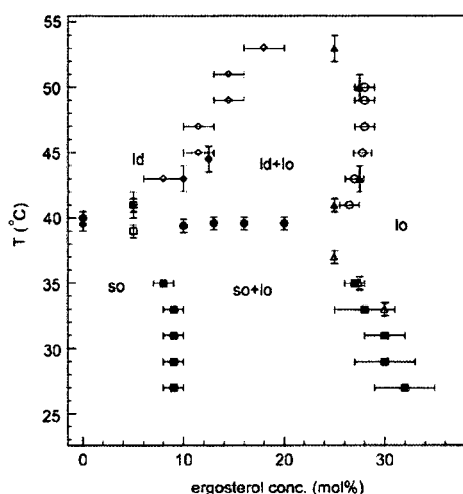


Figure 3.2: Partial phase diagram of DPPC-ergosterol mixture as reported by Thewalt *et al.* [11].

ison. Looking at the structures of these sterols it is apparent that cholesterol and ergosterol are structurally very similar except for the presence of additional double bonds at position C_7 and C_{22} and a methyl group at C_{24} , whereas lanosterol has two additional methyl groups protruding out of the steroid rings. It is suggested that structural differences of these sterols bring about changes in the physical properties of membranes. For example replacing cholesterol with ergosterol is believed to be responsible for the difference in the interaction of the membrane with an antibiotic such as amphotericin B [8]. A similar result was also obtained for another anti fungal agent known as nystatin [9, 10].

Many studies have been carried out on model membranes containing ergosterol and lanosterol to probe the influence of sterol structure on various properties of membranes.

A partial phase diagram of DPPC-ergosterol mixtures obtained by NMR and calorimetric studies was reported by Thewalt *et al.* (see fig. 3.2). Here the authors find a region of two phase co-existence (denoted as l_o - l_d) above T_m between 10 – 25 mol% of ergosterol concentration [11]. This phase behaviour is very similar to that of DPPC-cholesterol obtained from spectroscopic studies described in chapter-2.

In this chapter we present the results of a study of the comparative effects of ergosterol and lanosterol on the phase behaviour of DPPC membranes using x-ray diffraction. We also compare the values of chain orientational order parameter obtained from the wide angle x-ray scattering studies of these systems.

3.2 Experimental results

We have carried out x-ray diffraction studies on aligned multilayers of lipid and sterol. All experiments were done at $98\pm 2\%$ relative humidity (RH) as described in chapter-1. From the characteristic diffraction patterns, the different phases were identified. Macroscopic phase separation can easily be detected from non overlapping Bragg peaks in the small angle region (SAXS). Unlike the liposomal dispersions used in majority of diffraction studies on these systems, aligned samples have the additional advantage of ease of detection of any in-plane order that may exist in the bilayers. Also in such an experimental geometry the reflections corresponding to the lipid chains in the wide angle region can easily be analyzed. By analyzing the diffraction pattern we have determined partial phase diagrams of DPPC-ergosterol and DPPC-lanosterol membranes. Also by Fourier reconstruction method we have calculated the transbilayer electron density profiles on a relative scale. From such an electron density profile the peak to peak distance can be calculated which gives a measure of the bilayer thickness. In addition, by analyzing the WAXS data from these system we have studied the influence of sterol structure on the chain orientational order of the bilayer.

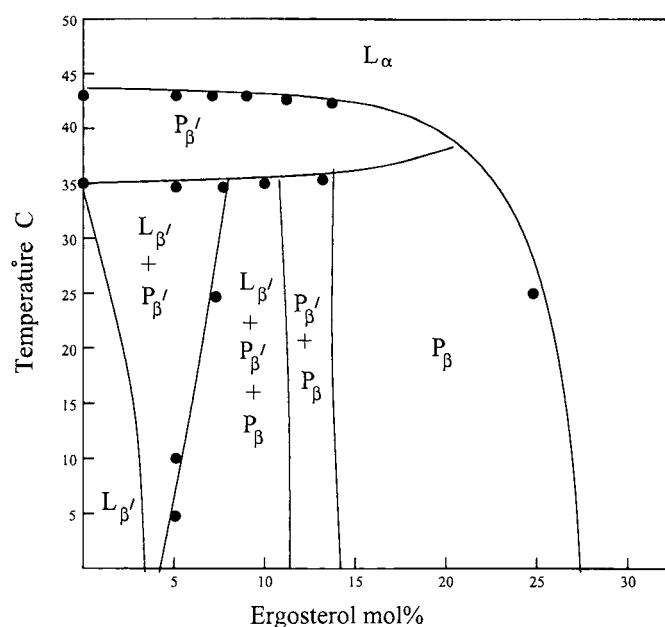


Figure 3.3: Phase diagram of DPPC–ergosterol mixtures at 98% RH.

3.2.1 Small angle x-ray scattering (SAXS) studies

3.2.1.1 Phase behaviour of DPPC-ergosterol mixtures

DPPC-ergosterol mixtures were probed at various sterol concentrations (X_e) and temperatures and a partial phase diagram for this system has been determined (fig. 3.3). As described in chapter-1, pure DPPC bilayers exhibit three lamellar phases at high hydration: the fluid phase (L_α) above the chain melting transition temperature T_m ($\sim 42^\circ\text{C}$), a ripple phase ($P_{\beta'}$) between T_m and the pre-transition temperature T_p , and the gel phase ($L_{\beta'}$) below T_p ($\sim 34^\circ\text{C}$).

Incorporation of ergosterol in the DPPC membrane alters this phase behaviour. At very low ergosterol concentrations ($X_e < 2.5$ mol%) the main and pre-transition temperatures remain the same as those of the pure sample and the corresponding phase sequence ($L_\alpha \rightarrow P_{\beta'} \rightarrow L_{\beta'}$) was observed. At $X_e \sim 5$ mol% a coexistence of $P_{\beta'}$ and $L_{\beta'}$ was observed below the pre-transition. At X_e between 15 to 25 mol% the modulated phase (P_β) was observed. The P_β phase was characterized by satellite peaks in the small angle region (fig. 3.4) which can be indexed on a rectangular unit cell. The T_m decreased slightly with ergosterol concentration

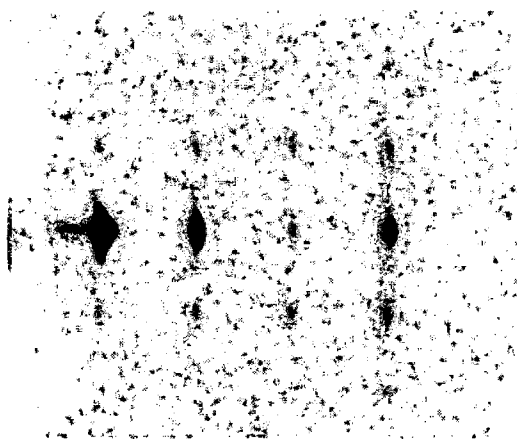


Figure 3.4: Diffraction pattern of P_β phase in DPPC-ergosterol mixture.

up to ~ 25 mol%. Thereafter an abrupt decrease in T_m was observed and both the main transition and the pre-transition were completely abolished. A fluid phase was observed at all temperatures for $X_e > 25$ mol% (fig.3.7).

Interestingly a three phase coexistence was observed at ergosterol concentration ~ 10 mol%. Three distinct sets of lamellar peaks were observed below the pre-transition up to 5°C . The three co-existing phases were found out to be $L_{\beta'}$, P_β and $P_{\beta'}$. Small angle diffraction pattern showing the coexistence of three phases is shown in fig. 3.5. Though the satellite peaks of the P_β phase can be visualized clearly, however the satellite peaks of the ripple phase ($P_{\beta'}$) was not observed prominently. But we could characterize the $P_{\beta'}$ by a: the smearing of the main peaks along q_\perp direction, b: the lamellar periodicity data. The $L_{\beta'}$ phase was identified by its characteristic wide angle chain scattering as discussed previously. As evident from the phase diagram (fig. 3.3), the three phase region was followed and preceded by narrow regions of two phase coexistence (fig. 3.6). Such a three phase coexistence region was reproducible in different samples at similar ergosterol concentrations. The three phase coexistence region is a broad region of width ~ 5 mol% along the concentration axis. Lamellar repeat spacing of DPPC-ergosterol mixtures as a function of temperature is given in table. 3.1. In the P_β phase the wave length of modulation increases with temperature. A plot of ripple wave length as a function of temperature at various ergosterol concentration is shown in fig. 3.8.

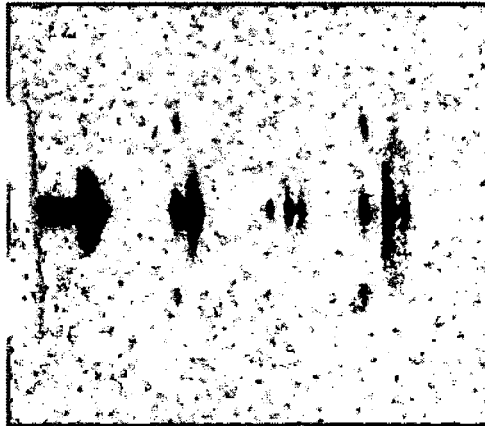


Figure 3.5: Diffraction pattern showing 3 phase coexistence in DPPC-ergosterol mixtures.

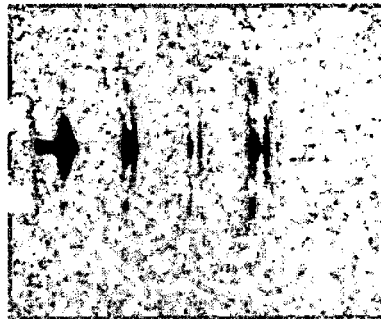


Figure 3.6: Coexistence of P_β and $P_{\beta'}$ at ergosterol concentration = 12.5 mol%, $T=15^\circ\text{C}$.

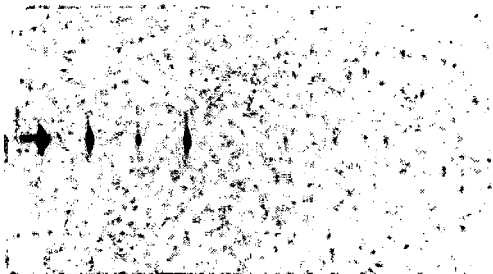


Figure 3.7: The fluid phase was observed at all temperatures for ergosterol concentration > 25 mol%.

Table 3.1: Lamellar spacings d (Å) of DPPC-ergosterol mixtures as a function of temperature. RH = 98±2 %. The error in d is ± 0.3Å.

T (°C)	X_c (mol%)								
	0	5	7.5	10	12.5	15	20	25	30
45	56.6	55.6	54.9	56.0	56.4	57.6	59.9	56.4	59.4
40	62.3	60.7	60.7	61.2	61.2	60.7	62.1	58.4	60.9
35	60.3	59.6 ; 61.8	60.7 ; 62.3	59.0 ; 61.2 ; 64.0	61.0 ; 63.6	64.2	64.3	61.2	62.1
30	50.0	59.4 ; 61.6	61.0 ; 63.8	59.2 ; 61.4 ; 64.8	61.0 ; 64.1	64.8	64.5	61.9	62.5
25	59.7	59.6 ; 61.8	61.0 ; 64.3 ; 58.8	59.6 ; 62.3 ; 64.8	62.1 ; 64.8	65.0	65.0	64.3	64.5
20	63.9	59.6 ; 61.8	62.1 ; 65.8 ; 59.9	59.6 ; 62.1 ; 66.3	61.9 ; 64.8	65.0	65.8	64.3	64.5
15	62.0	59.8 ; 62.1	62.1 ; 66.1 ; 59.6	59.6 ; 62.1 ; 66.3	61.9 ; 65.3	65.5	65.8	63.1	64.5
10	62.0	59.8 ; 62.1	62.1 ; 66.1 ; 59.4	59.4 ; 61.8 ; 66.1	61.4 ; 65.1	65.5	65.8	63.5	64.5
5		59.4 ; 61.6 ; 65.8	61.0 ; 65.1 ; 58.3	59.2 ; 61.4 ; 65.8	60.1 ; 63.6	65.5	65.8	63.5	64.5

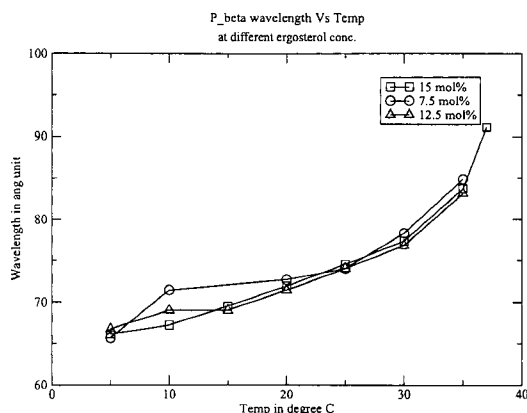


Figure 3.8: Ripple wavelength ($\lambda(\text{\AA})$) of P_β as a function of temperature at different ergosterol concentration.

3.2.1.2 Phase behaviour of DPPC-lanosterol mixtures

DPPC-Lanosterol mixtures at various lanosterol concentrations (X_l) were probed at 98% RH to compare the phase behaviour with that of DPPC-ergosterol mixtures. Gradual decrease in T_m was observed up to 25 mol% of lanosterol concentration after which the main and pre-transitions were completely abolished and a fluid phase was obtained for all temperatures. For $0 < X_l < 25$ mol% below T_m the normal ripple phase was observed for a temperature range of $\sim 5^\circ\text{C}$. At intermediate sterol content (~ 20 mol%) the modulated phase (P_β) was observed. At this concentration on cooling the observed phase sequence was ($L_\alpha \rightarrow P_{\beta'} \rightarrow P_\beta$). This region was preceded by a region of two phase coexistence ($L_{\beta'} - P_\beta$). The partial phase diagram of DPPC-lanosterol mixture is shown in fig. 3.9. The lamellar periodicity data of DPPC-lanosterol mixture are given in table 3.2.

3.2.1.3 Trans-bilayer electron density profiles: Influence of sterol on bilayer thickness

From the SAXS data we have calculated the transbilayer electron density profile (edp) using the procedure described previously. Though such an approach will only give the electron densities on a relative scale, some structural parameters, such as the peak to peak separation d_{pp} , which is a measure of the bilayer thickness can be accurately determined. The trans-bilayer edp for ergosterol and lanosterol system at 30°C at various sterol concentration is shown in fig. 3.10 and fig. 3.11. In fig. 3.12 a plot of lamellar periodicity (d) and the peak

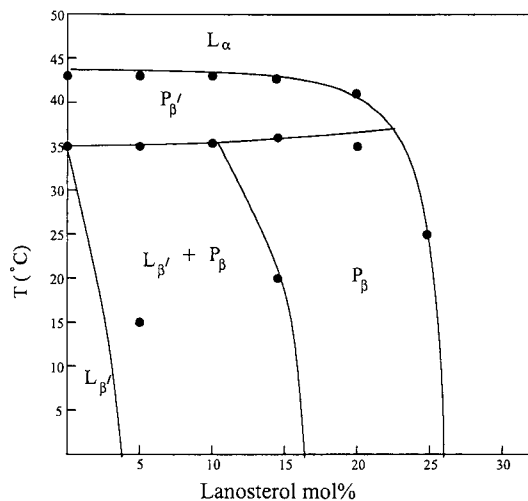


Figure 3.9: Phase diagram of DPPC–Lanosterol at 98% RH.

Table 3.2: Lamellar spacings d (Å) of DPPC-lanosterol mixtures as a function of temperature. RH = 98±2 %. The error in d is ± 0.3 Å.

T (°C)	X_c (mol%)						
	0	5	10	15	20	25	30
45	56.6	56.5	57.3	58.4	60.0	59.8	61.9
40	62.3	61.6	61.1	61.0	62.3	61.9	62.0
35	60.3	62.1 ; 59.7	60.4 ; 65.5,	64.1	63.5	63.1	62.2
30	60.0	64.8 ; 59.5	60.4 ; 65.6	65.1	63.6	63.3	62.2
25	59.7	64.8 ; 59.4	60.6 ; 66.7	66.4	64.8	64.2	62.3
20	63.9	64.8 ; 59.4	60.6 ; 66.7	66.7	64.2	64.1	63.1
15	62.0	65.6 ; 59.4	60.6 ; 66.7	66.4 ; 59.6	64.8	63.9	63.2
10	62.0	65.6 ; 59.4	60.2 ; 66.7	66.4 ; 59.6	64.8	63.9	62.7
5		65.6 ; 59.4	60.0 ; 66.5	66.4 ; 59.6	63.9		

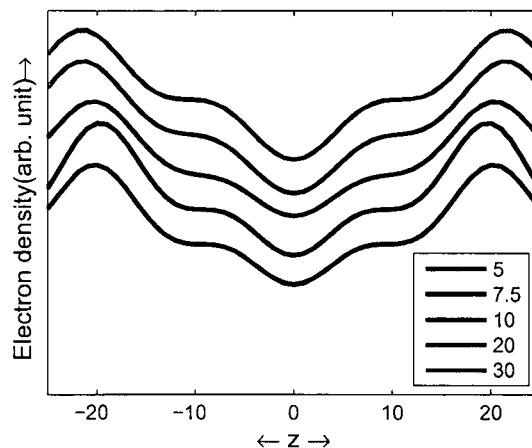


Figure 3.10: Electron density profiles of DPPC-ergosterol mixture for various sterol concentration at $T = 45^{\circ}\text{C}$.

to peak distance d_{pp} in edp are given for DPPC-ergosterol and DPPC-lanosterol systems as a function of sterol concentration at $T=45^{\circ}\text{C}$. The bilayer thickness increases with the sterol concentration. However no significant difference in the bilayer thickness was observed with different sterols.

3.2.2 Wide angle x-ray scattering (WAXS) studies

The ordering of acyl chains in a bilayer can be quantified by the chain orientational order parameter. Since the bilayer chains are not rigid, usually segment-wise order parameter values are reported. Most common method employed for measuring the segment-wise order parameter is by NMR spectroscopy where the bilayer chain is deuteriated selectively at different carbon numbers and the order parameter is measured from the quadrupolar splitting. Similarly an average value of the order parameter for the whole chain can also be deduced using NMR techniques from the first moment data. Though the segment-wise order parameter gives detailed information about the ordering of each molecular segment in the bilayer chain, the average orientational order parameter is a more useful quantity describing the acyl chain ordering of the bilayer in comparing the effects of different molecular species on the chain ordering.

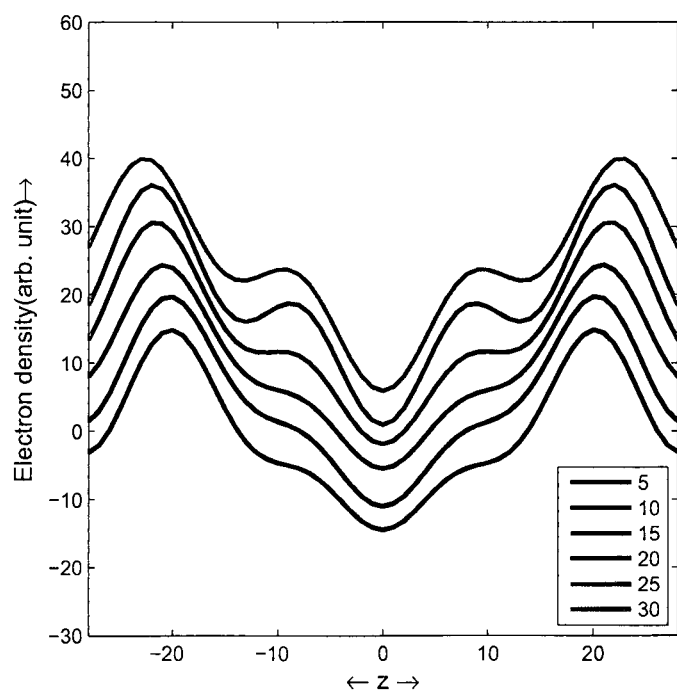


Figure 3.11: Electron density profiles of DPPC-lanosterol mixture for various sterol concentration at $T = 45^\circ\text{C}$.

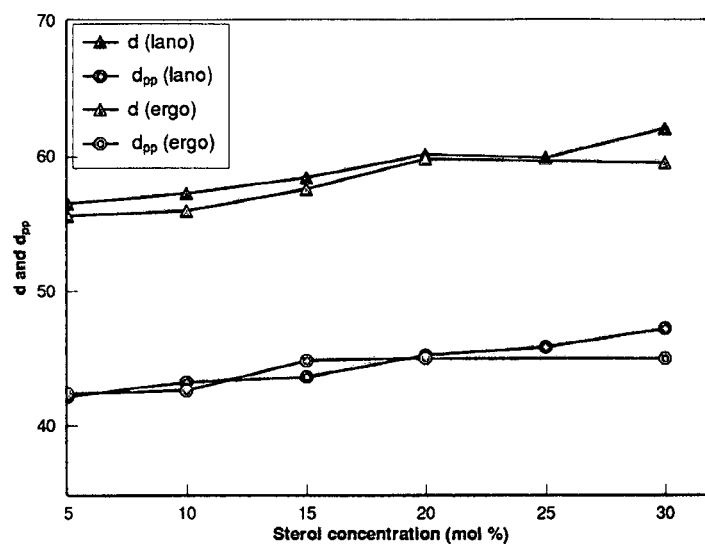


Figure 3.12: Lamellar periodicity (d in Å) and peak to peak separation in the edp (d_{pp} in Å) of DPPC-ergosterol and DPPC-lanosterol bilayers as a function of sterol concentration at $T = 45^\circ\text{C}$.

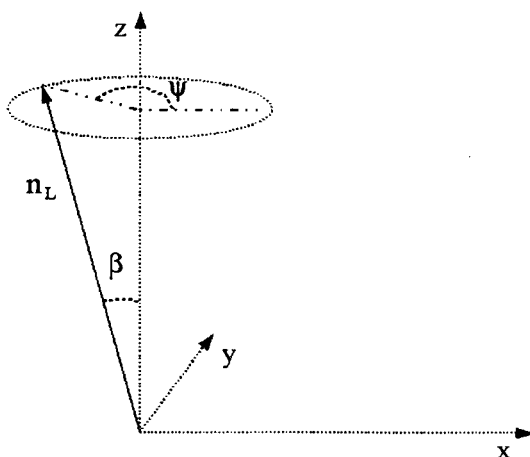


Figure 3.13: Geometrical representation of orientation of a single chain (rigid rod assumption). z axis defines the bilayer normal.

Such an average orientational order parameter can also be determined from the WAXS analysis. For analyzing the WAXS data we have employed a method reported by Nagle *et al.* [12]. As described there such an analysis is independent of experimental geometry. In the following section we give a very brief account of the approach following the above reference.

3.2.2.1 Theoretical background

In liquid crystal research it is often required to calculate the orientational order parameter of rod-like molecules especially in the nematic phase. The orientational order is quantified by the orientational distribution function ($f(\beta)$). $f(\beta)$ is the singlet orientational distribution function which describes the finite probability for a particular molecule to have its long molecular axis oriented at an angle β to the director field. $f(\beta)$ can not be measured directly. However several methods have been established to calculate the orientational order parameter by estimating $f(\beta)$ from scattering data [13, 14, 15, 16]. These methods work on the assumption that the system consists of rigid rods of length L separated by some average distance d_{avg} where $L \gg d_{avg}$. In the sample there exists several regions of rods with a particular local director (say \vec{n}_L). Locally the rods are assumed to be well correlated and rotationally symmetric about \vec{n}_L but the domains have a orientational distribution $f_d(\beta)$. Then $f_d(\beta)$ can be calculated from the intensity distribution. In general $f_d(\beta)$ is different from the

singlet distribution function $f(\beta)$. However it has been shown that $f_d(\beta)$ is similar to $f(\beta)$ [13, 14, 16].

Now if we assume a director distribution function $f(\beta)$, then the fraction of rods with a particular orientation can be described by $f(\beta) \sin\beta d\beta d\psi$ (see fig. 3.13). With this kind of geometry, scattered intensity $I(\phi)$ as a function of angle ϕ (see fig. 3.15) can be deduced. And from the $I(\phi)$ obtained from scattering experiment $f(\beta)$ can be computed either analytically [16] or numerically [15]. From $f(\beta)$ the orientational order parameter can be deduced. The average orientational order parameter (S) is defined in terms of the director angle β as -

$$S = \frac{1}{2}(3\langle \cos^2\beta \rangle - 1) = \frac{\int_{\beta=0}^{\beta=\pi/2} \frac{1}{2}(3\cos^2\beta - 1)f(\beta)\sin\beta d\beta}{\int_{\beta=0}^{\beta=\pi/2} f(\beta)\sin\beta d\beta} \quad (3.1)$$

Such an approach may not be strictly valid for a system like lipid bilayers in the fluid phase, where lipid chains can not be strictly assumed to be straight rods. However such methodology can give some kind of average value of the orientational order parameter and specially for comparison of the influence of different molecules such as sterols on chain ordering this method can be applied. The most common form of distribution function used to fit scattering data in liquid-crystalline system is the Maier-Saupe orientational distribution function [17] which is given by

$$f(\beta) = \frac{1}{Z} \exp(m\cos^2\beta) \quad (3.2)$$

where m is a parameter related to the width of the distribution and Z is a normalization factor. This kind of distribution function has been used in several occasions for fitting the scattering data [13, 18, 19, 20]. Using such a distribution function the final formula for the WAXS scattering can be written as [12]

$$I(\phi) = I_{back} + \frac{C}{8} \times \frac{\sqrt{m}}{\exp(m)D(\sqrt{m})} \times \exp\left(\frac{m\cos^2\phi}{2}\right) \times I_0\left(\frac{m\cos^2\phi}{2}\right) \quad (3.3)$$

where I_0 is a Bessel function of the first kind, D is the Dawson integral given by $D(x) = e^{-x^2} \int_0^x e^{y^2} dy$.

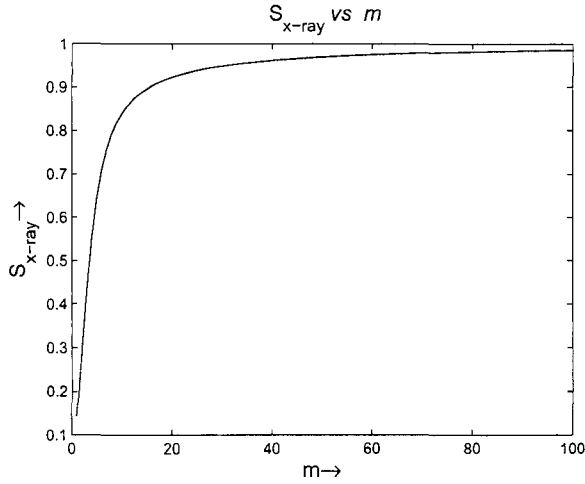


Figure 3.14: Variation of S_{x-ray} with (m)

This equation has three fitting parameters: I_{back} is the constant background introduced for accounting any additional scattering; C , a proportionality constant related to the beam intensity, amount of the sample and exposure duration; m as described above is related to the width of the Maier-Saupe distribution function. After extracting these parameters from the appropriate fit the chain orientational order parameter can be calculated using the relation-

$$S_{x-ray} = \frac{1}{2}(3\langle \cos^2 \beta \rangle - 1) \quad (3.4)$$

which for the Maier-Saupe distribution gives

$$S_{x-ray} = \frac{3}{4m} \left(\frac{\sqrt{m}}{D(\sqrt{m})} - 1 \right) - \frac{1}{2} \quad (3.5)$$

S_{x-ray} asymptotically goes to 1 with m (see fig.3.14). For the detail derivation of the fitting equation, S_{x-ray} and related discussion the readers are advised to refer to [12].

3.2.2.2 Results

The raw data from WAXS were collected from aligned sample of lipid-sterol mixtures. The typical exposure time was ~ 1 hour. A representative diffraction pattern of the wide angle region is shown in fig. 3.15. During the collection of WAXS data the small angle region of

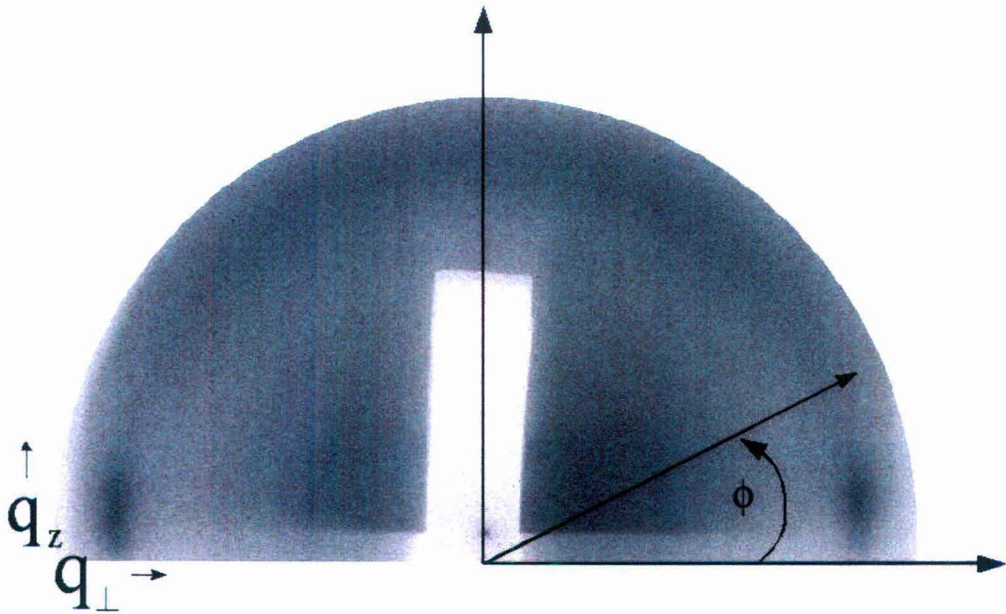


Figure 3.15: Diffraction pattern showing the peak in the wide angle region.

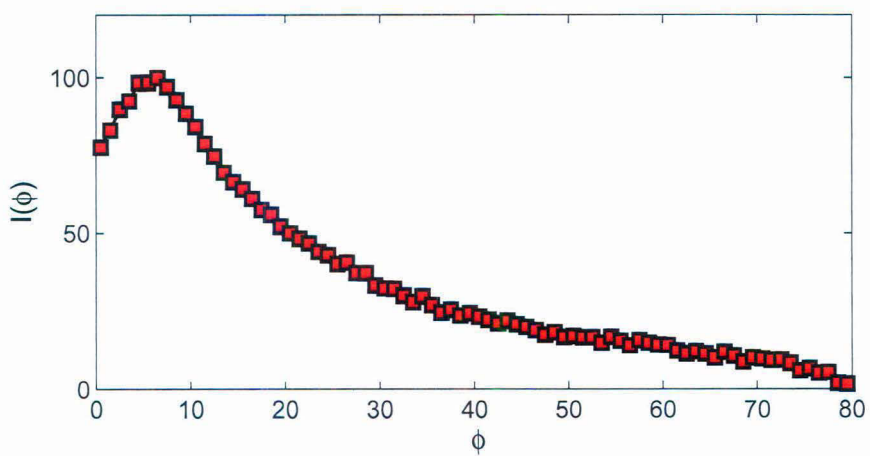
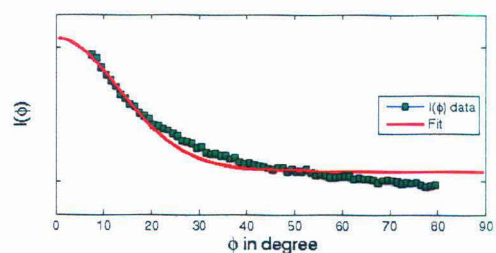
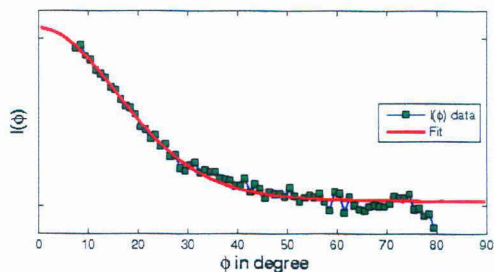


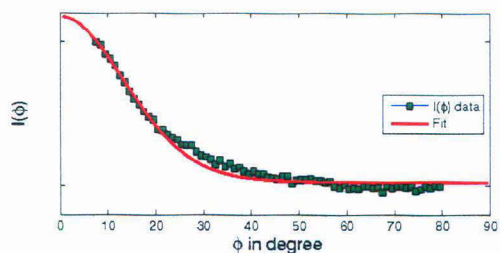
Figure 3.16: Variation of WAXS intensity as a function of ϕ .



(a)



(b)



(c)

Figure 3.17: Variation of normalized intensity ($I(\phi)$) of the wide angle peak with ϕ . The solid line is a fit obtained using eqn. (3.3) (a) ergosterol, (b) lanosterol and (c) cholesterol.

the detector was covered with lead sheet of appropriate dimension so as not to saturate the image plate due to high intensity. The background data were obtained with a very similar set up but without the sample. After the background subtraction the $I(\phi)$ data were obtained by averaging the Intensity values over a q range of 1.7 to 1.4 \AA^{-1} over the entire ϕ range of 0 - 90 degree. Then finally the intensity values were averaged over one degree to get the final data for fitting. Because of absorption within the sample and by the substrate the maxima does not occur at 0 degree rather the $I(\phi)$ curve looks like as presented in fig. 3.16. So the fitting is applied only from the maxima. The fitting was done using MATLAB curvefitting routine.

The width of the distribution (m) was calculated for ergosterol and lanosterol by fitting

Table 3.3:

Sample	m	$S_{x\text{-ray}}$
DPPC-cholesterol	9.78(\pm 0.36)	0.83(\pm 0.05)
DPPC-ergosterol	9.9(\pm 0.77)	0.87(\pm 0.09)
DPPC-lanosterol	6.94(\pm 0.44)	0.75(\pm 0.06)

the $I(\phi)$ data appropriately as described previously. The corresponding $S_{x\text{-ray}}$ values were obtained using equation. (3.5). The data were compared for a 30 mol % of cholesterol, ergosterol and lanosterol at a fixed temperature $T=45$ °C. The fitted curve along with the experimental data are shown in fig. 3.17. The values of m and $S_{x\text{-ray}}$ for the sterols are given in table. 3.3. The $S_{x\text{-ray}}$ values for the three different sterols follow the trend ergosterol > cholesterol >> lanosterol.

3.3 Discussion

Our experimental results on DPPC-ergosterol and DPPC-lanosterol mixtures have several interesting features. We do not observe any two phase coexistence region above T_m for both ergosterol and lanosterol systems. Whereas, as described earlier, a two phase coexistence region was reported in DPPC-ergosterol mixtures from spectroscopic studies [11]. Similar discrepancies are also seen in the DPPC-cholesterol system [21]. We think such a discrepancy can arise depending upon the way one probes the system. We believe that transient local concentration fluctuation exists within the lipid bilayer at intermediate cholesterol concentrations. In such a scenario techniques like NMR which probes the bilayer at molecular time scales can possibly pick up two different chain conformations corresponding to transient cholesterol-rich and cholesterol-poor regions in the bilayer. Whereas scattering techniques such as x-ray diffraction which probes the system at a much longer timescale, will average out all such fluctuations and hence will not indicate a macroscopic phase separation. This may explain the discrepancies in the observations [21].

The phase behaviour of DPPC-cholesterol mixtures under similar conditions (oriented

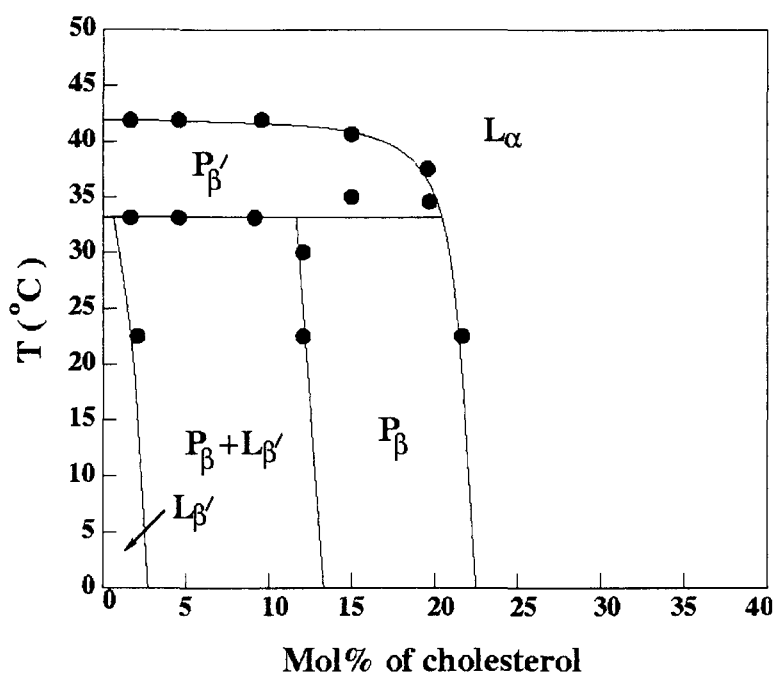


Figure 3.18: Phasediagram of DPPC-cholesterol mixture at $98 \pm 2\%$ RH [22].

samples at $98 \pm 2\%$ RH) was reported by Karmakar *et al.* [22] (see fig. 3.18). From our observation on DPPC-lanosterol mixtures, it is evident the influence of lanosterol on the phase behaviour of DPPC bilayers is very similar to that of cholesterol. However there are certain differences. The concentration at which the main and pretransitions are completely abolished is $< 25\text{mol}\%$ for cholesterol beyond which a fluid phase is observed which is referred to as the liquid-ordered (l_o) phase. Whereas a higher lanosterol concentration ($> 25 \text{ mol}\%$) is required to induce the l_o phase. The modulated phase which was proposed to be induced by cholesterol is also seen in case of lanosterol. This suggests that even though lanosterol differs structurally from cholesterol still the influence of lanosterol on DPPC membrane is very similar to that of cholesterol. For the case of ergosterol, major aspects of the phase behaviour remain similar. We also see the modulated phase in DPPC-ergosterol mixtures. However one intriguing feature in DPPC-ergosterol system is the observation of a three phase co-existence region. Because this three phase region is followed and preceded by two phase regions, it is not an experimental artifact. The three phases are characterized as $L_{\beta'}$, P_{β} and $P_{\beta'}$. However we could not observe the satellite peaks of the $P_{\beta'}$ phase. Also we have observed the

three phase coexistence region for three different concentrations of ergosterol i.e for 5 mol% at 5°C, for 7.5 mol% below 25 °C and for 10 mol% immediately below the pre-transition. This suggests that it is a broad region in temperature and concentration plane. Recalling the well known Gibb's phase rule in thermodynamics, this kind of observation raises a familiar question as discussed in the following.

According to Gibbs phase rule -

$$f = c - p + 2 \quad (3.6)$$

where c is the number of components, p is number of phases and f is the number of degrees of freedom.

For our experiments on two component lipid-sterol system the relative humidity (RH) can be considered as analogous to the pressure in the more familiar $T - P$ phase diagrams. Hence for a binary system of DPPC-ergosterol at constant relative humidity a three phase co-existence can only occur at a point in temperature-composition plane (as degrees of freedom=0), whereas we observe a three phase co-existence over an area in the phase diagram. There can be several possibilities for such discrepancies such as-

- There may be local fluctuation in relative humidity. Such a scenario can be ruled out because all the samples are equilibrated for long time at constant temperature and humidity. Local condensation is also avoided by proper air circulation as described in our experimental section in chapter-1. Also in other samples we do not observe such humidity fluctuations leading to different phase behaviour.
- The compositional purity of lipid and sterol sample : in case of impurity in either lipid or sterol the no of components increases thereby increasing the degrees of freedom. However we rule out such a reason, because other sterols with same lipid sample doesn't show such coexistence. Also as will be described in chapter-4 another sterol (7-dehydrocholesterol (7DHC)) which shares a very similar structure with ergosterol i.e two double bonds in the steroid skeleton, also induces a three phase coexistence in

DPPC bilayers.

- There may be a complex formation for particular type of sterols thereby increasing the no of components. The fact that we observe a similar three phase co-existence in DPPC-7DHC mixtures suggests that the steroid skeleton of such sterols might be somehow responsible for this. So a complex formation can not be ruled out. We could not test this possibility and it still remains an open question.

Another interesting feature in our observation is that the ripple phase ($P_{\beta'}$) is stabilized at low temperatures in DPPC-ergosterol mixtures. As evident from the phase diagram (see fig 3.3) and the lamellar repeat spacing data (see table 4.1) we observe $P_{\beta'}$ at several ergosterol concentrations (5, 7.5, 10, 12.5 mol%) down to 5°C. Interestingly a very similar observation was made in DPPC and dehydroergosterol(DHE) mixture at 13 mol% of DHE where the $P_{\beta'}$ was found to co-exist with the gel phase down to 5°C[23]. Both ergosterol and DHE has similar steroid ring structure (with two double bonds). This again suggests that the structure of the steroid ring influences the phase behaviour of the DPPC bilayers.

The earlier phase diagram determined from NMR and calorimetric study [11](See fig.3.2) shows a co-existence of a gel phase(denoted as S_o) and a sterol rich liquid-ordered phase (denoted as l_o) at intermediate ergosterol concentration below T_m . Whereas we observe the modulated phase instead of l_o phase. In DSC the phase behaviour is determined by measuring the change in enthalpy and in NMR the phase behaviour is determined from the first moment data. Hence it is difficult to find such a modulation of the lipid bilayers in such experiments. However in SAXS studies of aligned bilayer such a modulated phase can be easily identified [22].

The electron density profiles constructed for both ergosterol and lanosterol do not show any significant differences. The bilayer thickness is similar for both sterols. However the WAXS analysis suggests that ergosterol is more efficient in ordering the acyl chains of DPPC bilayers as compared to lanosterol. We have compared the WAXS results with those from DPPC-cholesterol bilayers. The average chain orientational order parameter follows the

sequence ergosterol > cholesterol > Lanosterol. From micropipette aspiration studies on POPC bilayer containing different sterols, it was shown that the area expansion modulus K_a of POPC bilayer increases with addition of sterol molecules and the increment in K_a follows the sequence cholesterol > lanosterol > ergosterol [6] whereas similar studies on DPPC bilayer shows the trend as ergosterol > cholesterol > lanosterol [24]. Similar results were also obtained for DMPC bilayer in presence of the three sterols. [25].

It is worth noting that WAXS analysis do not give the absolute value of the order parameter. The rigid rod assumption of the bilayer chains is not strictly valid. The segment-wise order parameter as measured by NMR can be an appropriate representation. Also the values of S_{xray} obtained by WAXS analysis is higher than that found by NMR (S_{NMR} from first moment data). It was found that S_{xray} is greater than S_{NMR} by a factor 1.3 [12]. This difference can be attributed to the fact that different quantities are measured by NMR and x-rays. However when comparing the effect of various sterol on chain ordering, WAXS can be used to calculate such an orientational order parameter.

3.4 Conclusion

We have carried out a comparative study of ergosterol and lanosterol in DPPC bilayers. The phase behaviour of DPPC-lanosterol mixtures is very similar to that of DPPC-cholesterol mixtures. Though major aspects of the phase diagram of DPPC-ergosterol system remain the same we have observed a three phase coexistence region at intermediate ergosterol concentrations. The bilayer thickness is increased similarly by all these sterols. But very dramatic changes in the chain orientational order parameter was observed.

Bibliography

- [1] K. Bloch, *Science*, **150**, 19 (1965).
- [2] K. Bloch, *CRC Crit. Rev. Biochem*, **14**, 47 (1983).
- [3] L. Miao, M. Nielsen, J. Thewalt, J. H. Ipsen, M. Bloom, M. J. Zuckermann and O. G. Mouritsen, *Biophys. J.* , **82** ,1429 (2002).
- [4] B. Alberts, D. Bray, J. Lewis, M. Raff, K. Roberts and J. D. Watson, *Molecular Biology of the Cell* Garland publishing, Taylor and Francis Group, (1994).
- [5] K. Bloch, *Cholesterol, evolution of structure and function.*, Benjamin/Cummins, Newyork (1985).
- [6] J. Henriksen, A. C. Rowat, E. Brief, Y. W. Hsueh, J. L. Thewalt, M. J. Zuckermann, and J. H. Ipsen, *Biophys. J.*, **90**, 1639 (2006).
- [7] A. Arora, H. Raghuram, and A. Chattopadhyay, *Biochem. Biophys. Res. Commun.*, **318**, 920 (2004).
- [8] J. Borald, *Biochim. Biophys. Acta* , **864**, 257 (1986).
- [9] L. Silva, A. Coutinho, A. Fedorov , and M. Prieto, *Biophys. J.*, **90**, 1067 (2005).
- [10] K. Hac-Wydro, P. Dynarowicz-Łatka , *Biophysical Chemistry*, **123**, 154 (2006).
- [11] Y. W. Hsueh, K. Gilbert, C. Trandum, M. Zuckermann and J. Thewalt, *Biophys. J.*, **88**, 1799 (2005).

- [12] T. T. Mills, G. E. S. Toombes, S. Tristram-Nagle, D. Smilgies, G. W. Feigenson and J. F. Nagle, *Biophysical J.*, **95**, 669 (2008).
- [13] A. J. Leadbetter and E. K. Norris, *Mol. Phys.*, **38**, 669 (1979).
- [14] A. J. Leadbetter and P. G. Wrighton, *J. Phys. Colloq. France*, **40**, 234 (1979).
- [15] A. J. Leadbetter, *Structural studies of nematic, smectic A, and smectic C phases. In The Molecular Physics of Liquid Crystals*, Edited by G. R. Luckhurst, and G. W. Gray, Academic Press, London (1979).
- [16] M. Deutsch, *Phys. Rev. A.*, **44**, 8264 (1991).
- [17] P. G. de Gennes and J. Prost, *The Physics of Liquid Crystals*, Clarendon Press, Oxford (1993).
- [18] P. Davidson, D. Petermann and A. M. Levelut, *J. Phys. II France*, **5** 113, (1995).
- [19] S. V. Savenko and M. Dijkstra, *Phys. Rev. E*, **70**, 011705 (2004).
- [20] V. K. Kelker and A. S. Paranjpe, *Mol. Cryst. Liq. Cryst.*, **4**, 2189 (1987).
- [21] S. Karmakar, B. R. Sarangi and V. A. Raghunathan, *Solid State Communication*, **139**, 630 (2006).
- [22] S. Karmakar and V. A. Raghunathan, *Phys. Rev. Lett.*, **91**, 098102 (2003).
- [23] S. Karmakar, *Phase Behaviour of lipid-cholesterol membranes*, Thesis submitted to JNU, Delhi, (2001).
- [24] E. Endress, S. Bayerl, K. Prechtel, C. Maier, R. Merkel, and T. M. Bayerl, *Langmuir*, **18**, 3293 (2002).
- [25] J. A. Urbina, S. Pekerar, H. B. Le, J. Patterson, B. Montez, and E. Oldfield, *Biochimica Et Biophysica Acta*, **1238**, 163 (1995)
- [26] K. Sabatini, J. P. Mattila and P. K. J. Kinnunen, *Biophys. J.*, **95**, 2340 (2008).

Chapter 4

Universal behaviour of sterols in PC membranes

4.1 Introduction

As described in previous chapters, the structure of a sterol molecule has significant consequences on its influence on the phase behaviour of lipid bilayers. There are many other sterols which are structurally similar to cholesterol. We have systematically studied the influence of such sterols on the phase behaviour of DPPC bilayers. Two such systems that is DPPC-ergosterol and DPPC-lanosterol were described in chapter-3. The hydrophilic -OH group helps the sterol molecule to anchor at the hydrocarbon-water interface in the lipid bilayers. Hence the hydrophilic part of the sterol influences the orientation of the sterol molecule inside the lipid bilayer. Any modification in the hydrophilic part of the sterol molecule can be expected to significantly influence its orientation in the bilayer and hence to affect its influence on the bilayer properties. To probe the effect of such changes we selected three different sterols namely 4-Cholesten-3-one (cholestenone), 25-hydrocholesterol (25HC), 5 α -cholestane (cholestane). Chemical structures of these three sterols are shown in fig. 4.1. All three sterols have very similar steroid skeletons. However they differ in the hydrophilic part. In cholestenone the -OH group is replaced by a ketone group. 25HC has an additional -OH group at the end of the hydrophobic tail, whereas cholestane does not have

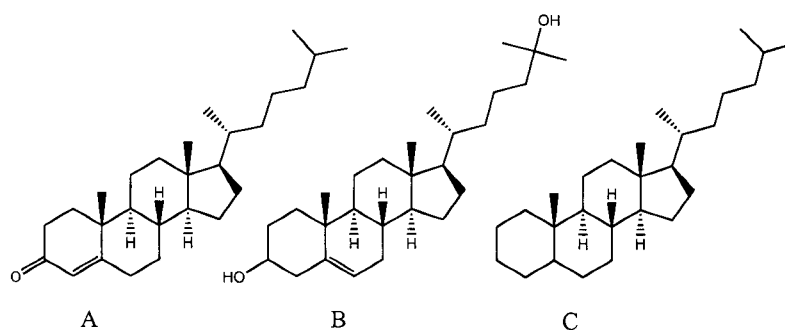


Figure 4.1: Chemical structures of A: cholestenone, B: 25-hydrocholesterol and C: 5 α -cholestane.

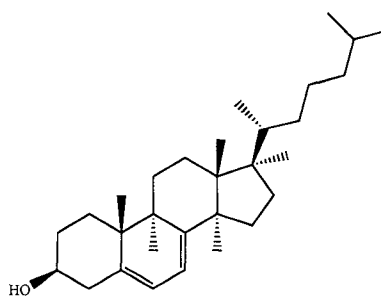


Figure 4.2: Chemical structures of 7-dehydrocholesterol.

any -OH group.

7-dehydrocholesterol (7DHC) is another sterol which has a very similar steroid skeleton as that of ergosterol (fig. 4.2). In view of the observation of the three phase coexistence in DPPC-ergosterol bilayers described in chapter-3, it is interesting to probe the influence of 7DHC on DPPC bilayers.

There have been a few studies on lipid monolayers and bilayers containing these sterols. Keller *et al.* have investigated the phase behaviour of DPPC monolayers containing various sterols [1]. From these studies, sterols were classified to be either membrane active or not. Sterols which are capable of changing the barrier properties and other membrane physicochemical properties are classified as “membrane active” sterol [2]. In this scheme cholesterol and ergosterol satisfy the membrane active criteria, whereas lanosterol, cholestane, 25HC and cholestenone do not [1]. The effect of sterol structure on domain formation in lipid bilayer was studied by fluorescence quenching measurement in the ternary raft mixtures and it was reported that several sterols like cholesterol and 25HC promote do-

main formation. Sterols like cholestane and lanosterol have little effect and a few other sterols like coprostanol, androstenol and 4-cholestenone strongly inhibit the domain formation [3]. Using fluorescence microscopy it was observed that some sterols promote the co-existing liquid phases ($l_o - l_d$) in GUVs of DPPC-DOPC and sterols. These sterols include cholesterol, ergosterol, 25HC and were classified as “promoters”. Whereas sterols like cholestenone, cholestane and coprostanol induce a gel-liquid coexistence and they were classified as “inhibitors” [4]. From pressure-area isotherm measurements on Langmuir-Blodgett films of EGG-PC bilayers with different sterols it was shown that 7DHC exhibits slightly larger molecular areas as compared to cholesterol [5]. From molecular dynamics simulation studies on DPPC bilayers containing cholesterol and cholestenone it was reported that though both sterols increase membrane order and induce chain condensation, but the effect of cholestenone is weaker than that of cholesterol and also cholestenone resides deeper in the bilayer and can easily flip-flop between bilayer leaflets [6]. From all such results it is evident that structural differences between sterols have differential effect on various properties of model membranes.

We have systematically investigated the influence of cholestenone, 25HC, cholestane and 7DHC on the phase behaviour of DPPC bilayers. In this chapter we describe our experimental results of x-ray scattering studies on these binary systems.

4.2 Experimental results

We have carried out x-ray diffraction studies on binary mixtures of DPPC with cholestenone, 25-hydrocholesterol, cholestane and 7-dehydrocholesterol. These samples were probed at various concentrations. The x-ray diffraction patterns were collected from oriented samples at $98\% \pm 2$ RH at various temperatures as described in earlier chapters. From the characteristic diffractions patterns different phases were identified. The partial phase diagrams were constructed for the above mentioned binary mixtures. The influence of these sterols on the phase behaviour of DPPC bilayers is described in the following.

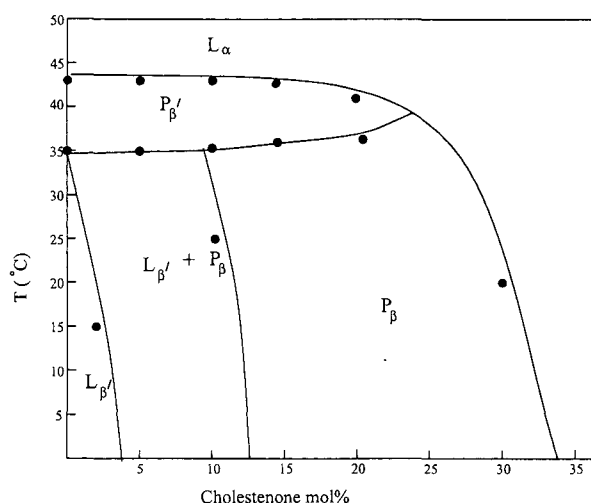


Figure 4.3: Phase diagram of DPPC–cholestenone mixtures at $98\% \pm 2RH$.

4.2.1 Phase behaviour of DPPC-cholestenone bilayers

A partial phase diagram of DPPC-cholestenone mixtures is shown in fig. 4.3. The phase behaviour of DPPC-cholestenone mixtures is very similar to that of DPPC-cholesterol mixtures described in chapter-1. Above the chain melting transition temperature (T_m) the fluid phase L_α is observed at all sterol concentrations. Just below T_m the ripple phase ($P_{\beta'}$) was observed up to $\sim 35^\circ\text{C}$. The T_m does not get affected significantly with sterol concentration up to ~ 25 mol% though it decreases slightly as compared to pure DPPC bilayers. For sterol concentrations > 35 mol% abrupt decrease in T_m was observed and the fluid phase is observed at all temperatures. At intermediate sterol concentrations (15 to 30 mol%) the modulated phase (P_β) was observed (see fig. 4.4). As described earlier the P_β phase was identified by the satellite peaks observed in the small angle region. The modulated phase was preceded by a coexistence region of the gel phase ($L_{\beta'}$) and P_β phase.

4.2.2 Phase behaviour of DPPC-25HC and DPPC-cholestane bilayers

The influence of 25HC and cholestane on the phase behaviour of DPPC bilayer was probed systematically as a function of sterol concentration and temperature. Above T_m the L_α phase was observed at all concentrations of 25HC. Just below T_m the ripple phase $P_{\beta'}$ was observed

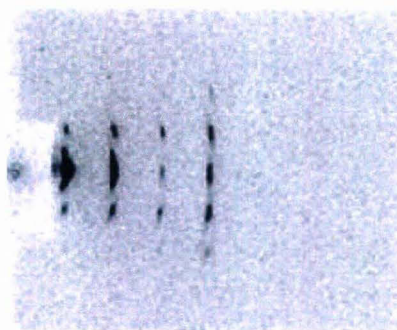


Figure 4.4: Small angle diffraction pattern of the P_{β} phase in DPPC–cholestenone mixtures at $98\% \pm 2RH$.

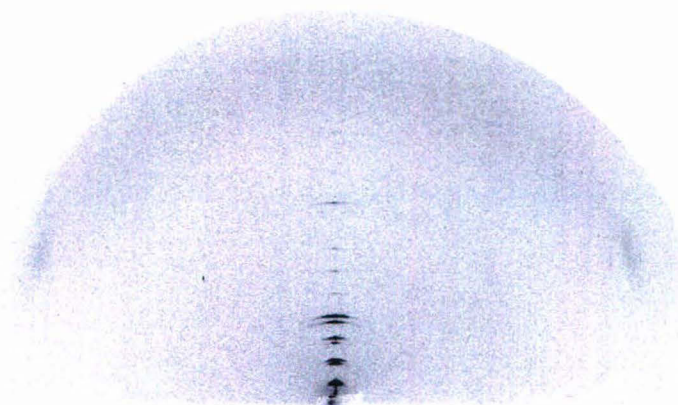


Figure 4.5: Small angle x-ray diffraction pattern of DPPC–25-hydrocholesterol mixtures at $98\% \pm 2RH$, sterol concentration = 10 mol%, $T = 30\text{ }^{\circ}\text{C}$. Off axis peaks in the wide angle region correspond to the chain lattice in the $L_{\beta'}$ phase.

for a temperature range $\sim 5^{\circ}\text{C}$. At low sterol concentrations ($< 5\text{ mol}\%$) the $L_{\beta'}$ phase was seen at lower temperatures. For sterol concentrations between $5 - 25\text{ mol}\%$ a coexistence of two phases were observed. The two phases were identified as the gel phase ($L_{\beta'}$) and the fluid phase or L_{α} phase. The $L_{\beta'}$ phase was characterised by the non-equatorial wide angle peaks which correspond to the scattering from the hexagonally packed chain lattice (see fig. 4.5). The small angle diffraction pattern from such a coexistence region is shown in fig. 4.6. At concentrations $> 25\text{ mol}\%$ of 25HC the fluid phase was observed at all temperatures (fig. 4.8). A partial phase diagram of DPPC-25HC mixtures is shown in fig. 4.7.

A very similar phase behaviour was observed in DPPC-cholestane mixtures where also we observed the coexistence of $L_{\beta'}$ and L_{α} phases for sterol concentrations in the range $5 - 25\text{ mol}\%$. Interestingly the modulated phase P_{β} was not observed in both DPPC-25HC

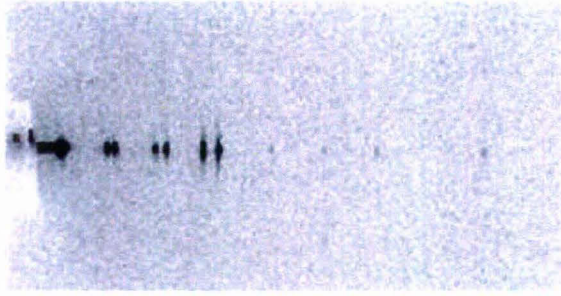


Figure 4.6: Two phase coexistence in DPPC–25-hydrocholesterol mixtures (sterol concentration= 15 mol%, Temperature= 25°C).

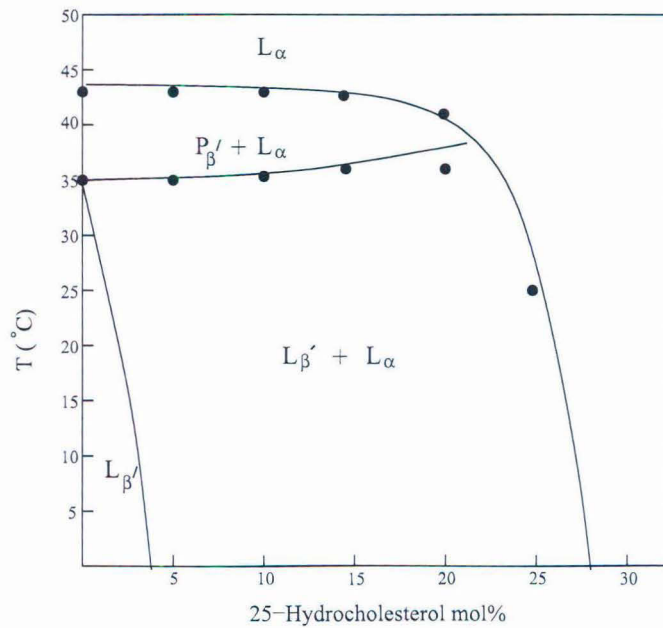


Figure 4.7: Phase diagram of DPPC–25-hydrocholesterol mixtures at $98\% \pm 2RH$.



Figure 4.8: Small angle diffraction pattern of l_0 phase of 25HC. Sterol conc= 30 mol%, Temp= 10°C

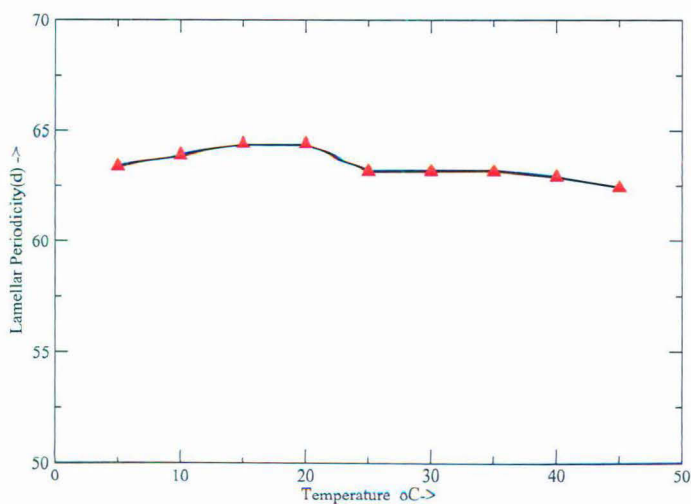


Figure 4.9: Plot of lamellar periodicity d (Å) as a function of temperature at 30 mol% of 25HC.

Table 4.1: Lamellar spacings d (Å) of DPPC-25HC mixtures as a function of temperature at $98 \pm 2\%$ RH. The error in d is ± 0.3 Å.

T (°C)	X_c (mol%)						
	0	5	10	15	20	25	30
45	56.6	56.8	58.2	58.0	59.4	60.8	62.4
40	62.3	61.4, 63.6	61.2, 63.4	63.4	63.1,	63.1	62.9
35	60.3	59.2, 63.6	58.8, 63.1	60.1, 63.4	59.4, 63.4	59.9, 63.6	63.1
30	60.0	59.4, 62.6	58.6, 62.9	60.1, 63.4	59.0, 63.4	59.4, 63.6	63.1
25	59.7	58.8, 63.6	58.8, 63.4	59.7, 64.1	59.0, 63.4	59.4, 63.6	63.1
20	63.9	59.2, 64.1	58.8, 63.4	59.9, 64.6	59.7, 64.4,	59.4, 63.6	64.4
15	62.0	59.2, 64.1	58.4, 63.1	59.9, 64.6	59.0, 63.9	59.4, 63.6	64.4
10	62.0	59.2, 64.4	58.3, 63.6	59.4, 64.4	59.4, 63.9	58.6, 63.4	63.9
5	62.0	58.8, 63.4	58.2, 63.1	59.4, 64.4	59.0, 63.9	58.8, 63.6	63.4

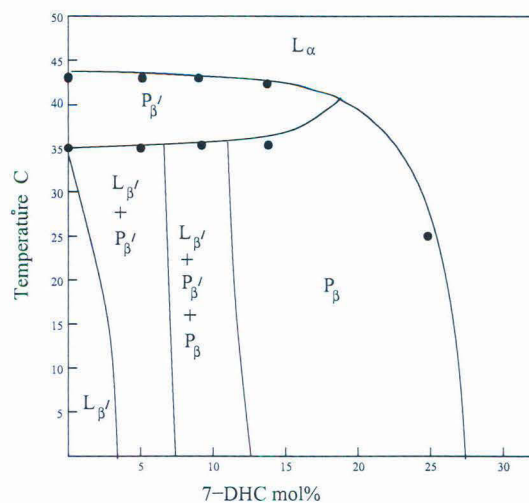


Figure 4.10: Phase diagram of DPPC–7DHC mixtures at $98\% \pm 2RH$.

and DPPC-cholestane bilayers.

4.2.3 Phase behaviour of DPPC-7DHC bilayers

As described earlier 7-DHC has a very similar chemical structure as ergosterol. The influence of ergosterol on DPPC bilayers has been described in chapter-3. To draw a comparison with ergosterol we have probed the phase behaviour of DPPC-7DHC bilayers. The phase diagram obtained from our scattering studies is shown in fig. 4.10. Similar to all other sterols in binary systems here also we see the L_α phase at temperatures $> T_m$. And the $P_{\beta'}$ was seen immediately below T_m . The main and the pre-transitions are completely abolished at sterol concentrations > 25 mol%. At low sterol concentrations (~ 5 mol%) we observed the phase sequence $L_\alpha \rightarrow P_{\beta'} \rightarrow L_{\beta'} + P_{\beta'}$. At intermediate sterol concentrations (15 – 25 mol%) the P_β phase was observed. Interestingly similar to the DPPC-ergosterol system, here also we observed a three phase co-existence at sterol concentrations ~ 10 mol%. The three phases were identified as the $L_{\beta'}$, P_β and $P_{\beta'}$. The small angle diffraction pattern showing the three phase co-existence is shown in fig. 4.11. A two phase co-existence region is expected after the three phase region as seen earlier in DPPC-ergosterol bilayers. But here we could not observe the two phase co-existence region. The reason for this may be that the two phase region is very narrow along the concentration axis. Hence we may not have seen it because

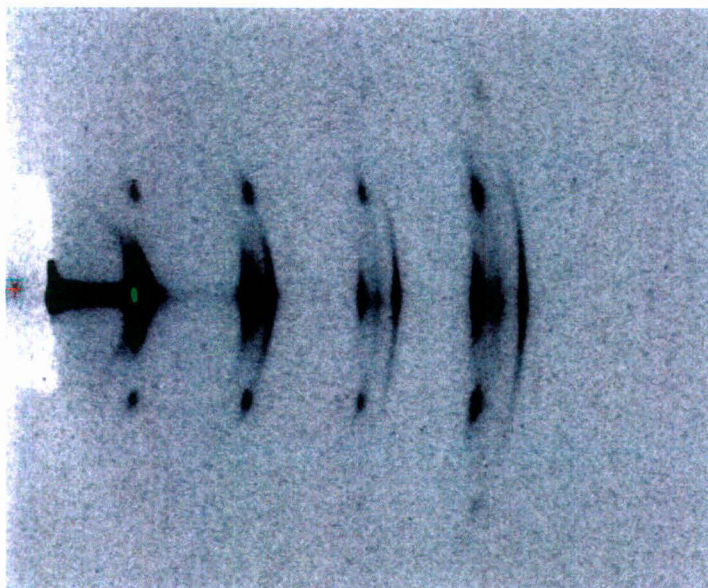


Figure 4.11: Small angle diffraction pattern showing three phase coexistence in DPPC-7DHC bilayers.

of our coarse steps in concentration.

4.3 Discussion

We have systematically studied the influence of cholesterol, 25HC, cholestane and 7DHC on the phase behaviour of DPPC bilayers. The phase behaviour of such binary systems has some universal features namely

- We don't observe a two phase coexistence above T_m for all sterols, in agreement with our earlier results on cholesterol, ergosterol and lanosterol. This result again ascertains the fact that the phase separation above T_m as observed by spectroscopic techniques in these lipid-sterol bilayers is not seen from scattering studies. Such apparent phase separation above T_m may indicate transient concentration fluctuations in the sterol concentration as described in the earlier chapters [7].
- At high sterol concentrations (> 30 mol%) the main and pre transitions are completely abolished and a fluid phase L_α is observed at all temperatures. However the phase boundary for such a fluid phase occurs at a slightly higher concentration for other

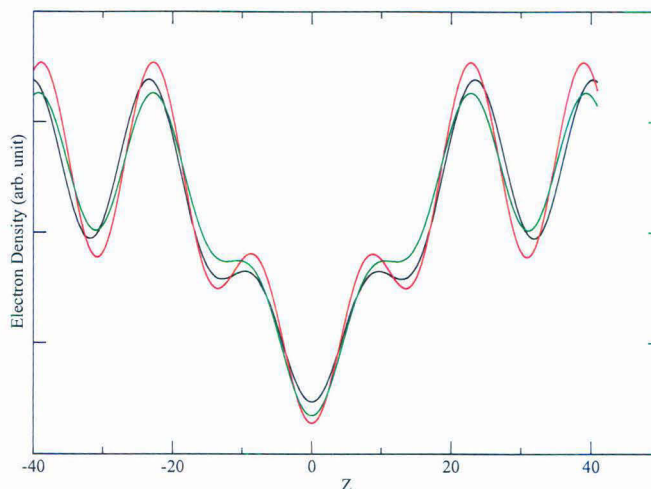


Figure 4.12: Electron density profile of DPPC bilayer containing cholestenone (red), cholestane (green) and 25HC (black) in the fluid phase.

sterols (~ 30 mol%) compared to cholesterol (~ 25 mol% [8]). And in particular for DPPC-cholestenone mixtures this phase boundary occurs at ~ 35 mol% of sterol concentration.

There are certain differences in the phase behaviour at intermediate sterol concentrations which may be arising due to the structural differences between these sterol molecules. Cholestenone in DPPC bilayers induces a similar phase behaviour as cholesterol. Though the $-OH$ group is replaced by a ketone group, still there is no significant difference in its influence on the phase behaviour. A comparative study on the influence of cholesterol and cholestenone on DPPC bilayers was done by measuring the temperature-dependent steady-state fluorescence anisotropy of different fluorophores [9]. Their results suggest that both cholesterol and cholestenone influence the bilayer properties like broadening the main transition in a similar way. In the case of 25HC, which contain an additional $-OH$ group at the end of its hydrophobic tail, we observed certain differences in its influence on the phase behaviour of the DPPC bilayers. The modulated phase P_β was not observed for DPPC-25HC system. P_β phase is proposed to be the consequence of the removal of chain tilt by the anchoring of sterol molecules at the bilayer-water interface [8]. In the case of 25HC the presence of the two $-OH$ groups at opposite ends may have a strong influence in orienting the

sterol molecule in the bilayer. Absence of the P_β phase and the observation of coexistence of L_β and L_α at intermediate sterol concentrations may be attributed to the fact that 25HC is not as effective as other sterols like cholesterol, cholestenone and even lanosterol to remove the chain tilt. Interestingly cholestane, which does not have a -OH group also induces similar phase behaviour in DPPC bilayers. So it seems that sterol orientation in the bilayer strongly influences the structure and phase behaviour of the lipid. Interestingly recently Huster *et al.* studied several cholesterol analog including cholestane in POPC membrane using electron paramagnetic resonance, nuclear magnetic resonance, and fluorescence spectroscopy [10]. Their results suggest that cholestane is not as effective as cholesterol in ordering the POPC bilayers. The acyl chain ordering in presence of cholestane was found out to be very similar to that of fluid phase of pure POPC bilayers. If cholestane has also similar influence on DPPC bilayer then below T_m the phase rich in cholestane will be in a fluid phase. And the cholestane poor phase will be in gel phase (L'_β) phase. Our observation of coexisting phases in DPPC-cholestane mixture is consistent with such a scenario.

We have constructed the electron density profiles of the high sterol concentration L_α phases of these three sterols in DPPC bilayers as shown in figure. 4.12. There is no significant change in the electron density profiles between the different sterols.

Both 7DHC and ergosterol have similar steroid skeletons. They differ only in the hydrocarbon tail where ergosterol has one additional double bond. The phase behaviour of DPPC-ergosterol system was described in chapter-3. A three phase coexistence was seen at ergosterol concentrations $\sim 10\text{mol}\%$. Interestingly we also observed a similar three phase coexistence region in DPPC-7DHC bilayers at similar sterol concentrations. This kind of coexistence was not seen with any other sterols. The presence of an additional double bond in the steroid ring of both ergosterol and 7DHC suggests that this feature may be responsible for such an observation. Further work is necessary to confirm this correlation.

4.4 Conclusion

We have systematically studied the phase behaviour of DPPC bilayers containing cholestenone, 25-hydrocholesterol, cholestane and 7-dehydrocholesterol. Small angle x-ray scattering was used to probe the phase behaviour of these binary mixtures. Our results show that the DPPC-cholestenone system has a similar phase behaviour as DPPC-cholesterol mixtures. However 25-hydrocholesterol shows a very different phase behaviour. The modulated phase was not observed in DPPC-25HC mixtures. Two phase coexistence was observed in a very broad region of this phase diagram. The two phases were identified as the gel phase and a fluid phase. DPPC-cholestane system also shows a very similar phase behaviour as that of DPPC-25HC. Our studies on DPPC-7DHC bilayers give similar results as those from DPPC-ergosterol bilayers described earlier, which indicates that structural changes in the steroid skeleton play a key role in influencing the bilayer phase behaviour.

Bibliography

- [1] B. L. Stottrup and S. Keller, *Biophys. J.*, **90**, 3176 (2006).
- [2] Y. Barenholz, *Prog. Lipid. Res.*, **41**, 1 (2002).
- [3] X. Xu and E. London, *Biochemistry*, **39**, 843 (2000).
- [4] M. E. Beattie, S. L. Veatch, B. L. Stottrup and S. L. Keller, *Biophys. J.* , **89**, 1760 (2005).
- [5] A. B. Serfis, S. Brancato and S. J. Fliesler, *Biochim. Biophys. Acta*, **1511**, 341 (2001).
- [6] T. Rog, L. M. Stimson, M. Pasenkiewicz-Gierula, I. Vattulainen, and M. Karttunen, *J. Phys. Chem. B*, **112**, 1946 (2008).
- [7] S. Karmakar, B. R. Sarangi and V. A. Raghunathan, *Solid State Communication*, **139**, 630 (2006).
- [8] S. Karmakar and V. A. Raghunathan, *Phys. Rev. Lett.*, **91**, 098102 (2003).
- [9] V. Benyashar and Y. Barenholz, *Biochim. Biophys. Acta* , **985**, 271 (1989).
- [10] H. A. Scheidt, P. Müller, A. Herrmann and D. Huster, *The Journal of Biological Chem.*, **278**, 45563 (2003).

Chapter 5

Phase behaviour of ternary mixtures with ergosterol and cholestenone and the problem of cholesterol partitioning between l_o and l_d phases

5.1 Introduction

The proposed existence of “rafts” in the plasma membrane has drawn considerable research interest over the past decade. These rafts which are believed to be rich in cholesterol and spingolipids, are often associated with many cellular processes [1, 2, 3, 4, 5]. As described in chapter-1, detergent solubility of plasma membranes under specific conditions showed that the detergent insoluble fraction of the membrane is rich in cholesterol and spingolipids. This detergent insoluble fraction called as detergent resistance membrane (DRM) is believed to come from pre-existing domains in the plasma membrane called “rafts” [6, 7, 8]. There have been several attempts to look for such domains in cell membranes. Nanoscale heterogeneity in lateral membrane organization has been observed using homo-FRET [9] and by stimulated emission depletion (STED) far-field fluorescence nanoscopy [10]. However the rafts have remained elusive till date.

In model membrane systems microscopic fluid-fluid phase separation has been observed in ternary mixtures of a saturated lipid, an unsaturated lipid and cholesterol [11, 12]. These two fluid phases are called as liquid-ordered (l_o) and liquid disordered (l_d) phases. Such kind of phase separation has been proposed to mimic the raft like domains of the biological membranes. Therefore to understand the domain formation, these ternary mixtures or the “raft mixtures” have been studied using a variety of experimental techniques [11, 13, 14, 15, 16, 17, 18, 19, 20, 21, 22, 23, 24, 25]. Studies on giant unilamellar vesicles (GUVs) and solid supported membranes have found domains of the liquid ordered (l_o) phase rich in the saturated lipid coexisting with the liquid disordered (l_d) phase rich in the unsaturated lipid. The ability of fluorescent dyes to partition differently into the two coexisting fluid phases was used to visualize phase separation in GUVs [13, 14, 11]. Partial phase diagrams of ternary raft mixtures have been constructed using fluorescence microscopy [14], fluorescence spectroscopic techniques such as fluorescence resonance energy transfer (FRET), fluorescence anisotropy, lifetime and quenching [16], and fluorescence correlation spectroscopy (FCS) [18, 26]. The single most important result of all these studies is the observation of the coexistence of the l_o and l_d phases at cholesterol concentrations from 10 to 33 mol% below the chain melting transition temperature (T_m) of the saturated lipid. It is believed that the l_o phase contains more cholesterol than the l_d phase. However the partitioning of cholesterol in these two fluid phases has not been found out conclusively. There are several reports with different conclusions regarding the partitioning [14, 16, 27].

Cholesterol has been used primarily as the sterol molecule in these so called “raft mixtures” because of obvious reasons. However many studies have been conducted on other sterols also which share a similar structure with cholesterol. The main aim of such studies has been to find out whether other sterols induce a fluid-fluid coexistence similar to that exhibited by cholesterol in ternary mixtures. Sterol miscibility and transition temperature of 1:1:1 DOPC/DPPC/sterol mixtures were studied for various sterols including ergosterol and cholestenone [28]. Based on their studies the authors classified sterols into two categories; promoters and inhibitors depending on whether a particular sterol induces fluid-fluid phase

separation or not. In their classification ergosterol is a promotor sterol whereas cholesterol is classified as an inhibitor sterol which induces fluid-gel phase separation.

This chapter describes the phase behaviour of ternary raft mixtures composed of equimolar ratio of dipalmitoyl phosphatidylcholine (DPPC) and dioleoyl phosphatidylcholine (DOPC) at various concentrations of ergosterol and cholesterol. We also describe an approach to find the partitioning of cholesterol between the two coexisting fluid phases from our x-ray diffraction studies of DSPC-DOPC-cholesterol mixtures. Subsequently we describe some critical aspects of the existing approaches for getting the absolute electron density profile from scattering data.

5.2 Experimental studies on ternary mixtures with ergosterol and cholesterol

We have studied ternary mixtures of DPPC, DOPC with ergosterol and cholesterol to compare the phase behaviour. From the small angle x-ray diffraction studies we have drawn partial phase diagrams for these systems. We have also studied giant unilamellar vesicles made from these mixtures for different sterol concentrations.

5.2.1 SAXS studies on DPPC-DOPC-ergosterol mixtures

Oriented bilayers of equimolar mixture of DPPC and DOPC at various ergosterol concentrations were studied using x-ray diffraction at 98% relative humidity. Different phases were identified from their characteristic diffraction patterns as described in earlier chapters.

The chain melting transition temperature of DPPC is 42 °C and that of DOPC is -18 °C. The equimolar mixture of DPPC and DOPC shows a single fluid phase (L_α) above 35°C. Below 35°C a coexistence of gel ($L_{\beta'}$) and fluid (L_α) phases was observed. The pre-transition is completely abolished for this mixture and the ripple phase ($P_{\beta'}$) was not observed.

At ergosterol concentration of 5 mol% a two phase coexistence is observed between 35°C and 20°C. The two phases were identified as L_α and $L_{\beta'}$. Below 20°C we have observed a

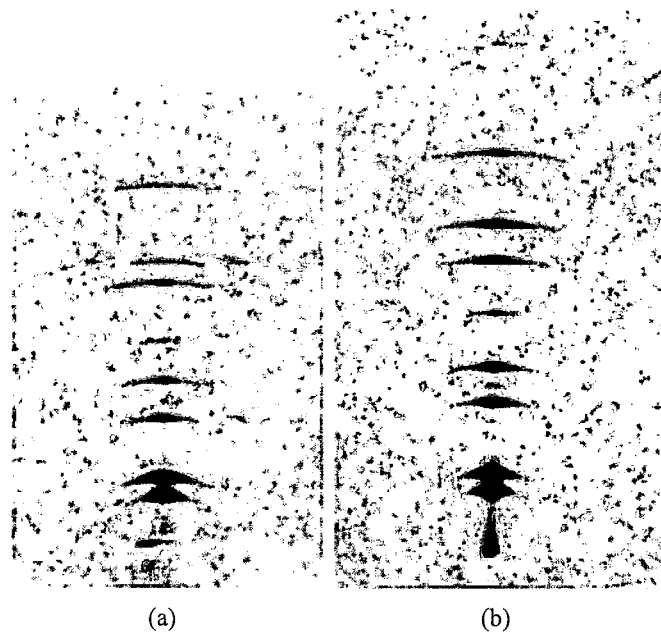


Figure 5.1: Small angle diffraction pattern of DPPC-DOPC-ergosterol mixture at a) 10 mol%, $T=5^{\circ}\text{C}$ showing the coexistence of P_{β} and $L_{\beta'}$ phases, b) 25 mol% $T=20^{\circ}\text{C}$ showing the coexistence of two fluid phases.

three phase coexistence of L_{α} , $L_{\beta'}$ and P_{β} . Above 15 mol% the coexistence of two fluid phases was observed below 30°C (fig. 5.1). Such a fluid-fluid coexistence was observed at 20 and 25 mol% of ergosterol.

At 33 mol% of ergosterol we have observed some additional reflections along with the lamellar peaks (see fig. 5.2). These additional reflections were observed even at high temperatures up to 70°C .

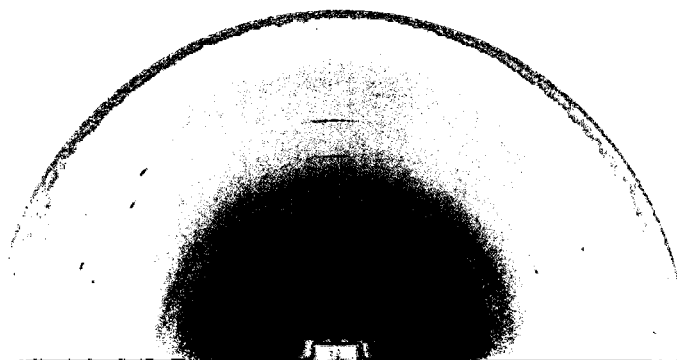


Figure 5.2: Diffraction pattern of 1:1 DPPC-DOPC mixture with 33 mol% of ergosterol at $T=65^{\circ}\text{C}$.

5.2.2 SAXS studies on DPPC-DOPC-cholestenone mixtures

To compare the phase behaviour of ternary mixtures we have carried out x-ray diffraction studies on aligned samples of DPPC-DOPC-cholestenone mixtures at various concentrations. Interestingly for these mixtures we observed significant decrease in the transition temperature. Down to $T=20^{\circ}\text{C}$ we observe the fluid phase up to 25 mol% of cholestenone. Small angle diffraction patterns of DPPC-DOPC-cholestenone mixtures at $T=5^{\circ}\text{C}$ for various cholestenone concentration are shown in fig. 5.3. From 5 to 15 mol% of cholestenone we observed two phase coexistence at low temperatures. The two phases were identified as the fluid phase L_{α} and the modulated phase P_{β} . At 20 mol% of cholestenone we saw a fluid-fluid coexistence. The two fluid phases were identified from the absence of any sharp peaks in the wide angle region. However at cholestenone concentration ~ 25 mol% we observed additional sharp spots (see fig. 5.4). Similar non lamellar peaks were also observed at 33 mol% (fig. 5.5). These sharp spots did not disappear even after heating up to 60°C .

5.2.3 Microscopy of GUVs

We have also studied giant unilamellar vesicles (GUVs) composed of ternary mixtures containing ergosterol and cholestenone at different sterol compositions. As described in chapter 1 electroformation method was used to form the GUVs. GUVs were labelled with the fluorescence dye rhodamine DHPE (Rh PE). Laser scanning confocal fluorescence microscope was used to study these GUVs. GUVs were formed at high temperature ($\sim 5^{\circ}\text{C}$ above T_m), and transferred to a coverslip for observation at room temperature. All studies were done at room temperature (23°C).

Mixtures of DPPC-DOPC-ergosterol were probed at 20 and 30 mol%. At both concentrations we observed a coexistence of two phases inferred by fluorescence dye partitioning. Black domains were observed on a bright background. Partitioning of Rho PE in the two phases suggests that the black domains are the more ordered phase coexisting with the disordered fluid phase. Though the domain shape appeared to be circular as would be expected

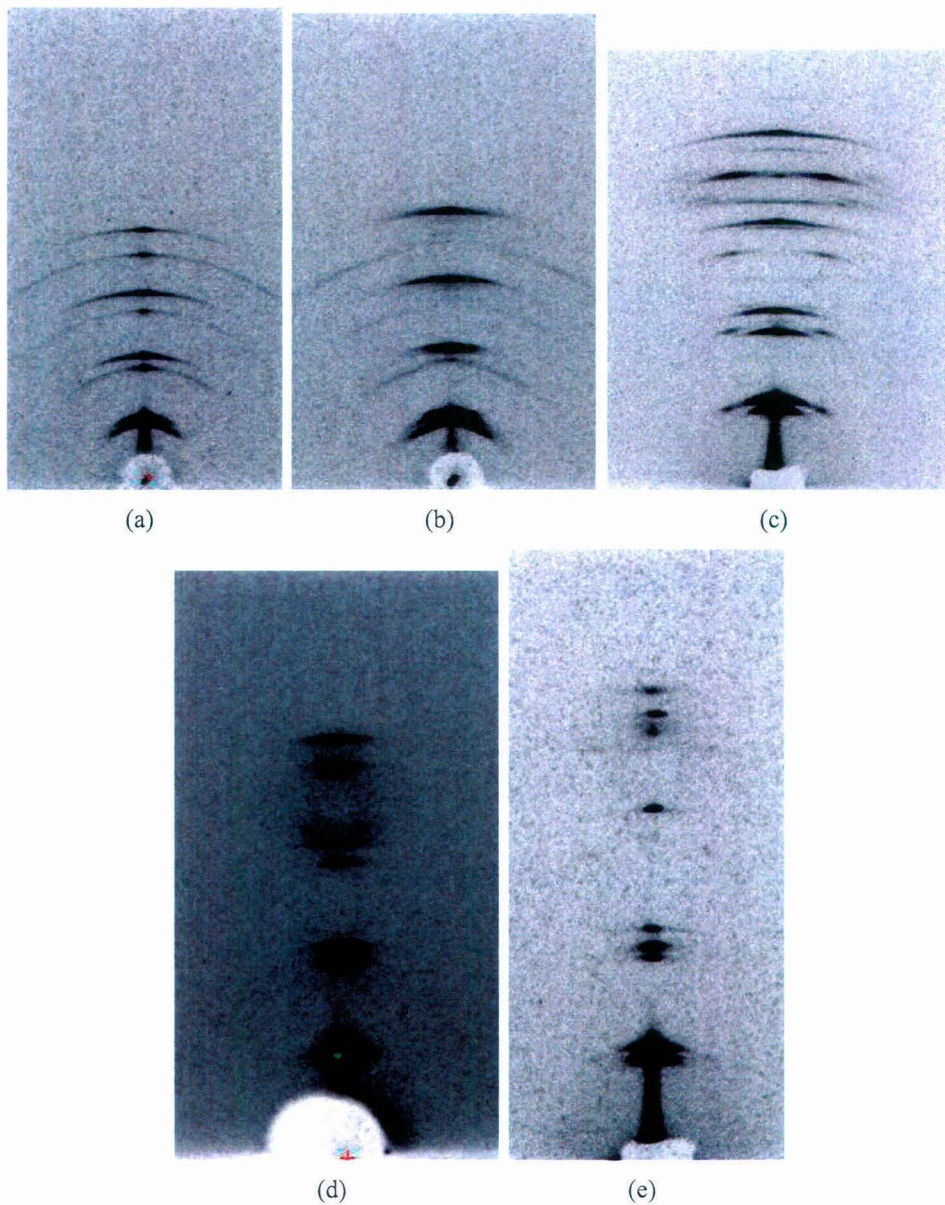


Figure 5.3: Small angle diffraction patterns of DPPC-DOPC-cholestenone mixtures at $T=5^{\circ}\text{C}$ for various cholesterol concentrations. a) 5 mol%, b) 10 mol%, c) 15 mol%, d) 20 mol% e) 25 mol%. At 20 mol% fluid-fluid co-existence was observed. At 25 mol% additional reflections were observed in the small angle region.

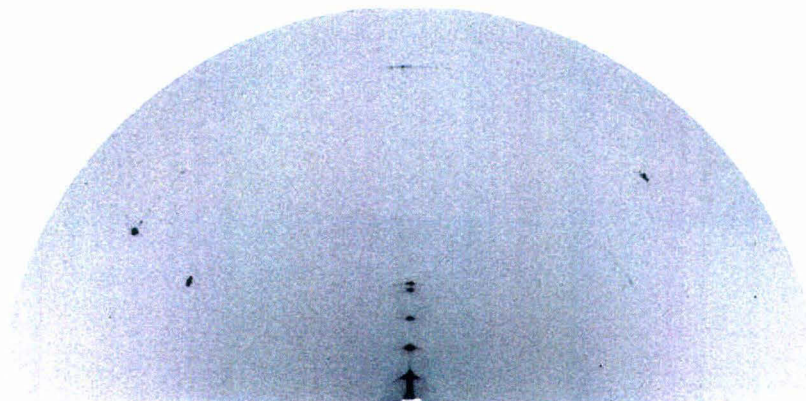


Figure 5.4: Diffraction pattern of DPPC-DOPC-cholestenone mixture at 25 mol% at $T=20^{\circ}\text{C}$.

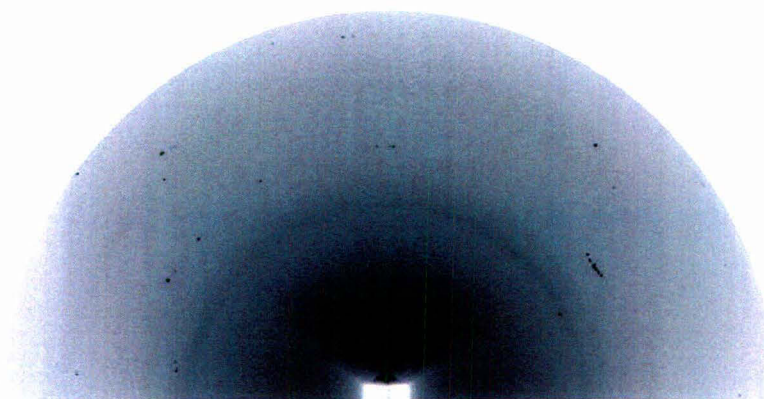


Figure 5.5: Diffraction pattern of DPPC-DOPC-cholestenone mixture at 33 mol%. The sharp spots seen in this pattern remained even at $\sim 60^{\circ}\text{C}$.

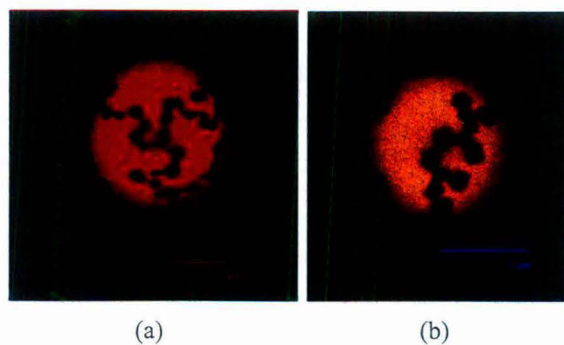


Figure 5.6: Fluorescence micrographs of GUVs of DPPC-DOPC-ergosterol mixtures showing the coexistence of two phases.

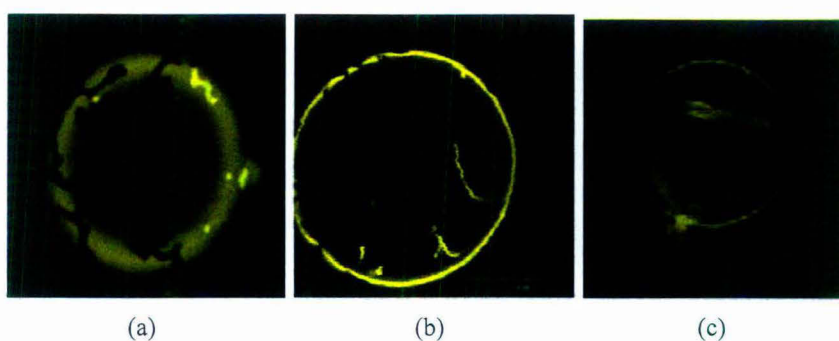


Figure 5.7: Fluorescence micrographs of GUVs of DPPC-DOPC-cholestenone mixtures showing (a) the gel-fluid phase separation (b) and (c) growth of tubules.

from a fluid phase, surprisingly we did not observe the coalescence of domains even after a long time (~ 1 hour). The domains seems to be frozen in a particular state with fused boundaries as shown in fig. 5.6.

In the case of DPPC-DOPC-cholestenone mixtures we first observed a gel-fluid coexistence. Gel domains do not contain the fluorescence dye and hence appear black. They appear in thread like structures and do not exhibit coalescence. The experimental result on GUVs of DPPC-DOPC-cholestenone mixtures at 30 mol% of cholestenone is shown in fig. 5.7. Interestingly after a time scale of ~ 30 minutes we observed nucleation of tubules from the GUVs. The tubules were observed growing both inward and outward directions from the vesicle surface. After a long time almost all vesicle showed this feature (see fig. 5.7).

5.3 Cholesterol partitioning between l_o and l_d phases

As described earlier the partitioning of cholesterol between l_o and l_d phases is a very important problem. In this section we first describe the earlier attempts made to calculate such a partitioning. Then we describe our approach to calculate the partitioning from the scattering data. Subsequently we highlight the problem of constructing absolute electron density profiles of lipid bilayer systems from scattering data.

Earlier attempts to find the partitioning

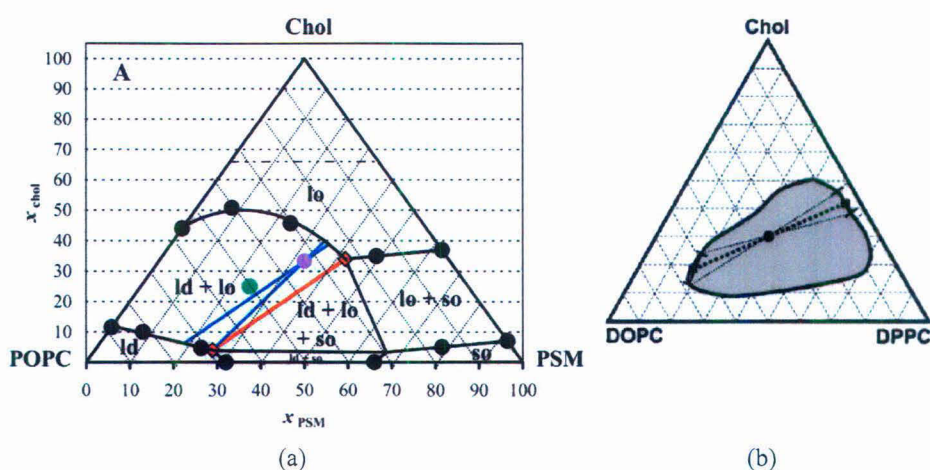


Figure 5.8: Tie lines obtained by different studies a) from fluorescence anisotropy studies [16], b) from NMR studies [14].

There have been a few attempts to determine such a partitioning. Using nuclear magnetic resonance techniques Veatch *et al.* estimated that the amount of cholesterol in both l_o and l_d phases are very similar [14]. The tie lines obtained by them are almost parallel to DPPC-DOPC axis (see fig. 5.8(b)) suggesting that both phases have similar cholesterol content. However the tie lines obtained in reference [16] clearly indicate that cholesterol content in the l_o phase is very different from that in the l_d phase (see fig. 5.8(a)). From x-ray scattering data in the three phase region (gel, l_d and l_o) of ternary mixtures of DPPC-DOPC-cholesterol

Chen *et al.* have calculated the partitioning utilizing the fact that the compositions of these three coexisting phases do not change over their coexistence range at fixed temperature [27]. The cholesterol contents of these phases are found to be 10, 9 and 29 mol% respectively. But the value obtained for the cholesterol content in the gel phase is surprising since all DPPC-cholesterol binary phase diagrams reported in the literature show that the gel phase becomes unstable at much lower concentrations of cholesterol [29, 30, 31].

5.3.1 Calculation from scattering data

In principle scattering data can also be used to find out such a partitioning. We describe a simple approach by which the scattering data from a phase separated system can be analyzed to find out the concentration of various components.

5.3.1.1 Principle

Ternary mixtures of a saturated lipid, an unsaturated lipid and cholesterol exhibit fluid-fluid ($l_o - l_d$) phase separation. It has been shown that the l_o phase predominantly contains the saturated lipid and the l_d phase contains the unsaturated lipid [14, 16]. Presumably both l_o and l_d phases will contain some amount of cholesterol though the concentration of cholesterol may be very different in the two phases. If the intermixing of lipids in the two phases are negligible then both l_o and l_d phases can effectively be treated as binary mixtures of lipid and cholesterol. Scattering studies of such phase separated mixtures shows two sets of lamellar peaks corresponding to l_o and l_d phases. From the scattering data it is possible to construct the electron density profile (edp) $\rho(z)$ on an absolute scale. The procedure for such a construction will be discussed subsequently. For now let us assume that we have the absolute edp of both phases.

Now we can divide the edp in to two regions at $z = d_c$ where d_c defines the boundary between the headgroup and the chain region of the bilayer. If the lateral area per lipid A_L , the volume of the lipid (V_L) and the volume of the headgroup (V_H) are known then d_c can be

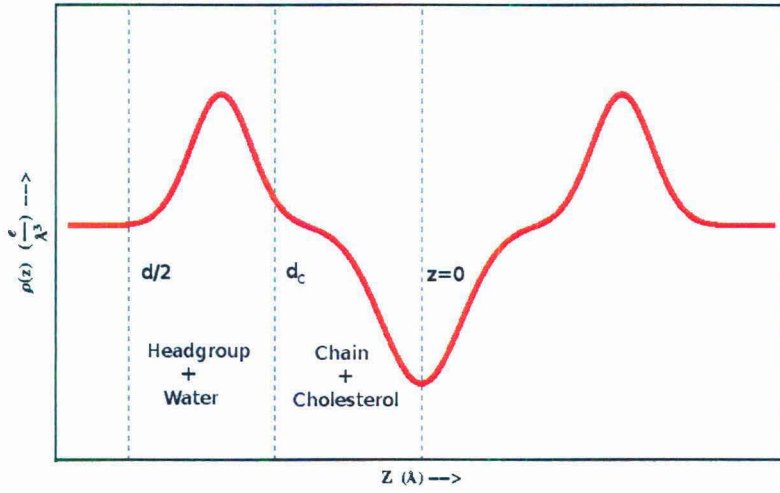


Figure 5.9: The edp of a lipid-cholesterol mixture can be divided into two regions at the boundary d_c . The head group region corresponds to the contribution by the head and water, whereas the chain region corresponds to the contribution from lipid chains and cholesterol

calculated as

$$d_c = \frac{V_L - V_H}{A_L} \quad (5.1)$$

Usually for PC lipids this boundary falls at $\sim 4\text{\AA}$ from the headgroup peak in the edp. For an one component lipid bilayer the region from $z = 0$ to $z = d_c$ reflects the contribution from the chains and the region defined by $z = d_c$ and $z = d/2$ reflects the contribution from water and head group. Hence if we integrate $\rho(z)$ in these two regions we can establish a relation with the number of electrons present in the head group and chain of that particular lipid. i.e

$$A_L \times \int_0^{d_c} \rho(z) dz = N_c \quad (5.2)$$

and

$$A_L \times \int_{d_c}^{\frac{d}{2}} \rho(z) dz = \rho_w \left(\frac{d}{2} - d_c \right) A_L - \rho_w V_h + N_H \quad (5.3)$$

where -

A_L = Lateral area per lipid.

V_H = Volume of the head group

N_C = Total number of electrons in the chain region

N_H =Total number of electrons in the head group.

ρ_w = Electron density of water ($0.332e/\text{\AA}^3$)

For a lipid cholesterol binary mixture we can assume that the cholesterol does not contribute to the electron density of the head group region. This assumption is prompted by the fact that cholesterol molecule is known to sit at the interface between head and chain. With this assumption we can again define two regions in the edp as discussed earlier. But now the chain region also includes the contribution from cholesterol as shown in the fig. 5.9. Therefore for a lipid cholesterol mixture all these structural parameters will be replaced by the weighted average values. If the cholesterol concentration is X_c then the new parameters in eqn. (5.2) and (5.3) will be

$$\overline{A} = (1 - X_c)A_{lipid} + X_c A_{chol}$$

$$\overline{V_H} = (1 - X_c)V_H$$

$$\overline{N_C} = (1 - X_c)N_C + X_c N_{chol}$$

$$\overline{N_H} = (1 - X_c)N_H$$

Therefore if we know $\rho(z)$ on absolute scale and d_c then we can calculate X_c using the head and chain integration from the edp. However as discussed subsequently, to get the edp on absolute scale one requires several structural parameters like the lateral area per lipid, volume of the lipid, volume of the head group etc. For a mixture one needs a careful approach to calculate these parameters.

It is difficult to get $\rho(z)$ on absolute scale if the values of these structural parameters are unknown. Use of a calibration sample will not serve the purpose. This is because, since our bilayer systems studied here are multilamellar vesicle dispersions, it is impossible to estimate the concentration of scatterer in the scattering volume for such a system. Without having this knowledge we can not use a calibration sample to determine $\rho(z)$.

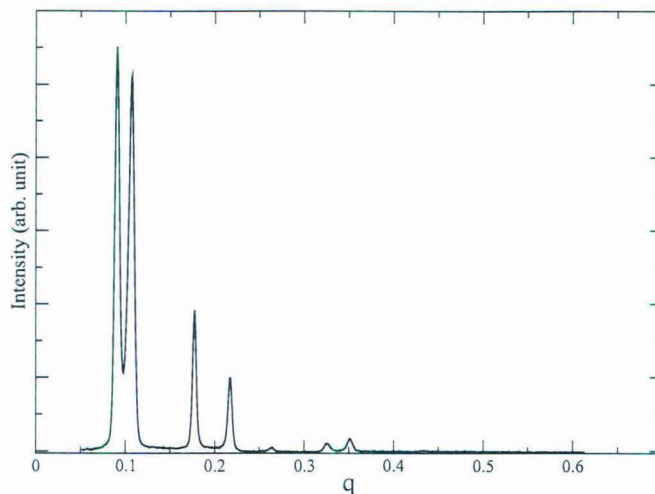


Figure 5.10: $I - q_z$ plot of phase separated equimolar mixture of DSPC-DOPC containing 20 mol% of cholesterol. The two sets of lamellar peaks correspond to l_o and l_d phases with lamellar periodicity of 69.26Å and 58.41Å respectively.

5.3.1.2 l_o - l_d phase separation in DSPC-DOPC-cholesterol mixtures

Even though there have been many studies on the fluid-fluid phase separation in ternary mixtures, but surprisingly some of the earlier scattering studies on these systems could not reveal such a co-existence. However fluid-fluid coexistence was observed in DPPC-DOPC-cholesterol mixtures by Karmakar *et al.* [12]. From the relative electron density profile constructed by Fourier synthesis of the diffraction data it was suggested that the l_o phase is rich in DPPC and the l_d phase in DOPC. But the cholesterol partitioning between these two phases could not be found [32].

In order to find the partitioning we have tried to analyze the scattering data from an unoriented samples of DSPC-DOPC and cholesterol. Most of the earlier studies on ternary mixtures have used DPPC-DOPC-cholesterol or spingomylin-POPC-cholesterol. We chose DSPC as the saturated part of the ternary mixture. The reason for this was that our aim was to find out the partitioning of cholesterol. Hence we wanted to match the two lipids in chain lengths to make them as similar as possible, so that the two coexisting phases can be considered essentially as binary lipid-cholesterol systems. Often only two orders of Bragg reflections are obtained from multilamellar lipid dispersions in the fluid phase. To obtain

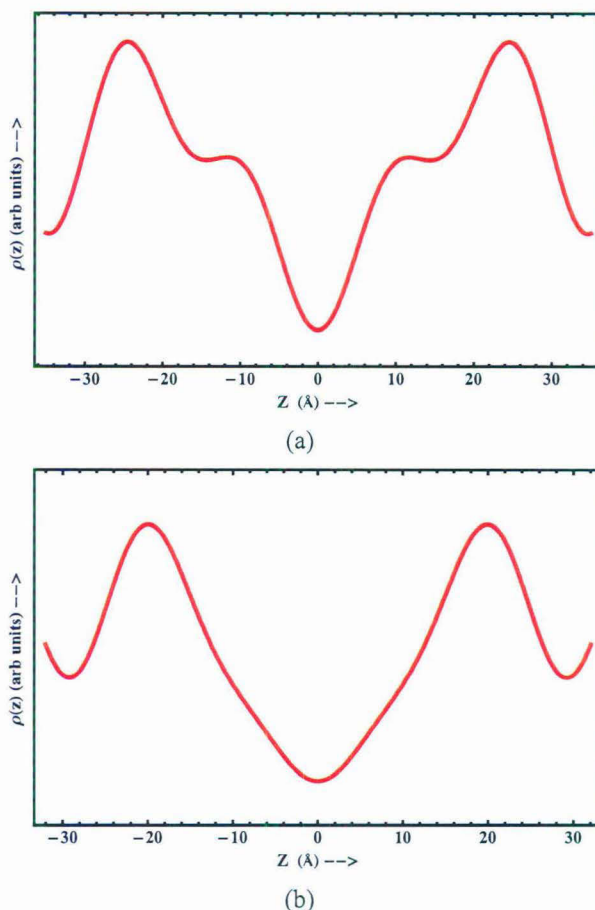


Figure 5.11: Relative electron density profile of (a) l_o and (b) l_d phases.

larger number of Bragg peaks we applied an osmotic pressure using a long chain polymer such as poly ethylene glycol (PEG). It is very similar to the condition of partial hydration. Small angle x-ray scattering was carried out at the ELLETRA-SAXS beamline. The data were collected on a PSD. The primary analysis was done using a software written by Dr. G. Pabst. The $I - q$ data showing the phase seapartion are shown in fig. 5.10.

Relative electron density profiles were constructed by Fourier synthesis of diffraction data. The relative edp for both l_o and l_d are shown in fig. 5.11. However to find the partitioning we need to put this edp on an absolute scale. To do so we followed a procedure existing in the literature as described in the following section.

5.3.2 Constructing electron density profile on absolute scale

Let us first consider the case of a one component lipid bilayer. The electron density of the bilayer is given by

$$\rho(z) = \rho_w + \frac{F(0)}{d} + \frac{2F_1}{d} \sum_{h=1}^{h_{max}} \alpha_h r_h \cos\left(\frac{2\pi h z}{d}\right) \quad (5.4)$$

where $\rho(w) = 0.332e/\text{\AA}^3$ is the electron density of water, $F(0)$ is the value of the form factor at $q = 0$, $\frac{2F_1}{d} = K$ is the scaling factor, α_h s are the phases of different Fourier components which can take the value ± 1 as discussed in chapter-1 and $r_h = \left|\frac{F_h}{F_1}\right|$ is the relative magnitude of the Fourier component corresponding to Miller index h.

As discussed in earlier chapters, in scattering studies of lipid bilayers most often an electron density in relative scale is presented. The reason for this is that from the scattering experiments only the absolute ratios $r_h = \left|\frac{F_h}{F_1}\right|$ can be correctly determined because F_h involves an unknown scaling factor. The electron density profile can be obtained on an absolute scale if the scaling factor is determined correctly.

One of the earlier attempts to put the edp on absolute scale was made by Weiner *et al.* [33], where the scattering data from DPPC in the gel phase was put on the absolute scale by a fitting procedure. A model describing the bilayer edp was fitted to the discrete form factors (r_h) obtained from the experimental data. For the gel phase the lateral area per lipid, which is an input parameter for getting the absolute edp, can be calculated accurately from the wide angle data. However in the fluid phase it becomes difficult to calculate the lateral area per lipid.

So the basic requisites for getting $\rho(z)$ on absolute scale are $F(0)$ and the scaling factor $k = \frac{2F_1}{d}$.

$F(0)$ which represents the contrast between the lipid bilayer and the solvent, can be calculated from the structural data of the lipid as-

$$F(0) = 2 \int_0^{d/2} (\rho(z) - \rho_w) dz = \frac{2(N_L - V_L \rho_w)}{A_L} \quad (5.5)$$

For lipids such as DPPC in the fluid phase $F(0)$ is very close to 0. Hence for a fluid phase data it is enough to calculate K correctly for constructing the absolute edp. In all our discussions we will be considering the case of the fluid phase.

However it is clear that accurate values of V_L , V_H , and A_L are essential for the calculation of $\rho(z)$. V_L and V_H values for many lipids are known to a reasonable accuracy from independent studies such as gravimetric measurements. A_L for a lipid in the gel phase can also be determined from the scattering experiments that is by calculating the lattice parameters from the wide angle peaks corresponding to the chain lattice. But in the fluid phase such area measurement is not possible because of the absence of any chain ordering. However with certain assumptions it is possible to get the fluid phase area of a lipid from its structural data in the gel phase. From the electron density profile in relative scale the separation between the head group peaks (X_{hh}) can be accurately determined. It has been shown that even with four order of diffraction X_{hh} can be determined to a fair accuracy. In addition, if the parameters like volume, hydrocarbon chain thickness (d_c) in the gel phase of a lipids are known, then the lateral area per lipid in the fluid phase of that particular lipid can be calculated [35]. The assumption that goes into such a calculation is that the change in volume in going from fluid to gel phase occurs only in the hydrocarbon chain region and the change in X_{hh} is mainly contributed by the change in d_c . This assumption is prompted by the fact that the head group which is buried in the water does not change its conformation in fluid and gel phases. Then we can write-(superscripts G and L are used for gel phase and fluid phase quantities)

$$V_L^F - V_L^G = A^F d_c^F - A^G d_c^G \quad (5.6)$$

and

$$\frac{X_{hh}^F - X_{hh}^G}{2} = d_c^F - d_c^G \quad (5.7)$$

Solving (5.6) and (5.7) we get an expression for lateral area in the fluid phase as -

$$A^F = \frac{V_L^F - V_L^G + A^G d_c^G}{d_c^G - \left(\frac{X_{hh}^G - X_{hh}^F}{2}\right)} \quad (5.8)$$

Since the structural information of the gel phase can be determined independently to get the fluid phase area one only needs the value of X_{hh} in the fluid phase, which can be determined from the edp in relative scale. Once A_L for the fluid phase ($= A^F$) is known then one can determine the scaling factor (K) in several ways as discussed below.

5.3.2.1 Using head group contrast

To calculate the scaling constant K we consider the contrast between the head group and water through the head group integral (H) which is defined as

$$A_L \times H = A_L \times \int_{d_c}^{d/2} (\rho(z) - \rho_w) dz = N_H - \rho_w V_H \quad (5.9)$$

where N_H is the number of electrons in the headgroup. $d_c = \frac{V_L - V_H}{A_L}$ defines the boundary between the head and chain region of the bilayer.

Now using eqn. (5.9) and (5.4) we obtain-

$$\begin{aligned} A \times \int_{d_c}^{d/2} (\rho(z) - \rho_w) dz &= \frac{A_L F(0)}{d} (d/2 - d_c) + A_L K \int_{d_c}^{d/2} \sum_h^{\alpha_h r_h} \cos\left(\frac{2\pi h z}{d}\right) dz \\ \Rightarrow N_h - V_h \rho_w &= \frac{A_L F(0)}{d} (d/2 - d_c) + A_L K \sum_h^{\alpha_h r_h d} \left[\frac{\sin(\pi h)}{2\pi h} - \sin\left(\frac{2\pi h d_c}{d}\right) \right] \end{aligned}$$

Hence the scaling constant K is given by

$$K = \frac{N_H - \rho_w V_H - F(0) \left(\frac{1}{2} - \frac{d_c}{d}\right)}{A_L \sum_h^{\alpha_h r_h d} \left[\frac{\sin(\pi h)}{2\pi h} - \sin\left(\frac{2\pi h d_c}{d}\right) \right]} \quad (5.10)$$

After we calculate the scaling constant K and $F(0)$ the electron density profile on a absolute scale can be determined from eqn. (5.4).

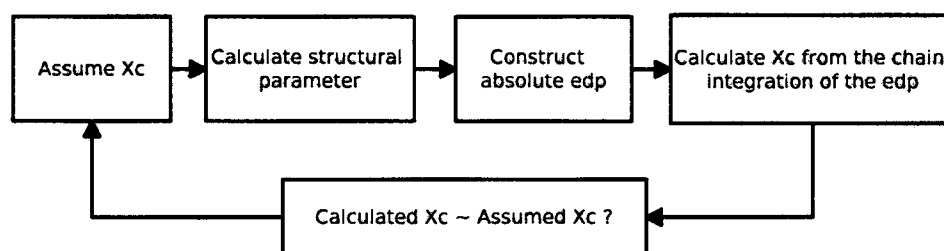


Figure 5.12: A self consistent way of calculating cholesterol partitioning from edp on absolute scale.

Now for a two component system we can calculate the edp on a absolute scale if we know the concentration of each component. Then the structural parameters required for the edp calculation as described above can be calculated using weighted average of the two components. But for the case of coexisting l_o and l_d phases since we do not know the concentration of cholesterol we can not calculate these parameters. Hence we tried a self consistent way. As depicted in the flow chart (see fig. 5.12) we first assume a cholesterol concentration then calculate the structural parameters. With that we constructed the edp on the absolute scale. Since we use the head integral to put on the absolute scale, we integrated the chain region of edp to find out X_c using eqn. 5.3 hoping that only for a particular value of X_c the initially assumed value and calculated value will converge. However we could not find a convergence. This is because these two integrals are not independent, since they add up to give $F(0)$. To our knowledge till date there have been no attempt to put the edp of a binary bilayer system on absolute scale.

5.3.2.2 Using a model

To analyze several data sets obtained from swelling experiments Nagle *et al.* used a model fitting procedure for getting the edp on absolute scale [35]. Here the authors used a model electron density profile known as 1G model to fit the experimental data from DPPC bilayers in the fluid phase. In the model the two head groups of the bilayer are defined by two Gaussian functions with mean position at $z = +X_{hh}/2$ and $z = -X_{hh}/2$. Where X_{hh} is the peak to peak distance between two head groups. Similarly the methyl trough is defined by another

Gaussian function with mean at $z = 0$. The height and the width of the head group Gaussian are defined by ρ_h and σ_h respectively. Similarly the methyl trough is defined by ρ_m and σ_m . With this the experimental data were fitted to get the absolute values of Fourier components. However the authors had to put several constraints in the model to get the lateral area per lipid similar to that obtained from gel phase data (for fluid phase DPPC $A_L = 62\text{\AA}^2$). Such an approach seems to produce inconsistent results when we tried to calculate A_L separately from head and chain regions using the scaling form factors obtained from the model as described in the following.

Inconsistency in A_L calculation in the model approach

From the absolute electron density profile of a bilayer one can get the relations for the lateral area per lipid as shown previously in eqn (5.2) and (5.3).

If we denote C_{int} and H_{int} as the head and chain integration respectively then -

$$C_{int} = \int_0^{d_c} \rho(z) dz$$

and

$$H_{int} = \int_{d_c}^{d/2} \rho(z) dz$$

Now using (5.2), and (5.3) we can get an expression for lateral area per lipid from head and chain integral as -

$$A_{chain} = \frac{N_C}{C_{int}}$$

and

$$A_{head} = \frac{N_H - V_H \rho_w}{H_{int} - \rho_w(\frac{d}{2} - d_c)} \tag{5.11}$$

If the edp is correctly obtained then $A_{chain} \approx A_{head} \approx A_L$. To test this we took two data set along with the scaling factor obtained from 1G model as reported in reference [35]. From

these two data sets we calculated edp on absolute scale using-

$$\rho(z) = \rho_w + \frac{2F_1}{d} \sum_{h=1}^{h_{max}} \alpha_h r_h \cos\left(\frac{2\pi hz}{d}\right) \quad (5.12)$$

Then using the structural parameter as given in the same reference we calculated the re-

Table 5.1: Form factor data for DPPC and the calculated areas from head and chain integrals.

$d(\text{\AA})$	f_2	f_3	f_4	$F_1(1G \text{ fit})$	$A_{head} (\text{\AA}^2)$	$A_{chain} (\text{\AA}^2)$
58.38	0.89	0.65	0.61	1.77	84.8	58.1
55.06	0.60	0.59	0.65	1.89	81.3	58.5

spective lateral areas from chain and head integration. The data are given in the table-5.1. Surprisingly we find that the values of A_{chain} and A_{head} differ significantly as can be seen from the table.

Using the head group contrast method the same data set produces consistent result for A_{chain} and A_{head} . This suggests that the scaling factor can be determined accurately using the head group contrast rather than using a model. Although using a model makes it possible to combine different data sets at different hydration levels, the method is complicated by the fact that many constraints have to be applied to the model to get consistent values of some of the parameters. Further the width of the Gaussian in the model turns out to be too small for the fluid phase. Hence this method is not satisfactory for many reasons.

5.3.2.3 Another way for obtaining electron density profile with minimum constraints

If A_L is known then one can also employ a very simple procedure for getting the edp on absolute scale. Let us revisit our parent equation which describes the electron density in absolute scale i.e

$$\rho(z) = \rho_w + \frac{F(0)}{d} + K \sum_{h=1}^{h_{max}} \alpha_h r_h \cos\left(\frac{2\pi hz}{d}\right) \quad (5.13)$$

To put the electron density profile on absolute scale we only need two parameters: One parameter(say ρ_b) which gives the constant added to the profile, and the second parameter

(say β_s) which gives a scaling factor. As described above $\rho_b = \rho_w + \frac{F(0)}{d}$ and $\beta_s = K$. With such a description equation (5.13) can be rewritten as -

$$\rho(z) = \rho_b + \beta_s \times \sum_{h=1}^{h_{max}} \alpha_h r_h \cos\left(\frac{2\pi h z}{d}\right) \quad (5.14)$$

If we know the lateral area per lipid molecule (A_L) and the hydrophobic thickness (d_c) it is possible to obtain ρ_b and β_s . We only use the constraint that the calculated areas from both the chain integral and the head integral should converge to A_L . In other words

$$A_{head} \cong A_{chain} \cong A_L \quad (5.15)$$

Then we can get corresponding H_{int} and C_{int} using eqn (5.11). From that ρ_b and β_s can be calculated easily. Then using those values the absolute edp can be obtained by eqn (5.14).

To test this approach we evaluated the edp on absolute scale using the form factor data of DPPC in fluid phase obtained from reference [35] as given in table-5.1. For $A_L = 62\text{\AA}^2$ and $d_c = 14.6$ using the first data set in the table we get $\rho_b = 0.33$ and $\beta_s = 0.083$ and for the second data set we obtain the values as $\rho_b = 0.33$ and $\beta_s = 0.090$. The corresponding F_1 values are 2.42 and 2.48 respectively.

5.3.2.4 Effect of the limiting number of Bragg peaks

As described earlier the electron density profile on an absolute scale should be deemed correct only when we get similar values for the lateral area per lipid from both head group (H_{int}) and chain (C_{int}) integration. To test whether the presence of only a few peaks in the data has significant influence on the areas calculated from H_{int} and C_{int} we followed a simple procedure.

Let us define the electron density profile of a bilayer using the 1G Gaussian model as discussed earlier. With such a description the model electron density profile can be written as -

$$\rho(z)_{model} = 0.332 + [\rho_H \{e^{-\frac{(z+x_h)^2}{2\sigma_h^2}} + e^{-\frac{(z-x_h)^2}{2\sigma_h^2}}\} - \rho_M e^{-\frac{z^2}{2\sigma_M^2}}] \quad (5.16)$$

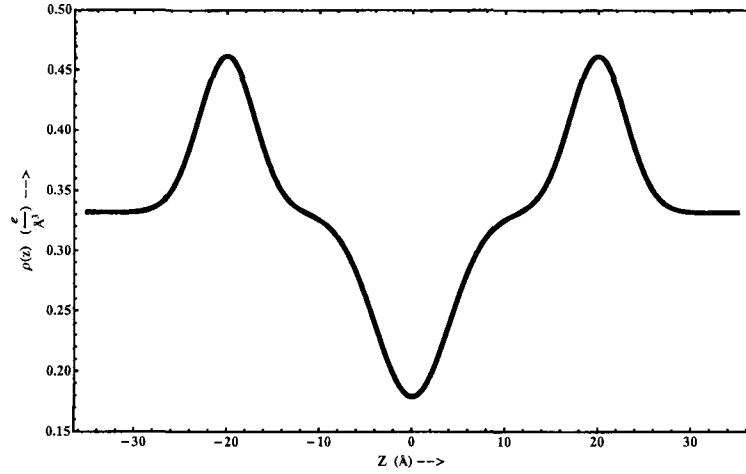


Figure 5.13: Electron density profile as described in eqn.5.16

In this model we took the width of the head group and methyl group gaussian as $\sigma_h = 3$ and $\sigma_m = 5$. With this we applied the area constraint as described in eqn. (5.15). We took the parameters as described in ref. [35] such as $d = 58.38$, $d_c = 14.6$, $A = 62\text{\AA}^2$. We varied the relative heights ρ_H and ρ_M in small incremental step of 0.001. Only those values of ρ_H and ρ_M were picked for which the calculated area from the head group integral and chain integral converge to a value of $62 \pm 0.5\text{\AA}^2$. With the values of the parameters mentioned above only a few sets of ρ_H and ρ_M satisfied our condition. We chose the value for which we observe the closest match between A_h and A_c . The values are $\rho_M = 0.156$, $\rho_H = 0.13$. Note that these values are with reference to the water level i.e 0.332. Hence the head group peak and the terminal methyl peak value will be 0.462 and 0.176. And the corresponding calculated areas are $A_c = 61.92\text{\AA}^2$ and $A_h = 61.93\text{\AA}^2$. With this the electron density profile on absolute scale looks like as given in fig. 5.13.

Then we obtained the Fourier transform of $\rho(z)_{model}$ to get the continuous form factor $F(q_z)$ as shown in fig. 5.14. Using the continuous form factor we created a data set (F_h) corresponding to $q_h = \frac{2\pi h}{d}$. $\rho(z)$ is then calculated using eqn. (5.13) by keeping F_h values upto a maximum order h_{max} . For every such profile we calculated the corresponding areas. The result of such an analysis is shown in fig. 5.15. Areas calculated from head and chain integral are shown on the plot. Our analysis suggests that even with a few Fourier components

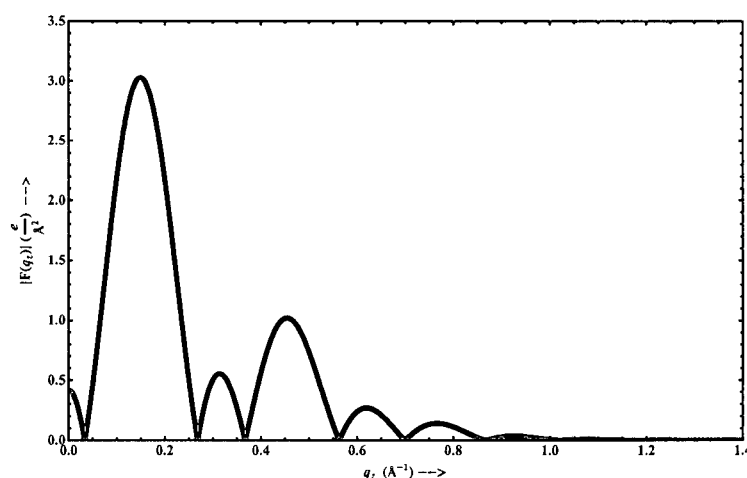


Figure 5.14: The continuous form factor $F(q_z)$ as obtained from the model edp.

the areas can be calculated within an error of 5\AA^2 . The convergence increases slightly on including a larger number of co-efficients. This suggests that higher order contribution is negligible and the edp can be represented with fair accuracy with discrete form factor data. Hence the difference between A_c and A_h in table-1 can not be attributed to having only a few peaks in the diffraction data.

5.3.3 Scheme of calculation of partitioning in two component system

As described earlier for a two component system the edp can be calculated on absolute scale if we know the value of A_{avg} . To get A_{avg} we need to know the molar fractions of each component in the mixture and their respective structural parameters such as molecular volumes, headgroup volumes. Also we need to know d_c . With all these we can calculate A_{avg} and subsequently put the edp on absolute scale. However for a system where the molar fractions of individual components in the mixtures are not known this calculation has to be done in a self consistent way. One approach is discussed below

- Construct edp on absolute scale for several known compositions of that particular system by collecting scattering data.
- Construct edp on absolute scale for the mixture of unknown composition by assuming

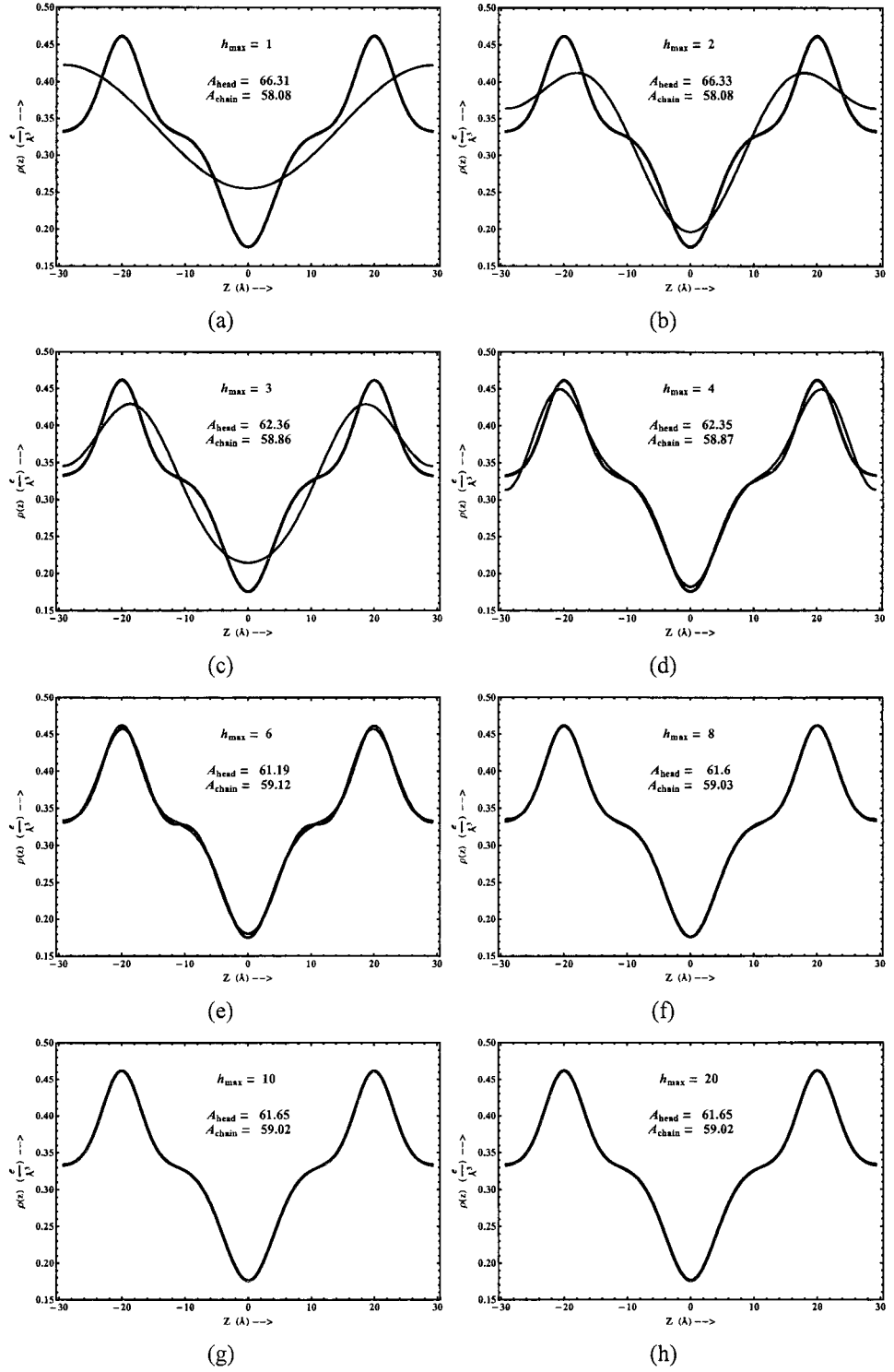


Figure 5.15: Reconstructed edp with varying no of Fourier components (up to h_{\max}) added (see eqn (5.13)). In each plot red curve represents the model edp and green curve represents the reconstructed profile

a molar ratio. Do this for different values of the molar ratio and compare the resulting edps with those obtained from each mixtures of known composition. Since the data corresponds to a particular composition (X^*), the edp of the mixture of unknown composition at $X_c = X^*$ will match best with that obtained from the mixture of composition X^* .

Now to test this procedure we first constructed a model edp for a binary mixture taking the A_{avg} for a particular molar fraction. Now if one were to do the scattering experiment with such a model bilayer then the data should contain the information about the molar ratios of individual components. However the question is from such experimental data can one extract that information. To address this question we took three different model bilayers with different compositions ($X_m, m = 1, 2, 3$). Then we constructed the model edp (ρ_{model}) for each of them. After that we generated the experimental data by taking the ratios of the form factors from one of these models. From the form factor ratios we obtained edp (ρ_{expt}) on absolute scale by assuming a particular composition with area constraint as described previously. This was repeated for different values of X_c . Then we compared ρ_{expt} with ρ_{model} by-

$$\rho_{diff}^2 = \int_0^{d/2} [\rho_{expt}(X_c) - \rho_{model}(X_m)]^2 dz$$

We plotted ρ_{diff}^2 for several values of X_c for each model. We used this method for three different cases which are described in the following

5.3.3.1 Binary mixture with cholesterol

We took the structural parameters of DSPC and cholesterol as follows

$$\text{DSPC} : V_{lipid} = 1264 \text{\AA}^3, V_{Head} = 319 \text{\AA}^3$$

$$\text{Cholesterol} : V_{chol} = 623 \text{\AA}^3,$$

The number of electrons in the lipid and cholesterol is 436 and 216 respectively. For lipid the number of electrons in the head group is taken as 164. For cholesterol the head

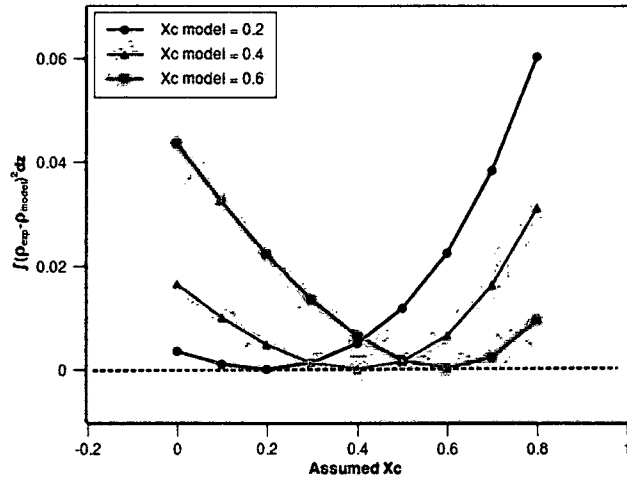


Figure 5.16: ρ_{diff}^2 as a function of X_c for the models with value of X_c given in the inset, for a bilayer of DSPC-cholesterol mixture

group volume is taken to be zero as we assume that the contribution of cholesterol only occurs in the chain region. Assuming the cholesterol concentration $X_c = 0.4$ we calculated $A_{avg} = \frac{(1-X_c)(V_{lipid}-V_{Head}) + X_c V_{chw}}{d_c}$. With this A_{avg} we constructed a model edp as described in 5.3.2.4. From such a model we calculated the experimental form factor ratios. Now this experimental ratios should contain the information about the composition of the binary mixture from which it was constructed. We constructed the edp by assuming different cholesterol molar fractions (X_c). Then we compared the obtained profiles with the models corresponding to 3 different values of X_c . Note that the experimental data is constructed from model X_c of 0.4. However when we matched the profile by calculating ρ_{diff}^2 we found that the profiles match equally well with all these models. This shows that we can not estimate the cholesterol concentration from such an analysis. The reason for this is that there is no contrast between cholesterol and water, since the electron densities are $0.34e/\text{\AA}^3$ and $0.332e/\text{\AA}^3$ respectively.

5.3.3.2 Binary mixture with a cholesterol like molecule with higher electron density

In our next part model we replace cholesterol with another toy molecule having higher electron density. The structural parameter taken for the second molecule are volume = 600, number of electrons = 250, Hence the electron density of this molecule = $0.416e/\text{\AA}^3$. Here also we

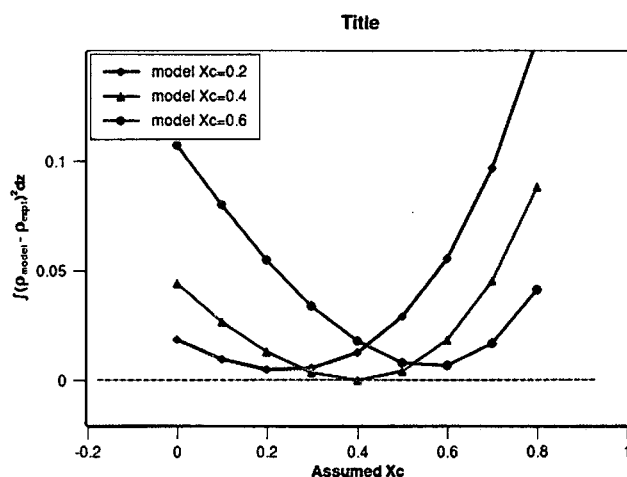


Figure 5.17: ρ_{diff}^2 as a function of X_c for the models with values of X_c given in the inset, for a mixture of DSPC with a cholesterol like molecule with higher electron density.

assumed that the molecule only contributes to the chain region similar to cholesterol. With such a binary system we again followed the previous procedure to calculate ρ_{diff}^2 . The result is shown in fig. 5.17. Here the profile matched only at $X_c=0.4$. At $X_c=0.2$ though we see a minimum in ρ_{diff} still the values are significantly higher than the minimum at $X_c=0.4$.

5.3.3.3 Binary mixture of two lipid molecules with contrast in electron density

Finally we took a more general case of a binary mixture of two lipids. lipid 1 is DSPC. lipid 2 is again another toy molecule having structural parameters as volume= 900 \AA^3 , headgroup volume = 400 \AA^3 , total number of electrons = 300, number of electrons in head group= 100. Hence for this molecule the overall electron density = $0.300 e/\text{\AA}^3$ which is less than that of DSPC. With such a binary mixture we again calculated ρ_{diff}^2 for three different model edp at $X_c=0.2, 0.4, 0.6$. The experimental profile was constructed from $X_c=0.4$. As seen in figure. 5.18 the experimental profile matched well only at $X_c=0.4$.

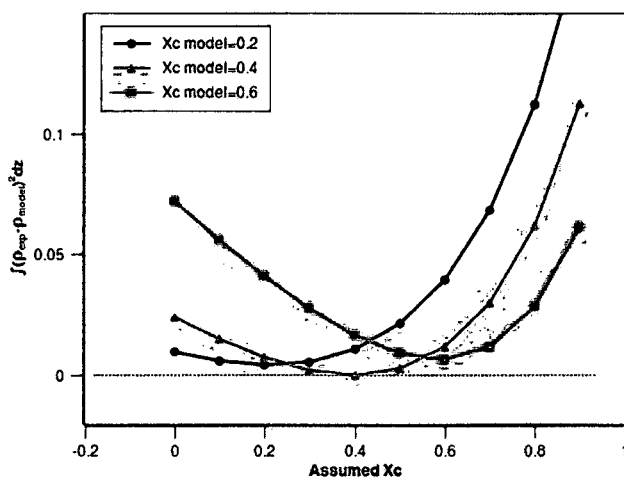


Figure 5.18: ρ_{diff}^2 as a function of X_c for the models with values of X_c given in the inset, for a mixture of two lipids with different electron densities.

5.4 Discussion

We have carried out systematic investigation of the phase behaviour of ternary mixtures containing ergosterol and cholesterol. The phase behaviour was studied using x-ray diffraction on aligned bilayer stacks of the above mixtures. We have also studied GUVs prepared from these mixtures at a few sterol concentrations.

A partial phase diagram of DPPC-DOPC-ergosterol mixtures obtained from diffraction studies is shown in fig. 5.19. The transition temperature increases slightly with sterol concentration ($\sim 4^\circ\text{C}$ up to 25 mol%). The important feature of this phase diagram is the observation of fluid-fluid coexistence at intermediate sterol concentrations. At relatively higher concentrations (~ 33 mol%) we observed additional scattering. These sharp peaks do not disappear even at very high temperatures. This may arise because of some highly ordered phase (i.e. crystallites). It appears that at ~ 33 mol% ergosterol phase separates. This is an interesting observation as for DPPC-DOPC-cholesterol mixtures the fluid-fluid coexistence is observed up to ~ 35 mol% [32]. This suggests that ergosterol concentration in both DPPC and DOPC saturates at relatively lower values than those of cholesterol. We have only investigated equimolar mixtures of DPPC and DOPC at different ergosterol concentrations. Further investigations at various other concentrations of lipids may provide additional insights in this

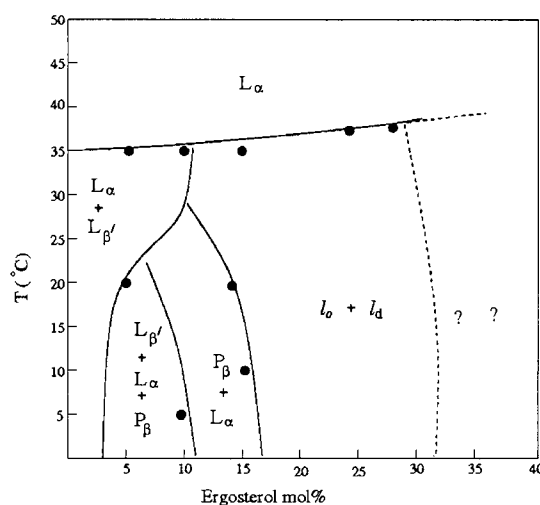


Figure 5.19: Partial phase diagram of DPPC-DOPC-ergosterol mixtures with equimolar DPPC and DOPC. The region marked by ? corresponds to a highly ordered phase observed at high concentrations of ergosterol.

comparison with cholesterol system.

Our microscopy observations on GUVs prepared from equimolar mixtures of DPPC and DOPC at 30 mol% of ergosterol also complement the diffraction results. Though the domains observed have circular shape resembling fluid domains, the fact that they do not coalesce with each other suggests that they are more ordered than the normal fluid phase domains. We have not done a controlled experiment with temperature variation. So we can not infer anything about the kinetics of such ordered domain formation. The sudden change in temperature from high temperature electroformation chamber to the room temperature coverslip for observation may be responsible for the observed chains of small circular domains. However under similar procedure ternary mixtures with cholesterol show fluid-fluid phase separation and coalescence of domains.

The phase behaviour of DPPC-DOPC-cholestenone mixtures has several interesting features. First the observation of fluid phase at temperature $\sim 20^\circ\text{C}$ suggests a significant decrease in the transition temperature from that of the DPPC-DOPC mixture (1:1), for which the transition temperature is close to 35°C . Though we observed fluid-fluid coexistence at 20 mol% of cholestenone, we could not conclusively establish it. This is because of the fact that sharp scatterings along with additional peaks in the small angle region started appearing at

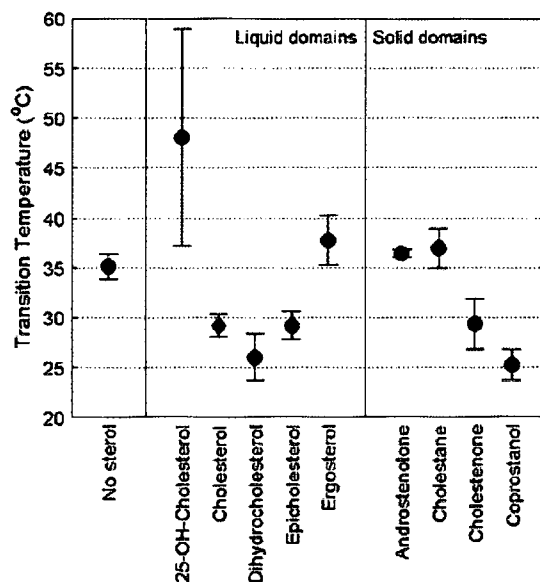


Figure 5.20: Transition temperature of 1:1:1 mixture of DPPC-DOPC-Sterol with various sterols (taken from ref [28])

25 mol%. And at 33 mol% these sharp peaks were recorded even at high temperatures suggesting a demixing transition. Microscopic studies on GUVs of DPPC-DOPC-cholestenone mixtures at 30 mol% showed the presence of gel like domains. But interestingly after ~ 30 minutes we observed tubule formation in these GUVs. Similar observation of tubules were noted also for 20 mol% of sterol concentration and binary mixtures of DOPC-cholestenone. At present we do not know the reason for such an observation.

Using fluorescence microscopy on GUVs Beattie *et al.* studied the effect of sterol structures on the miscibility and transition temperature of 1:1:1 mixture of DPPC/DOPC/sterol [28]. According to their results for ergosterol the transition temperature at equimolar concentration is slightly above that of DPPC-DOPC mixtures. Whereas for cholestenone the transition temperature was observed to be significantly lower. A plot of transition temperature with several sterols taken from [28] is shown in fig. 5.20. Our observations on both ergosterol and cholestenone ternary mixtures also show very similar results though for the case of cholestenone we observe still lower transition temperature even for lower concentrations. Moreover in their studies Beattie *et al.* have classified the sterols as promoters or inhibitors

depending upon the ability to induce fluid fluid phase separation. According to them ergosterol is a promotor and induces a fluid-fluid coexistence but cholesterol does not. Our studies on GUVs of ergosterol system seems to suggest that one of the two fluid phases is more ordered and does not coalesce. However in DPPC-DOPC-cholesterol mixtures we also observed a fluid-gel coexistence.

Using x-ray diffraction we have observed a fluid-fluid (l_o - l_d) phase separation in ternary mixtures of DSPC-DOPC-cholesterol. We could obtain up to four orders of Bragg peaks from the multilamellar dispersions of the above mixture by using a long chain polymer (PEG) to apply an osmotic pressure. We have constructed the electron density profile for both l_o and l_d phases by Fourier reconstruction method. The partitioning of cholesterol can be found out from the scattering data by putting the edp on an absolute scale as discussed earlier. However while doing so we came across some shortcomings of previous methods to get the absolute edp. We showed the inconsistency in this method by analyzing available data in the literature. We also show that the scaling factor can be carefully calculated by incorporating the area constraint so that both head and chain integrals give consistent values for the lateral area per lipid.

However we could not determine cholesterol partitioning between l_o and l_d phases using a self consistent approach. We think the reason for this is that there is no contrast between cholesterol and water, since the electron densities of water and cholesterol are 0.332 and 0.34. Our model calculation for binary system also suggests that for two molecules having sufficient contrast in electron density one can obtain the partitioning by comparing the profiles with the profiles obtained from known concentrations. Therefore to calculate the partitioning from the scattering data one needs to create a contrast between the species. One possible way to do so is to use a functionalized cholesterol molecule with an electron heavy group or neutron diffraction with deuterated species.

5.5 Conclusion

We have studied the phase behaviour of DPPC-DOPC-ergosterol and DPPC-DOPC-cholestenone mixtures using small angle x-ray scattering. The phase behaviour of both these system have several differences. Fluid-fluid coexistence was seen in the ergosterol system. Our studies on DSPC-DOPC-cholesterol mixtures show l_o - l_d coexistence. We could not find out the partitioning of cholesterol form the x-ray data because of inherent problem which arises due to the lack of contrast between the electron densities of cholesterol and water. Hence we propose a procedure to find such partitioning by varying the contrast. We also showed that the existing methods to get absolute electron density profile leads to some inconsistency in the lateral area calculated from head and chain regions of the lipid bilayer. We propose a simpler method to avoid such a discrepancy.

Bibliography

- [1] M. Edidin, *Annu. Rev. Biophys. Biomol. Struct.*, **32**, 257 (2003).
- [2] R. Lipowsky, *J. Biol. Phys.*, **28**, 195 (2002).
- [3] K. Simons and E. Ikonen, *Nature*, **387**, 569 (1997).
- [4] K. Gaus, E. Gratton, E. P. W. Kable, A. S. Jones, I. Gelissen, and L. Kritharides, *Proc. Natl. Acad. Sci. U.S.A.*, **100**, 15554 (2003).
- [5] T. P. W. McMullen, R. N. A. H. Lewis and R. N. McElhaney, *Curr. Opin. colloid Interface Sci.*, **8**, 459 (2004).
- [6] D. A. Brown and E. London, *J. Biol. Chem.*, **275**, 17221 (2000).
- [7] E. London and D. A. Brown, *Biochim. Biophys. Acta*, **1508**, 182 (2000).
- [8] T. J. McIntosh, A. Vidal, and S. A. Simon, *Biophys. J.*, **85**, 1656 (2003).
- [9] P. Sharma, R. Varma, R. C. Sarasij, K. G. Ira, G. Krishnamurthy, M. Rao, and S. Mayor, *Cell*, **116**, 577 (2004).
- [10] C. Eggeling, C. Ringemann¹, R. Medda¹, G. Schwarzmann, K. Sandhoff, S. Polyakova, V. N. Belov¹, B. Hein, C. Middendorff, A. Schnle¹ and S. W. Hell, *Nature*, **457**, 1159 (2009).
- [11] T. Baumgart, S. T. Hess, and W. W. Webb, *Nature*, **425**, 821 (2003).

- [12] S. Karmakar, B. R. Sarangi and V. A. Raghunathan, *Solid State Communication*, **139**, 630 (2006).
- [13] S. L. Veatch and S. L Keller, *Phys. Rev. Lett.*, **89**, 268101 (2002).
- [14] S. L. Veatch and S. L Keller, *Biophys. J.*, **85**, 3074 (2003).
- [15] S. L. Veatch, I. V. Polozov, K. Gawrisch, and S. L Keller, *Biophys. J.*, **86**, 2910 (2003).
- [16] R. F. M. de Almeida, A. Fedorov, and M. Prieto, *Biophys. J.*, **85**, 2406 (2003).
- [17] M. Gandhavadi, D. Allende, A. Vidal, S. A. Simon, and T. J. McIntosh, *Biophys. J.*, **82**, 1469 (2002).
- [18] D. Scherfeld, N. Kahya, and P. Schwille, *Biophys. J.*, **85**, 3758 (2003).
- [19] G. W. Feigenson and J. T. Buboltz, *Biophys. J.*, **80**, 2775 (2001).
- [20] H. M. McConnell and M. Vrljic, *Annu. Rev. Biophys. Biomol. Struct.*, **32**, 469 (2003).
- [21] H. M. McConnell and A. Radhakrishnan, *Biochim. Biophys. Acta*, **1610**, 159 (2003).
- [22] H. A. Rinia, M. M. E. Snel, J. P. J. M. van der Eerden, and B. de Kruijff, *FEBS Lett.*, **501**, 92 (2001).
- [23] J. Korlach, P. Schwille, W. W. Webb, and G. W. Feigenson, *Proc. Natl. Acad. Sci. U.S.A.*, **96**, 8461, (1999).
- [24] M. Ge, K. A. Field, R. Aneja, D. Holowka, B. Baird, and J. H. Freed, *Biophys. J.*, **77**, 925 (1999).
- [25] P. E. Milhiet, C. Domec, M. Giocondi, N. V. Mau, F. Heitz, and C. Le. Grimellec, *Biophys. J.*, **81**, 547 (2001)
- [26] N. Kahya, D. Scherfeld, K. Bacia, B. Poolman, and P. Schwille, *J. Biol. Chem.*, **278**, 28109 (2003).

- [27] L. Chen, Z. Yu and P. J. Quinn, *Biochim. Biophys. Acta*, **1768**, 2873 (2007).
- [28] M. E. Beattie, Sarah L. Veatch, Benjamin L. Stottrup and Sarah L. Keller, *Biophys. J.*, **85**, 3074 (2003).
- [29] R. P. Rand, V. A. Parsegian, J. A. C. Henry, L. J. Lis and M. McAlister, *Can. J. Biochem.*, **58**, 959 (1980).
- [30] S. Karmakar and V. A. Raghunathan, *Phys. Rev. E*, **71**, 061924 (2005).
- [31] M. R. Vist and J. H. Davis, *Biochemistry*, **29**, 451 (1990).
- [32] S. Karmakar, *Phase Behaviour of lipid-cholesterol membranes*, Thesis submitted to JNU, Delhi, (2001).
- [33] M. C. Wiener, R. M. Sutter and J. F. Nagle, *Biophys. J.*, **55** 315 (1989).
- [34] J. F. Nagle and M. C. Wiener, *Biophys. J.* **64**, 1476 (1989).
- [35] J. F. Nagle, R. Zhang, S. Tristram-Nagle, W. Sun, H. 1. Petrache and R. M. Suter, *Biophys. J.*, **70**, 1419 (1996).

Chapter 6

Preparation of a simple cellular environment: Cell blebs

6.1 Introduction

In earlier chapters we have described studies on model membranes. Considering the fact that model membranes often consist of a small number of lipid components, it is rather easy to study model membrane systems. On the other hand cell membranes which possess greater complexity are more challenging to study quantitatively. It is, however, possible that this complexity of cell membranes could lead to qualitatively new behaviour not seen in model membranes. Therefore, recently there has been growing interest in detached cell blebs as a more relevant "model" system.

Blebs are spherical cellular protrusions that occur in many physiological situations such as cytokinesis, cell spreading, virus uptake, and apoptosis [1, 2]. Blebbing is quite common in animal cells. Blebs have been observed both *in vitro* and *in vivo*. Freshly plated fibroblast cells with a dynamically unstable cortical actin mesh exhibit spontaneous blebbing [3, 4]. The cell volume during blebbing is conserved [3]. The mechanism of such a bleb formation has been addressed in ref [5]. In the case of natural blebbing in cells, blebs form on the cell surface and retract back. The time scale for formation is ~ 30 seconds, whereas the retraction timescale is ~ 120 seconds [5]. Blebbing can also be induced artificially by a variety

of methods [4]. These blebs have been shown to be free of cellular organelles, with lipid compositions representative of the plasma membrane, and phospholipid/cholesterol ratios of $\approx 2 : 1$ [6, 7, 8]. Also these blebs can be detached from the cell surface [6, 9, 10]. These detached blebs are sometimes referred to as giant plasma membrane vesicles (GPMVs). Since blebs are part of the plasma membrane, the GPMVs provide a very ideal cellular environment to study many biological processes. Recently the membrane organization of these GPMVs was studied using fluorescence markers. Large scale fluid-fluid phase separation was observed in these GPMVs below physiological temperatures. The fluid-fluid phase separation was inferred by the partitioning of the fluorescence markers [10]. This kind of phase separation is analogous to the $l_o - l_d$ phase separation observed in ternary mixtures in model membrane systems and is of immense importance in view of the “raft hypothesis” described in earlier chapters.

Recent studies suggest that the cytoskeleton plays an active role in the organization of lipids in the plasma membrane [11]. The cell free blebs give an ideal system to study such coupling between the cytoskeleton and membrane organization. If cell detached blebs can be produced with actin cytoskeleton inside then the activity of the cytoskeleton inside the blebs can be controlled. For example actin monomers inside the blebs can be polymerised by ATP. With such control the membrane organization of the blebs can be studied as a function of the activity of the cytoskeleton. Motivated by this idea we tried to prepare cell detached blebs following several existing protocol. In this chapter we describe our studies on these cell blebs.

6.2 Experimental results

6.2.1 Cell culture and imaging

Chinese Hamster Ovarian (CHO) cells stably transfected with GFP-GPI anchored proteins were used for all our experiments (*source : Dr. S. Mayor, NCBS, Bangalore, India*). Cells were grown in Ham’s F12 medium (HF12) (*HiMedia, Bombay, India*) supplemented with

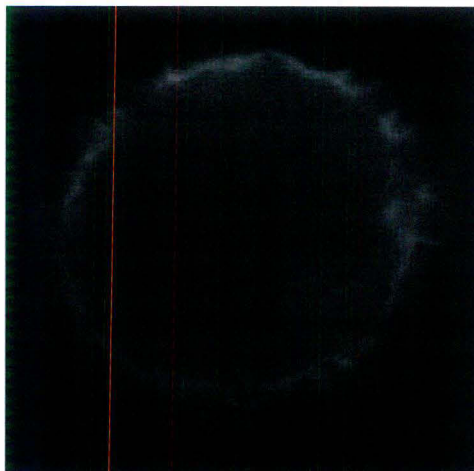


Figure 6.1: Spontaneous blebbing in freshly plated CHO cells.

10 % fetal bovine serum (FBS) (*GIBCO, Carshland, CA, USA*). Appropriate selection antibiotic and combination of penicillin and streptomycin as antibacterial agents were used in the medium . Cells were cultured at 37°C at 5% CO_2 . All necessary buffers such as PBS, imaging buffer etc were prepared in the laboratory using required reagents purchased from *Sigma-Aldrich, USA*. Cell imaging was done with the help of fluorescence labelling. All the imaging was performed either on a TE-2000 or a TE-300 (*Nikon, Japan*) microscope.

6.2.2 Cell blebbing

As described in the previous section cells bleb under various conditions. Spontaneous cell blebbing can occur in response to a stressfull environment [2]. We have also observed this kind of spontaneous blebbing in freshly plated CHO cells. After replating the cells on a petridish, it was observed under a microscope. Blebbing was observed when cells approach the surface of the petridish (fig. 6.1). The time scale for bleb growth was observed to be ~ 30 seconds and the retraction timescale was about 1 – 2 minutes.

Blebbing can also be induced by chemical treatments. We followed various well documented protocols to induce blebbing as described in the following.



Figure 6.2: Blebbing in ethanol treated CHO cells.

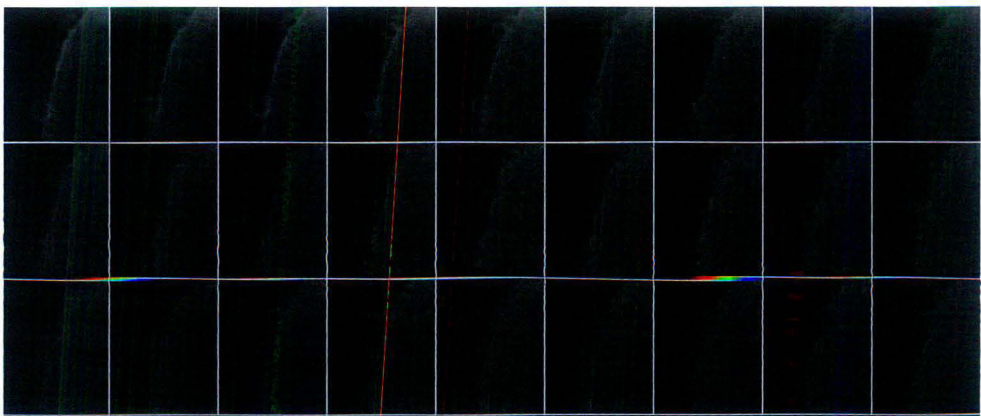


Figure 6.3: Formation and retraction of cell blebs. Each picture differs from the previous one by a time difference of 10 s. To be seen from left to right and top to bottom.

6.2.2.1 Ethanol treatment

In this method the adhered CHO cells were treated with ethanol(5% v/v) in the petridish and observed under the microscope. A few minutes after the treatment the cells start to blebb (fig. 6.2). All the blebs were attached to the cells and retract within a time scale of 1-2 minutes. A montage showing the bleb formation and retraction in ethanol treated CHO cells is given in fig. 6.3. The size of the blebs was of the order of 5 microns. But with this method we did not get detached blebs. Even rigorous shaking could only produce a very small number of detached blebs.

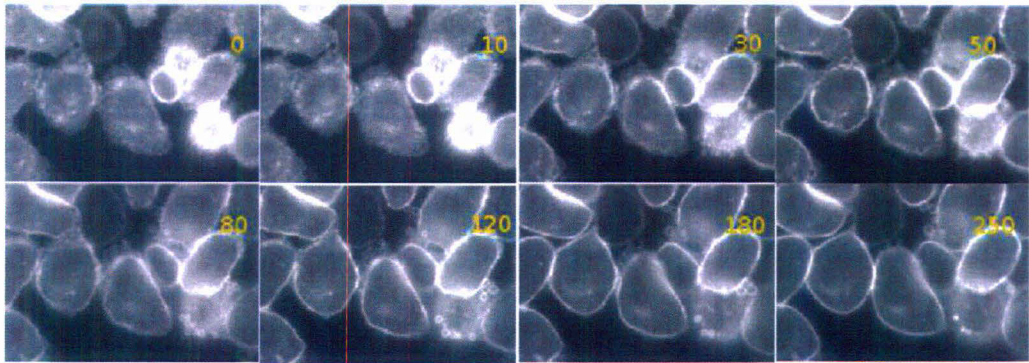


Figure 6.4: Cells after osmotic shock. Timeline in seconds is shown in top right corner of each image. Blebs can be seen appearing after $\sim 30s$.

6.2.2.2 Osmotic shock

In this method the cells were subjected to a high osmotic shock within a short timescale. The osmotic shock was applied by replacing the medium in the petridish by double distilled water. To have maximum possible osmotic pressure, all the medium in the petridish was replaced by water. Because of such a shock the cells swell within a few seconds and reach a limiting value. The swelling of cells after the application of osmotic shock is depicted in fig 6.4. As seen in the figure the observed projected area of the cells increase with the application of osmotic shock which is due to the influx of water in to the cell. The increase in projected area as a function of time is shown in fig. 6.5. It is rather difficult to measure the observed area of a fully spread adhered cell. Hence we normalize the area to a value observed at 30 second after the application of osmotic shock where we could see the projected edge of the cell with reasonable accuracy. However the qualitative feature of the swelling remains unperturbed with such a normalization. Our measurements show that , the projected areas of most of the cells increase by $\sim 30\%$ from our reference point (= Area at 30 s).

Because of such a shock some portions of the membrane protrude out in the form of blebs. As seen in fig 6.4 we observed these blebs $\sim 30s$ after the application of the osmotic shock. Though blebbing was observed with such a treatment, the number of blebs produced was very less and very few of them were detached from the cell.

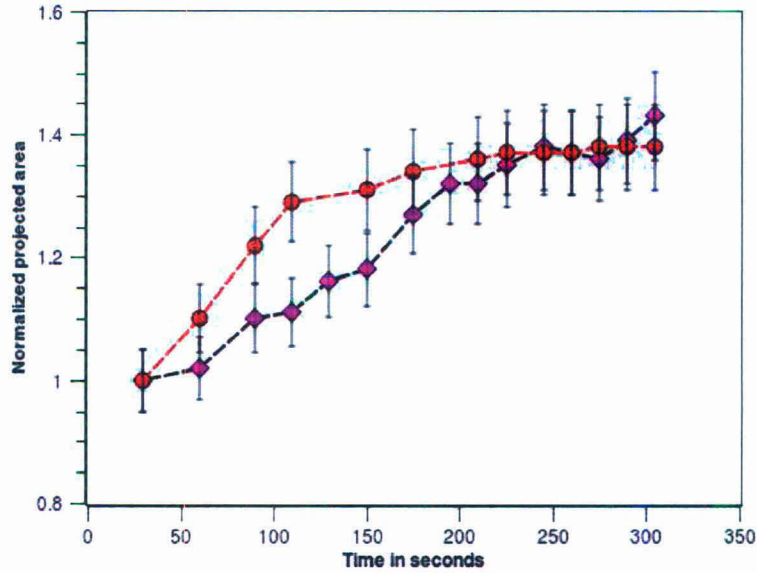


Figure 6.5: Normalized projected area as a function of time.

6.2.2.3 Formaldehyde treatment

We adopted a method described in [10] to produce cell detached blebs . In this method the cells were treated with 20mM formaldehyde and 2mM dithiothreitol (DTT) along with a buffer known as GPMV buffer. Then the cells were incubated for 1 hr at 37°C and 5% CO_2 . With this treatment blebs come out of the cell surface into the buffer. This buffer which contains the suspended blebs was then transferred to another petridish for observation under the microscope. We observed a lot of detached blebs or the GPMVs suspended in the medium. This method produces a large number of detached blebs (fig.6.6). The typical size of the blebs was in the range 5-20 microns.

6.2.2.4 Actin detection in detached cell blebs

To find out the presence of actin in these detached blebs we labelled the actin with the red fluorescent protein cherry (actin-cherry)(CA). Then we followed the formaldehyde treatment as mentioned above to produce detached blebs. The blebs detached from transfected cells were observed for the CA signal. Two channel fluorescence microscopy was performed to see both the GFP tagged membrane and CA tagged actin. The results are shown in fig.

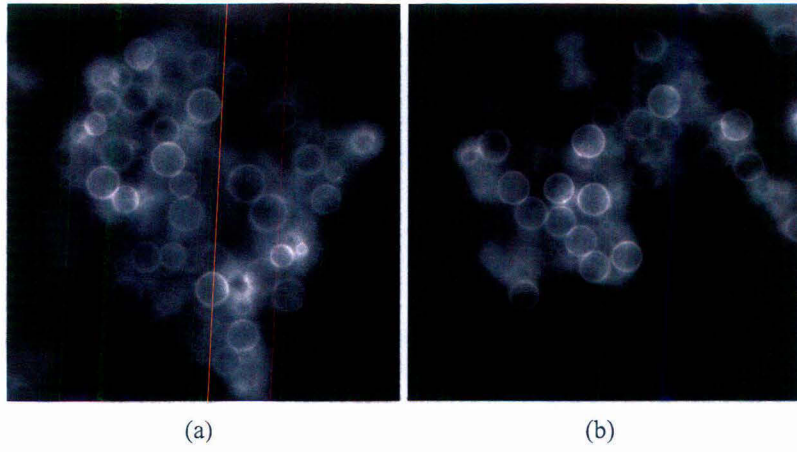


Figure 6.6: Detached blebs.

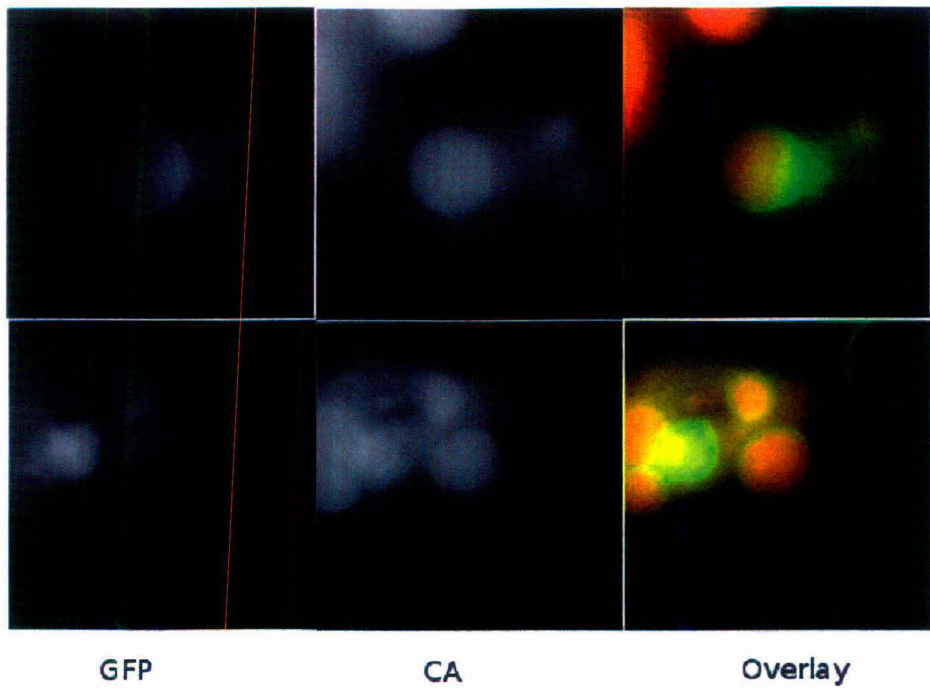


Figure 6.7: Actin in detached cell blebs. GFP Channel and CA channel is colored with green and red respectively in the overlay image.

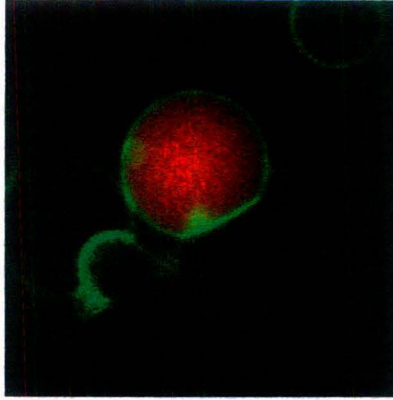


Figure 6.8: Detached blebs labelled with GFP (green) and CA (red).

6.7 and 6.8. The blebs which would have detached from the CA transfected cells show the presence of actin inside them.

6.3 Discussion

Blebs which are representative of plasma membranes provide a simpler cellular environment, compared to the plasma membrane itself. Hence they are an ideal platform to perform various biological experiments in a controlled way. In particular it is a nice system to study coupling of the cytoskeleton to the lipid organization within the membrane.

The osmotic swelling of cells can be understood by the following as described in reference [12]. Briefly, the osmotic pressure difference across the membrane can be written as-

$$\Delta\Pi = kT(\Delta\phi) \tag{6.1}$$

where $\Delta\phi$ is the difference in concentration of osmotically active particles (such as ions) inside and outside the cells. With this the change in volume can be approximated as -

$$\Delta V \propto L_p \Delta\Pi \tag{6.2}$$

where L_p is the membrane permeability. Hence the steady state is defined by the osmotic pressure balance. The water influx will continue till a steady state is reached. This influx

will cause cell swelling and after a steady state is reached the swelling will also stop. Our measurement of the projected area as a function of time, reflects such a feature. At longer time scales the cell tries to counteract the osmotic imbalance via some active mechanism such as opening of ion channels [12]. However we have not observed for longer timescales as our main aim was to produce cell free blebs using such a osmotic shock.

We have tried several protocols existing in the literature to produce detached blebs called as Giant plasma membrane vesicles(GPMVs). In ethanol induced blebbing and the spontaneous blebbing case we have observed the formation and retraction time scales of the cellular blebs. The formation of a bleb takes place within $\sim 20s$ and retraction takes 1 – 2 minutes. These observations are in accordance with earlier observations [5]. Ethanol treatment and the osmotic shock do not produce cell detached blebs . In both cases some separation method such as shaking or centrifuging has to be employed to get detached blebs. Cell free blebs are easily produced by formaldehyde treatment. We obtained a large number of detached blebs following such a procedure. We also found the presence of actin in the detached blebs. But we could not confirm whether the actin is in filamentous form or monomeric form. This is because of the reason that CA labels both F-actin and monomers. However formaldehyde treatment has a serious disadvantage. Formaldehyde fixes the cells by crosslinking the proteins. We have observed that after such a treatment to produce cell free blebs, the parent cells do not survive. Hence using formaldehyde the detached blebs produced will have most of its proteins non-functional. So further biological experiments on such a system will not be useful. However such a system can be used to study some of the passive behaviours of the plasma membranes such as the membrane organization. Such a study was reported recently in reference [10] where the authors observed fluid-fluid co-existence below physiological temperature in these GPMVs obtained from various cell lines.

However for certain experiments the proteins within the GPMVs might have to remain active. Then it may be necessary to use a protocol which does not perturb the cell chemically. As we have shown, detached blebs can be obtained using a purely non-chemical treatment such as osmotic shock. Though the number of detached blebs produced with osmotic shock is

small, the yield can be enhanced using some separation techniques like shaking, centrifuging etc. We have not studied in detail the effectiveness of such procedures. We have shown the presence of actin in the cell free blebs. Therefore, it is very likely that the actin meshwork in these blebs can be made active by providing proper physiological conditions. In such a scenario the coupling of the membrane organization to the activity of actin can be studied in a controlled environment.

6.4 Conclusion

We have tried several documented protocols to prepare cell blebs using CHO cells. Both cell attached and cell detached blebs were produced. We also found out that such cell detached blebs contain actin, and hence can be ideal for studying the coupling of the cytoskeleton to membrane organization. Although formaldehyde+DTT treatment produce cell detached blebs, we believe the blebs produced by this method will not have any biological activity. On the other hand, detached blebs produced using osmotic shock may retain their biological activity and could be very useful for a variety of experiments aimed at understanding the plasma membrane.

Bibliography

- [1] T. Tokumitsu , K. Maramorosch, *J. Cell Biol.*, **34**, 677 (1967).
- [2] G. J. Gores, B. Herman and J. J. Lemasters, *Hepatology*, **4**, 609 (1990)
- [3] G. T. Charras, J. C. Yarrow, M. A. Horton, L. Mahadevan and T. J. Mitchison, *Nature*, **435**, 365 (2005).
- [4] H. Keller, P. Rentsch, and J. Hagmann, *Exp. Cell Res.*, **277**, 161 (2002).
- [5] G. T. Charras, M. Coughlin, T. J. Mitchison and L. Mahadevan, *Biophys. J.*, **94**, 1836 (2007).
- [6] R. Scott and P. Maercklein *J Cell Sci*, **35**, 245 (1979).
- [7] A. Gidwani, D. Holowka and B. Baird, *Biochemistry*, **40**, 12422 (2001).
- [8] E. K. Fridriksson, P. A. Shipkova, E. Sheets, D. Holowka, B. A. Baird and F. M. McLafferty, *Biochemistry*, **38**, 8056 (1999).
- [9] R. Scott, *Science*, **194**, 743 (1976).
- [10] T. Baumgart, A. T. Hammond, P. Sengupta, S. T. Hess, D. A. Holowka, B. A. Baird and W. W. Webb, *Proc. Nat. Acad. of Sc.*, **104**, 3165 (2007).
- [11] G. R. Chichili and W. Rodgers, *Cell. Mol. Life Sci.*, **66**, 2319 (2009).
- [12] P. A. Pullarkat, P. Dommersnes, P. Fernández, J. F Joanny and A. Ott, *Phys. Rev Lett*, **96**, 048104, (2006).

Summary and outlook

In this thesis we have systematically studied the structure and phase behaviour of PC-sterol bilayers. We have used several sterols such as cholesterol, ergosterol, lanosterol, cholestenone, 25-hydrocholesterol (25HC), cholestane and 7-deydrocholesterol (7DHC) to study their influence on the phase behaviour of DPPC bilayers.

The hydration level strongly influences the phase behaviour of PC-cholesterol bilayers. In agreement with earlier studies a significant increase in the main transition temperature (T_m) was observed at low hydration. The gel phase is stabilized at low relative humidities (RH) and we do not see the ripple phase at these low RHs. However the modulated phase (P_β) exists at low RH as long as the tilt angle of the chains in the gel phase is non zero. This result highlights the importance of the chain tilt in the formation of this phase. Our results on DPPC-cholesterol in excess water seems to suggest that the modulated phase ceases to exist in excess water. Instead we observe a fluid phase (L'_α) with higher lamellar periodicity, which can arise from a lowering of the membrane rigidity due to the coupling between cholesterol concentration and the curvature of the bilayer.

The phase behaviour of DPPC bilayers in the presence of above mentioned sterols has some universal features. Firstly at high sterol concentration the main transition is completely abolished and we see a fluid phase at all temperatures. The concentration at which it occurs is slightly higher for other sterols as compared to cholesterol. Secondly we do not observe fluid–fluid immiscibility above T_m in any of the sterol systems. This result is consistent with earlier diffraction studies. However as discussed in previous chapters the observation of fluid-fluid coexistence above T_m by spectroscopic probes can be attributed to transient concentration fluctuations of cholesterol and the very short time scale of spectroscopic measurements which can pick up such inhomogeneity.

At intermediate sterol concentrations the phase behaviour has certain differences. Sterols such as cholesterol, lanosterol, ergosterol and 7-DHC induce a modulated phase (P_β) in DPPC bilayers. Whereas in 25HC and cholestane we did not observe the modulated phase.

Instead we observed a gel-fluid coexistence in that part of the phase diagram. Such a difference in the phase behaviour probably arises from the difference in their orientation in the bilayers.

The binary phase behaviour of DPPC-ergosterol and DPPC-lanosterol are very similar to that of the cholesterol system. However we have observed a three phase coexistence at ~ 10 mol% of ergosterol in DPPC bilayers. At present we do not know the reason for such an observation. Our order parameter measurements suggest that the influence of ergosterol and cholesterol on acyl chain ordering is similar. However lanosterol is not as efficient as the above two sterols in ordering the acyl chains.

We have also investigated ternary mixtures containing ergosterol and cholestenone to compare the phase behaviour. We observed a fluid-fluid ($l_o - l_d$) coexistence for both sterols at intermediate sterol concentrations. However a demixing transition was observed for both these sterols at a much lower concentration than that of cholesterol. Our microscopy observations on GUVs prepared from equimolar mixtures of DPPC and DOPC at 30 mol% of ergosterol also complement the diffraction results. Similar studies on GUVs of DPPC-DOPC-cholestenone mixtures at 30 mol% showed the presence of gel like domains.

Earlier studies to find the partitioning of cholesterol between l_o - l_d phases have contrasting results. We have tried to find such a partitioning from x-ray data. However we could not succeed in it because of inherent problem which arises due to the lack of contrast between the electron densities of cholesterol and water. From our model calculation we showed that it is possible to extract the information about the composition of bilayer system from scattering data provided there is sufficient contrast in electron densities between the species.

Detached cell blebs can be used as biologically intermediate system between the model membranes and cell membranes. However the usability of such a system depends on how it is prepared. The appropriate way to prepare such cell detached blebs is by a non chemical method like osmotic shock.

Open questions

Our investigation on PC-sterol mixtures leaves a few unanswered questions

- The origin of modulated phase (P_β) is an interesting problem. There are two aspects for this problem. (i) Since we do not observe P_β in excess water condition where the bilayer separation is more, the role of interbilayer interaction in inducing this phase can not be ruled out. (ii) Our studies on various sterols suggests that only sterols which have a single anchoring site (-OH) group could induce P_β phase, sterols like 25HC and cholestane do not. It is an interesting problem to investigate the orientation of these sterols in the bilayers. This could possibly help in understanding the origin of the modulated phase.
- The structural differences between sterol molecules have significant influence on the phase behaviour of binary mixtures. The changes in steroid ring structure, anchoring part, and hydrocarbon chains in the sterol molecule seem to have different influence on the bilayers. Hence a detailed investigation is required to understand the influence of such structural changes on the bilayer properties.
- In view of the observation of a three phase coexistence in DPPC-ergosterol and DPPC-7DHC mixtures it is an interesting problem to probe the role of the steroid ring structure in lipid-sterol interaction. Whether such an interaction leads to some kind of complex formation needs to be addressed.
- Cholesterol partitioning between $l_o - l_d$ phases still remains an open question. As proposed here such a partitioning can be found out by varying contrast which can be done using neutron diffraction techniques.